MONASH University

Molybdenum complexation in chloride- and hydrosulphide- bearing hydrothermal fluids: Insights from *ab initio* molecular dynamics simulations

Submitted in fulfilment of the requirement for the degree of

Doctor of Philosophy

by

Julia Alexandra Sen

MSc, BSc

Supervisor : Professor Joel Brugger

School of Earth, Atmosphere and Environment

Monash University, Clayton, Victoria, Australia

2019

Copyright notice

Abstract

The development of computational methods has been taking place since the last century, and it has allowed us to gain greater insights into the geological processes, hydrothermal ore formation being one of them. Computational methods make it possible to expand our knowledge by supplementing and cross-checking experimental results, as well as predicting geological processes under the conditions which are very difficult/ impossible to replicate in experiments (for example very high P/T).

Molybdenum is an industrially important element which plays an irreplaceable role in metallurgy. Despite the fact that the geology of Mo deposits is quite well-known, a lot of questions related to this metal's transport and deposition in hydrothermal fluids associated with its deposits, remain unanswered.

In the current study, *ab initio* (from first principles) molecular dynamics (MD) simulations based on density functional theory (DFT) were applied to investigate the speciation of molybdenum in hydrothermal chloride- and hydrosulphide- bearing aqueous fluids under the P/T conditions ranging from ambient to magmatic. The obtained data was used to cross-check some of the existing experimental results as well as to provide brand new insights into the behavior of Mo complexes.

The results reveal that molybdenum oxo-chloro complexes are more important than previously assumed. The calculated stability constant for the reaction $[MoO_2(OH)(Cl)]^0 + H_2O = [MoO_2(OH)_2]^0 + HCl$ shows that the chloride bearing species is very stable at 750 °C / 2 kbar in 6 m Cl^- , thus confirming that complexation with chloride under these conditions is favourable. This result means that the chloride bearing species probably have a more significant role in transport of Mo in hydrothermal fluids than previously assumed.

The findings of the Mo-O-S calculations show that the Mo-S complexation is dependent on the concentration of hydrosulphide in the solution, where high HS^- is favourable for the formation of sulphur bearing species.

Plain language summary

Everything in the material world is made up of molecules, both solid things, liquids and gases. In this thesis, I take a close-up look at several different molecules, composed of atoms such as molybdenum, chlorine, sulphur, oxygen and hydrogen. By using a very powerful computer and software based on mathematical approaches, I model how these molecules behave in geological environments, where they are influenced by high temperature and pressure. The aim of this work is to gain more knowledge about the processes related to the formation of metal enrichments deep in the earth crust.

Declaration

This thesis is an original work of my research and contains no material which has been accepted for the award of any other degree or diploma at any university or equivalent institution and that, to the best of my knowledge and belief, this thesis contains no material previously published or written by another person, except where due reference is made in the text of the thesis.

Signature:……

Print Name: … Julia Alexandra Sen…

Date: ……08/10/2019……

Acknowledgements

I would like to thank the Faculty of Science, Monash University, for providing me with a scholarship which made it possible for me to undertake this degree, and the Pawsey Supercomputing Centre in Perth, WA , for providing the necessary computational time needed to generate the data for this thesis.

There are so many people who have contributed to my completion of this work. So, a huge **thanks** to:

- Professor Joel Brugger, for being such a knowledgeable, kind, understanding, patient & available supervisor. I would not be able to finish without your support and I'm immensely grateful for all your guidance!
- Dr Yuan Mei, CSIRO. I owe you most of my the computational skills and I'm so grateful for your generosity in sharing your knowledge and experience with me.
- Dr Weihua Liu, CSIRO, for making time to help me out and providing so many useful insights.
- My fellow student Qiushi Guan, for answering my shockingly unintelligent questions without judgement. I admire your talent for explaining very complex things in a very clear and simple way.
- Dr Barbara Etschmann for providing the experimental data (and organic lemons ☺)
- My panel members: Shayne McGregor, Yona Nebel-Jacobsen & Andy Tompkins for the useful feedbacks after my milestones (some extra gratitude to Andy for offering help in a last-minute emergency situation!)
- Johanna Laurent and Steven Guo at the Faculty of Science, for approving all of my many extensions and leave requests and also for being so approachable and helpful
- Tien, Silvana, Emily, Yuzhou, Rob, Christine and Ada for taking care of the practical things and making my stay at Monash a pleasant experience.
- To my office buddy Anung for all the useful tips about the visa, milestones & thesis submission
- To Marianne Richter for the help, support, encouragement, for taking care of my pot plants and most of all for our friendship ☺
- Jenny, Jess, Vicki, Zuzana, Sunshine, Rhian and James for being my dream team at the MPA Monash, I really enjoyed working with you!

Table of Contents

List of abbreviations and terms

A-Type magma- granitic magma from an extensional tectonic setting.

ab initio – from First Principles (= based on quantum mechanical principles).

COORSP- this parameter defines the coordination number (CN) of one selected atom *i* with respect to only one selected species *jsp*. The CN is defined by a Fermi- like function, but in this case *j* runs only over the atoms belonging to the selected species *jsp*.

DFT- Density Functional Theory

EXAFS- Extended X-ray Absorption Fine Structure

FPMD- Extended firs-principles Molecular Dynamics Method

GOE- Great Oxidation Event

I-Type magma- granitic magma from an igneous source

in situ – applied directly at the point of interest and in contact with the investigated subject

K-edge XAS- X-ray Absorption Spectroscopy based on K-edge (excitation of the 1s- orbital electron)

LA-ICP-MS- Laser Ablation Inductively Couples Plasma Mass Spectrometry

QMF buffer- quartz-muscovite-K-feldspar buffer

QM methods- methods based on quantum mechanical principles

REE- Rare Earth Element/s

UV-vis spectroscopy- Ultraviolet- visible Spectroscopy

XANES- X-ray Absorption near edge structure

XRF- X-ray fluorescence

1 Introduction

Molybdenum (Mo), with an atomic number 42 has an atomic weight of 95.96 g/mole and is located in the second row of the transition metal elements. It has 5 oxidation states, 2-6, of which 4 and 6 are predominant in nature (Krauskopf, 1972). Pure molybdenum is a silver-white metal and also occurs as black or dark-grey powder (Barceloux & Barceloux, 1999).

Although molybdenum has been used since the Middle Ages, for long time it was confused with graphite (Barceloux & Barceloux, 1999) and its history as a separate element starts in 1778, when it was recognised by Swedish-German chemist Carl W. Scheele (Scheele, 1778). He discovered that molybdenite (MoS_2) produced a "metallic acid" when it was treated with nitric acid. In 1782 Swedish chemist Peter Hielm (Hielm, 1788) reduced this compound to the metal and named it molybdenum. The name "molybdenum" is derived from the Greek word *molybdos* which means "lead" and was originally used to describe both graphite, lead and other metallurgical materials (Agricola and Hoover & Hoover, 1950) long time before molybdenum metal was discovered. (Braithwaite, 1994).

The first industrial application of molybdenum took place in 1893, when French chemist Henri Moissan heated impure metal in an electric furnace in a CO_2 atmosphere and produced pure Mo (99.88%) (Braithwaite, 1994). The element was thought to be rare and didn't find its applications for many years (Jarrell et al.,1980). It is first during the World War I that molybdenum became important in industry because its chemical properties made it an excellent replacement for tungsten in high performance alloys (Giussani, 2011).

Nowadays, molybdenum is an important element which has a variety of applications in modern society (**Table 1.3**) (e.g., Henckens, et al., 2018). When it comes to scientific research, Mo can be used as a reliable paleo-redox tracer in a variety of disciplines due to its redox sensitivity, (Dahl et al., 2013). Moreover, it has been discovered that Mo is one of the essential trace elements for living organisms, including humans (Zoroddu et al., 2019). Molybdenum is necessary for functioning of a large number of enzymes which are involved in the cycle of nitrogen, carbon and sulphur in plants, animals and humans (Mendel, 2007; Schwarz et al., 2009).

1.1. Ore Deposits & Industrial Uses

Molybdenite, MoS_2, is the main economic Mo-containing mineral. In order to be profitable, an ore must contain a minimum of ~0.1% MoS_2, although a lower Mo concentration is acceptable in case of very large deposits (e.g. 0.053%Mo at Endako, Canada (Selby & Creaser, 2001; Pohl, 2011). About ~75% of Mo is produced as a by-product of porphyry copper ore mining, where very large masses of ores are processed. It allows even low Mo-grades to be recovered economically (Pohl, 2011).

According to (Henckens et al., 2018), the total amount of ultimately extractable molybdenum resources on Earth is 50-180 Mt. Table 1.1 summarizes their and other authors' estimates.

Table 1.1

Estimates of the extractable global amount of molybdenum (from Henckens et al., 2018)

Source	Specification	Estimated amount of Mo resources (Mt)
USGS(2017a), identified resources based on UNEP (2011a)	Identified resources	19.4
	"Not unreasonable upper limit" of extractable resources, based on 0.01% of the total amount of Mo in the Earth's crust (upper 1km)	60
Calculation according to Rankin (2011, p.303)	Identified plus undiscovered resources, based on as assessment of the ratio between identified and undiscovered resources for five metals in the USA	76
Sverdrup et al. (2015)	Ultimate recovery rate	46
Henckens et al. (2018)	Ultimately recoverable amount of molybdenum, based on the estimated recoverable amount of molybdenum in porphyry copper resources	180

The world's most important molybdenum resources are mainly located in 5 countries (see **Table 1.2**), with the biggest deposits located in East Qinling-Dabie Mo belt, China, which hosts

8.43 Mt of proven Mo metal reserves (Mao et al., 2011). The biggest in history Mo-only mine was located in Climax, Colorado, USA (Giussani, 2011).

Table 1.2

Percentage of world's reserves of molybdenum per country. Numbers derived from USGS (2018b)

Country	Percentage of Mo resources
China	49%
USA	16%
Peru	13%
Chile	11%
Russia	6%
Total:	95%

The demand for molybdenum is growing quickly. In 2015 global production of Mo reached 235.000 metric tons. This number, compared to 14.500 metric tons in 1950, is equivalent to an annual growth rate of 4.4% (USGS 2017c).

Table 1.3

Applications of molybdenum in 2012. Data from (International Molybdenum Association (IMOA), 2015).

Application of Mo	
Mo grade alloy steels & irons	59%
Stainless steel	22%
Chemicals	12%
Molybdenum metal	5%
Super alloys	3%
Total	100%

Molybdenum has a high melting temperature (2623°C), high thermal conductivity (142 W m^{-1} K^{-1} at 20 °C), low thermal expansion coefficient (4.3 x 10^{-6} per centigrade), and relatively low atomic weight (95.9 g mol^{-1}). All of these properties make Mo and its alloys important for several industrial applications (Giussani, 2011).

Table 1.3 shows that the biggest consumer of molybdenum is metallurgy, which uses over 80% of this metal. The metal plays an important role in production of high-quality steels. Addition of Mo improves steels' ability to withstand high temperatures, improves resistance to seawater and corrosive chemicals, as well as enhances hardenability (Henckens et al., 2018). The importance of molybdenum as an alloying agent in steel production has grown with the development and globalisation of non-fossil energy sources such as wind and solar power. High performance steels containing Mo are used in manufacturing wind turbines (International Molybdenum Association (IMOA), 2011). Molybdenum is also used as one of the metals in the back electrodes of thin film solar panels (International Molybdenum Association (IMOA), 2013). The second main application of molybdenum is in the chemical industry, where is it used in pigments, corrosion inhibitors, lubricants, smoke suppressants, sulfurization catalysts and as a micronutrient in fertilizers (International Molybdenum Association (IMOA), 2015).

Given current knowledge and technology the role of Mo in industry is not replaceable by another element. At the same time, according to the most optimistic scenario, the global molybdenum resources will be exhausted within 70-160 years from now (Henckens et al., 2019), so it is important to acquire as much knowledge as possible about the mechanisms behind the formation of Mo deposits and the behaviour of this element in various natural environments, in order to improve its recovery rates from the ores.

1.2 Molybdenum in the environment

1.2.1. Biochemistry of Molybdenum

Molybdenum is unique, being the only 4d transition metal that is utilized by biological systems and it is essential for all forms of life (Tunney et al., 2004). In the early stages of the evolution of life on the Earth, molybdenum is thought to be bound in the insoluble molybdenite (MoS_2) (Tunney et al., 2004). The element became available for incorporation into biological systems with the development of photosynthetic organisms and the following production of oxygen, which took place about 2.7×10^9 years ago (Howard & Rees, 1996).

Similar to humans (Zoroddu et al., 2019), plants take up Mo as $[Mo(VI)O_4]^{2-}$, which is the most common soluble Mo compound present in soils (Gupta, 1997). This species becomes biologically active as a Mo cofactor in pterin; molybdopterin is found in virtually all molybdenum-containing proteins (Tejada-Jimenes et al., 2018). Mo cofactor works as an activator for a number of enzymes critical in biogeochemical cycles of nitrogen as well as carbon and sulphur.

The first study to discover that molybdenum is essential for nitrogen fixation in plants was conducted by Bortels (1936). The role of nitrogen in plant growth and biomass production is vital. Nitrogen is required in the synthesis of amino acids, nucleic acids, proteins, lipids as well as it is a major component in chlorophyll (Wang et al., 2014).

Two of the most important enzymes which require Mo in plants are nitrogenase and nitrate reductase (Jarrell et al.,1980). Nitrogenase is the enzyme which catalyses the reduction of atmospheric nitrogen gas (N_2) to ammonium (NH_4^+) in legume plants, thus enable the plant to utilize nitrogen (Jarrell et al.,1980; Tejada-Jimenes et al., 2018). In non-leguminous plants Mo is required as a constituent of the nitrate reductase, an enzyme which catalyses the reduction of nitrate (NO_3^-) absorbed from the soil into biologically available nitrite (NO_2^-). This process is the first stage toward incorporation of the nitrogen into proteins (Jarrell et al.,1980).

In natural environment, Mo has not been shown to reach toxic concentrations in plants (Jarrell et al.,1980). According to Tejada-Jimenes et al. (2018), high contents of molybdenum in plants appear to negatively affect animals which are fed these plants to a much higher extent than the plants themselves.

In higher animals, molybdenum takes part in oxygen transfer reactions in a number of enzymes (e.g. sulphite oxidase and xanthine oxidase) and it is required in very low doses in the diet (Hall, 2018). While molybdenum deficiency in animals has not been observed and efforts to produce it in laboratory experiments were not successful (Giussani, 2011), toxic effects of excess molybdenum are known to occur in animals (e.g., Beeson & Matrone, 1976; Underwood, 1977 ; O'Connor et al., 2001). The amount of Mo which leads to the development of adverse reactions, depends on several factors, such as species, age, previous dietary history, as well as relative amount of molybdenum, copper and sulphur in the diet (Rajagopalan, 1988). While horses and pigs can tolerate >1000 ppm of molybdenum in their feed, ruminants, such as sheep and cows exhibit negative reactions from 2-30 ppm Mo. The adverse reactions as a result of toxic concentration of Mo in animals include anorexia, anaemia, osteoporosis, severe

diarrhea, hair discoloration and even death (Dick, 1956). Because elevated concentrations of MoO_4^{2-} lead to disturbances in the distribution and elimination of copper (Mason, 1986), feed which is low on sulphates and copper can contribute to the development of adverse reactions to Mo in ruminant animals (Dick, 1956). The effects of molybdenum toxicity observed in ruminants are almost not known to occur in monogastric animals even in cases where the intake of dietary molybdenum had taken place (Giussani, 2011).

Out of the 2nd and 3rd rows of the periodic table, molybdenum is the only essential transition metal for humans. The amount of Mo contained in an average adult human is 5 mg, and mostly stored in liver, kidneys and small intestine (Schwarz & Belaidi, 2013; Burguera & Burguera, 2007). However, this dose would be dangerous as a single intake and the average intake for humans is about 0.3 mg/day. Molybdenum is taken up by the cells in human body only as molybdate oxyanion, $[Mo(VI)O_4]^{2-}$(Zoroddu et al., 2019). The richest dietary sources of molybdenum are legumes, leafy vegetables, nuts, dairy products and cereals (Giussani, 2011). Some of the important functions of Mo-containing enzymes in the human body are: 1) production of uric acid – a process which removes unwanted nitrogen compounds from the body and 2) metabolism of alcohol (Zoroddu et al., 2019). According to Giussani (2011), molybdenum is readily bioavailable with >85% of the element being efficiently absorbed in the intestine. Naturally occurring Mo deficiency has been reported only once in a patient with Crohn's disease.

1.2.2. Geochemistry of Molybdenum: Mo in natural waters & its role as a redox proxy

The electronic configuration of molybdenum is $[Kr]5s^14d^5$ and all six outer electrons are capable of bonding. As a result of this, the oxidation state of Mo in complexes with other elements can vary between 0 and 6 (Rickard, 2012). This makes the chemistry of molybdenum very versatile and complex. Redox sensitivity of Mo is the major controlling factor of the element's geochemical behaviour. The size, charge and physical properties of the Mo ion depend on its oxidation state. In its reduced tetravalent state (IV), Mo is not soluble in aqueous fluids, but becomes soluble in its oxidised hexavalent state (VI) (Greany et al., 2018). This distinct geochemical behaviour of Mo in sulphidic (reduced) and oxic environments is the foundation of this element's use as a paleo-redox proxy (Crusius et al., 1996; Arnold et al.,

2004; Algeo & Lyons, 2006). Analysing Mo-bearing minerals in modern oceans, modern and ancient euxinic sediments, as well as in crustal rocks, is a widely accepted method for obtaining information on Earth's ocean oxygenation over time (Arnold et al., 2004; Wille et al., 2007; Pearce et al., 2008; Scott et al., 2008; Dahl et al., 2010; 2011).

In most oxygenated natural waters, Mo has an oxidation state 6^+ (Mo(VI)), and occurs as a relatively inert tetrahedral anion $Mo(VI)O_4^{2-}$. At pH < 5, protonated forms $HMoO_4^-$ and H_2MoO_4 form (Cruywagen, 1999). In seawater, Mo forms a variety of metal-molybdate species such as $CaMoO_4$ and $MgMoO_4$. Molybdenum can react with solid matter (like minerals) and organic matter, although it is more typical for environments with highly reducing conditions and low pH (Smedley & Kinniburgh, 2017). In presence of Fe-Mn-Al hydroxides, $Mo(VI)O_4^{2-}$ may be immobilized via adsorption. This process takes place for example during the formation of deep-sea manganese nodules. While in presence of Pb, $Mo(VI)O_4^{2-}$ will form mineral wulfenite (Pohl, 2011).

In the modern oceans, Mo shows a conservative behaviour and a very long residence time of ~440,000 years (Miller et al., 2011). It is in fact the most abundant transition element in ocean water with a concentration of 10-11µg/L (Pohl, 2011; Smedley & Kinniburgh, 2017). Concentrations of Mo in seawater are higher than what can be utilized by marine organisms, and therefore are not significantly affected by biological activity (Dellwig et al., 2007). Most of the marine Mo is supplied by rivers which carry weathered continental material into the oceans (e.g., Bertine & Turekian,1973; Brumsack & Gieskes, 1983). The element is transported into the waterways through association with organic matter and Fe/Mn oxyhydroxides (Wichard et al., 2009; Glass et al., 2013), such as for example ferrimolybdite ($Fe^{3+}{}_2(MoO_4)_3 \cdot 8(H_2O)$), which easily dissolves in water (Pohl, 2011).

In anoxic environments the picture is quite different. In presence of sulphur, the oxygens in the molybdate anion are progressively substituted by S atoms and form thiomolybdate species, $MoO_{4-x}S_x^{2-}$ (Helz et al., 1996; Erickson & Helz, 2000; Vorlicek et al., 2015). Further on, through the interactions between thiomolybdates and Fe-S mineral phases or/and with organic matter, Mo precipitates in the bottom sediments (Helz et al., 2011; Dahl et al., 2013; Chappaz et al., 2014; Ardakani et al., 2016), thus exhibiting a non-conservative behaviour under sulphidic conditions. This process leads to formation of molybdenum rich sediments where the

concentration of Mo can exceed its crustal concentration by two orders of magnitude given that a sufficient amount of sulphur is present in the water column (Chappaz et al., 2016).

Although Mo now exists on the Earth's surface and in oxic water reservoirs in its oxidated and soluble form, there is a scientific evidence that it was not the case during the Earth's first ~ 2 billion years, when atmospheric oxygen was almost absent (Greaney et al., 2018). It was first during the Great Oxidation Event (GOE) which occurred between 2.4 Ga and 2.3 Ga that the levels of oxygen in the atmosphere started to rise (Lyons et al., 2014 and references therein). Studies conducted on minerals containing Mo (as well as other redox- sensitive metal proxies, such as U, Cr, Re) support the GOE theory. There is evidence that the minerals in which these elements were incorporated started to break down when a sufficient amount of O_2 had accumulated in the atmosphere, and thus, weathering processes of the existing bedrock could commence. In the case of Mo, the indicative minerals are sulphides, mainly pyrite and molybdenite (Anbar et al., 2007; Miller et al., 2011). During the process of sulphide breakdown, Mo becomes oxidised and consequently soluble. Now Mo can be transported in waterways as molybdate anion, and it will eventually reach the ocean, where it will start to slowly incorporate into Fe-Mn oxides under oxygenated conditions, or precipitate in black shales in case of euxinic (contain both oxygen and sulphur) and anoxic environments. The uptake of Mo by Fe-Mo-S minerals under euxinic conditions (Heltz et al., 1996; Erickson & Heltz, 2000) requires a high amount of sulphur in the water column so that the oxidation state of Mo can be reduced. It is likely that like oxygen, sulphur became first abundant in the Archean oceans during the GOE, when the emergence of atmospheric oxygen caused weathering of sulphur-bearing minerals in the continental crust (Canfield, 2005). According to Gaschnig et al. (2014), Mo depletion in the upper continental crust (UCC) coincides with Mo enrichment in black shales during and after GOE. In the UCC, Mo has been depleted relatively to the light REE of comparable compatibility (such as Pr and Ce) since the Paleoproterozoic and until the present day. This is an important observation as it supports the hypothesis that Mo was removed from the weathering continental crust and transported into the ocean during and after the GOE.

1.2.3. Geochemistry of Molybdenum: formation of Mo-bearing ore deposits and related hydrothermal processes

According to Pohl (2011), the estimated crustal abundance (Clarke value) of Mo is 1.2 ppm, which means that Mo is less abundant than most REE (Rare Earth Elements). Among magmatic rocks, granitic rocks have higher concentrations of Mo (~1 ppm) than basalts (~0.7 ppm). In nature, Mo is always found in association with elements such as O, S, W, Pb, U, Mg to name a few, and it does not exist in a pure metallic form. Molybdenum occurs in several minerals. The most important ones are molybdenite MoS_2 (amorphous MoS_2 is called jordisite), wulfenite ($PbMoO_4$), powellite ($Ca(Mo)O_4$) and ferrimolybdite ($Fe^{3+}{}_2(MoO_4)_3 \cdot 8(H_2O)$) (Jarrell et al.,1980). Apart from these minerals, molybdenum in igneous rocks is readily incorporated in amphibole and biotite (Voegelin et al., 2014; Yang et al., 2017).

Today, economically profitable concentrations of Mo are almost without exceptions related to magmatic-hydrothermal ore deposits, more specifically, I-type (of igneous origin) subvolcanic granitic and monzonitic intrusions and associated high temperature hydrothermal processes (Pohl, 2011).

There are two main types of such deposits:

1) Magmatic-hydrothermal molybdenum porphyry deposits related to granite or rhyolite, where Mo is the main metal being mined and W is by-product **(Figure 1.1 (B))** (e.g., Endako deposit, Canada (Selby & Creaser, 2001)
2) Magmatic-hydrothermal copper porphyry deposits related to monzonite or latite, where Mo is a by-product of Cu mining (e.g., Chuquicamata open pit, Chile (Ossandon et al., 2001)

Other types of Mo-bearing ores include:

- Polymetallic skarn deposits related to carbonate rocks (Mo, W, Sn, Be, Cu + other elements).
- Sandstone type uranium infiltration deposits (U, Mo by-product) (**(Figure 1.1 (D)**).
- Ocean-floor hydrothermal ore shales (Mo, Ni, Cu, Co, Zn) **(Figure 1.1 (C))**.

Molybdenum porphyries have many similarities with copper porphyries, but there are also some noticeable differences. For example, when it comes to the deposits in the US, the Mo-porphyries are younger and were formed during phases of relaxation and extensional

deformation of the crust as opposed to the active subduction setting typical for Cu-porphyries. Whereas Cu-Mo deposits are thought to have originated from mainly I-Type parental magmas, Mo-porphyries were formed from A-Type magmas. Parental magmas of Mo deposits are enriched in alkali elements and silica compared to those of Cu porphyry systems (Pohl, 2011).

Pohl (2011) suggests the following general pattern of formation of Mo-Cu-deposits: originating in the lower crust, the parental magma body is enriched in K, Rb, Nb, Sn, W, Mo and water. On its way upwards it undergoes fractionation which leads to formation of water-saturated melt pockets. These batches of melt ascent to subvolcanic level. Further decrease in pressure causes segregation of fluids and frothing of the melt. At this stage, the melt contains a big volume of volatile phases, which leads to a powerful convection of the melt. The part of the melt which contains bubbles will be brought upwards, while the degassed portion will sink downwards (Shinohara et al., 1995). Interactions with surrounding halogen-rich fluids will effectively remove trace elements such as Cu, Ag, Sn, W, Re as well as Mo from the melt. In the end, single-phase intermediate density fluids will rise upwards and start to boil under hydrostatic pressure at about 420 °C. The resulting brine, rich in Mo and other elements, will precipitate molybdenite and quartz. The characteristic potassium alteration observed at the sites of large Mo-deposits is caused by the high K-content of the fluids. Pb, O, S and Sr isotope data confirm that the ore fluids are of magmatic origin. However, in some locations an involvement of meteoric water has also been observed, suggesting that fluid mixing can also contribute to ore precipitation mechanism locally (Selby et al, 2000).

It is clear why the current consensus is that hydrothermal fluids play a major role in the formation of Mo-rich deposits. This would also be true for most industrially important metals such as Fe, Au, Ag, Zn, Pb, U, Mn, to name a few (Heinrich et al., 1996) and should not come as a surprise given the crucial role of aqueous fluids in geological process: redistribution of metals in the Earth's crust via dehydration reactions taking place during major geological processes such as regional metamorphism and subduction (Bebout & Penniston-Dorland, 2016; Zhong et al., 2015); exsolution from ascending magmas deep below the surface; convection of surface fluids **(Figure 1.1 (A))**. Therefore aqueous fluids play a key role in controlling the composition of the crust (Heinrich et al., 2004). By definition, hydrothermal fluids are electrolyte solutions with temperatures varying from 25 to > 600° C and pressure from 0.1 to > 500MPa. Hence, hydrothermal fluids cover a wide range of compositions and physical states,

from low-density vapours, to medium density supercritical fluids and brines. These fluids can contain high proportions of volatiles such as H_2O, CO_2, SO_2, CH_4 and their salinities can vary from diluted to very saline brines (> 60% salt), where the most common electrolytes are NaCl, KCl and $CaCl_2$. Hydrothermal fluids carry a wide range of metals, which exist either as hydrated ions or form complexes by binding with ligands such as Cl^-, HS^-, NH_3, OH^- and CH_3COO^- (review in Seward & Barnes, 1997).

Several authors, e.g., Zajacz et al. (2008), Lerchbaumer & Audétat (2012), Seo et al. (2012), present evidence that a significant part of Cu-Mo porphyry deposits formed in magmatic hydrothermal systems characterized by presence of low- to intermediate density supercritical aqueous fluids, which likely transported a major part of Mo and led to its mineralisation. According to Hurtig & Williams-Jones (2014a), the P/T conditions relevant for the formation of molybdenum porphyries are 350-800 °C, 300-1500 bar.

When it comes to the composition of hydrothermal fluids involved in the formation of Cu-Mo and Mo-porphyry deposits, Cl^- and HS^- are the major ligands of interest. Roedder et al. (1984) states that chloride is one of the most significant anions in porphyry fluids, and the amount of NaCl in some natural solutions can exceed 50 wt%. Audétat et al. (2011) discovered that many ore-forming volcano-plutonic systems reach the point of molybdenite (MoS_2) saturation already at the magmatic stage. This suggests that the behaviour of Mo in hydrothermal fluids depends on the stability of molybdenite during the ore-forming process, which leads to a logical conclusion that sulphur-bearing systems should be investigated as well.

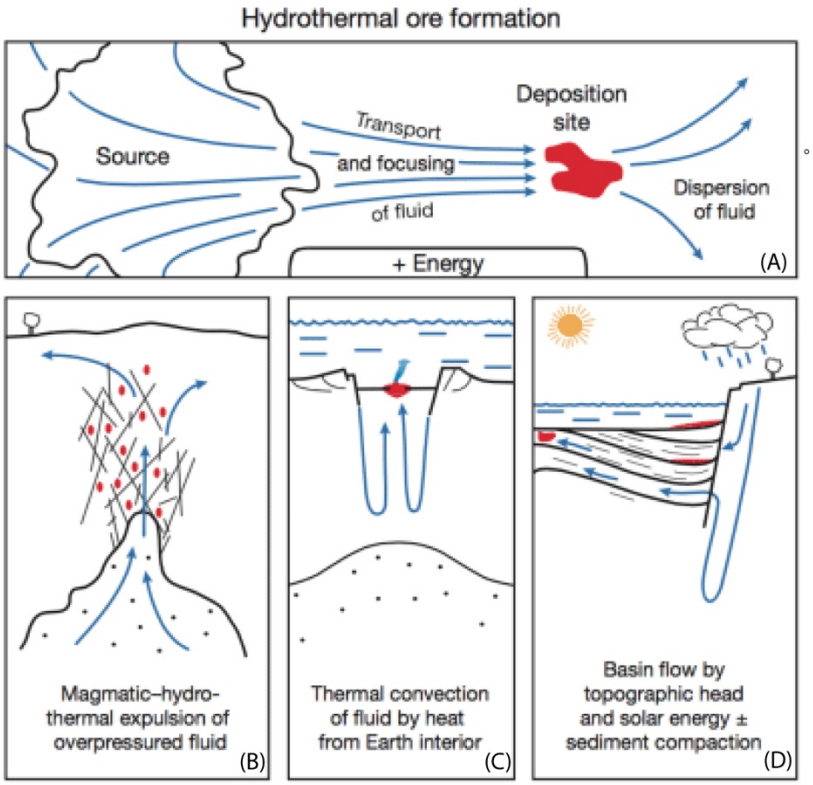

Figure 1.1 Schematic illustration of the process of metal enrichment by hydrothermal fluids (modified after Kesler, 1994).

1.3 Previous studies

Because Mo is a metal of interest in many fields of science and industry, there has been a number of experimental and theoretical studies to find the structure and speciation of Mo complexes. Some of these studies feature the two main anions in hydrothermal ore-forming processes - Cl^- and HS^-, while others describe experiments and computational investigations of molybdic acid and related protonated Mo-O-H species. The most significant and relevant (for my study) research is presented in Table **1.4**.

Ulrich & Mavrogenes (2008) conducted an experimental study of Mo solubility in KCl-H_2O solutions at 150-300 MPa and 500-800 °C, using LA-ICP-MS and XANES on synthetic fluid inclusions. Their results show that under these P/T conditions the solubility of Mo was temperature but not pressure dependent, and that it correlated positively with salinity, suggesting the formation of Mo-Cl complexes. However, due to the nature of the techniques,

the authors were not able to determine with certainty the nature of the Mo-Cl complexes present in the investigated solution. It is also worth to note that this study did not have independent K^+ and Cl^- measurements, so they suggested possible species based on calculated Mo/Cl and Mo/K ratios and comparison of XANES spectra with other studies (e.g. Cramer et al., 1978; Takenaka et al., 1998). Ulrich & Mavrogenes (2008) also conducted an experiment in pure water under the same P/T conditions. The conclusion is that H_2MoO_4 with the structure $[MoO_3 \cdot H_2O]$ is the dominant species. These results are in reasonable agreement with the work of Oyerinde et al. (2007), however the latter study was pH dependent and did not account for the effects of temperature. Based on their Raman spectroscopy data combined with DFT calculations, Oyerinde et al. (2007) concluded that the most likely structure of $H_2MoO_4^0$ is $[MoO_3(H_2O)_3]^0$ at pH < 6, but $[MoO_4]^{2-}$ becomes the predominant species at pH > 6. Tossel (2005) came to a similar conclusion in his study on stability of gaseous oxidic molybdenum species at 25 °C by performing free energy calculations (QM methods). Tossel (2005) reports that $[MoO_3(H_2O)_3]^0$ is more stable than the previously reported $[Mo(OH)_6]^0$ (Ozeki et al.,1988;1996), however, Tossel (2005) points out that according to his results, the dissociated 3-fold structure of $[MoO_3]^0$ is favoured under acidic conditions compared to $[Mo(OH)_6]^0$ and $[MoO_2(OH)_2]^0$, the latter two being highly unstable. In a neutral environment, $[MoO_3(H_2O)_3]^0$ decomposes to $[MoO_4]^{2-}$, according to the author.

Table 1.4 An overview over previous studies on Mo(VI) speciation & solubility which are relevant for the current study

Methods	Conditions	Results/Conclusions	Coordination/ geometry	Mo-O *d* (Å)	Mo-Cl *d* (Å)	Study
LA-ICP-MS on synthetic fluid inclusions & XANES	500-800 °C 150-300 MPa Mo in pure H_2O Mo in KCl-H_2O	Mo solubility is T but not P dependent, and it correlates positively with salinity $[MoO_3 \cdot H_2O]$ (H_2MoO_4(aq)) is dominant in pure water. At > 20 wt % KCl Mo-oxo-chloro complexes may be present.	N/A	N/A	N/A	Ulrich & Mavrogenes (2008)
Raman spectroscopy & DFT analysis	10 & 0.1mM of molybdate solution, 25°C	$[MoO_3(H_2O)_3]$(aq) is the most likely structure of molybdic acid in solution at concentration below 10^{-3} M Mo and pH < 6 $[MoO_4^{2-}]$ predominate at pH > 6 at all concentrations	Mononuclear species are predominant at concentrations of Mo below 10^{-3} M	Mo-O 1.69-1.73 Mo-OH 1.89-1.99 Mo-H_2O 2.20-2.68	N/A	Oyerinde et al. (2007)
Free energy calculations by molecular QM methods	Gas phase at 25 °C	$[MoO_3(H_2O)_3]$(aq) & $[MoO_3]$(aq) are stable in acidic environment	Dehydration from 6-fold to 4-fold geometry is favored	1.762-1.837	N/A	Tossell (2005)
Autoclave experiment & ICP-MS	300-500 °C 13-425 bar (vapor) ρ 0.005- 0.343 g cm^{3-} Mo concentration 3-481ppm in HCl vapor	Dissolution of MoO_3 increases with fH_2O	Hydration number increases with increasing fH_2O	N/A	N/A	Huritg & Williams-Jones (2014a)
Geochemical modelling with GEM-Selektor	Dry Cl_2(g), H_2O dominated gas, H_2S bearing gas	$MoO_3 \bullet yH_2O$(g) are the most stable gas species at all conditions, and are likely to be found in aqueous vapors and low- to intermediate density supercritical fluids.	Hydration number decreases with increasing T and constant P in gas phase. Constant T and increasing P promotes stability of hydrated Mo complexes	N/A	N/A	Huritg & Williams-Jones (2014a)

Methods	Conditions/Solution composition	Results/Conclusions	Coordination/ geometry	Mo-O *d* (Å)	Mo-Cl *d* (Å)	Study
XANES & EXAFS	25-385°C, up to 600 bar Mo in H_2O-HCl-NaCl brine Cl^- concentration up to 6.2 m.	Mo speciation is dominated by tetrahedral molybdate species in basic to near neutral solutions. Complexation with Cl^- occurs only in highly acidic fluids	Distorted octahedral oxo-chloro complexes predominate in highly acidic solutions. Tetrahedral $[MoO_4]^{2-}$ predominates in basic to near neutral solutions with Cl^- concentration up to 5.5 m without complexation with Cl^-	1.574-2.556	Mo-Cl 2.204-2.991	Borg et al. (2012)
Autoclave experiment	Crystalline MoO_3 in HCl-$HClO_4$-NaCl up to 1 m of Cl^- at 300 °C.	$[MoO_2(OH)_2Cl]^-$ is the most likely speciation, $\log_{10} K^0$ =-(0.87± 0.2)	$[MoO_2(OH)_2Cl_n(H_2O)_{2-n}^{-n}]$ is the most likely stoichiometry under small to moderate Cl^- concentrations	N/A	N/A	Dadze et al. (2018)
UV-spectrophotometry	30-300 °C Equilibrium saturated water pressure	$[HMoO_4]^-$ & $[MoO_4]^{2-}$ predominate in high-density natural hydrothermal fluids low in sulfur. $[H_2MoO_4]^0$ becomes insignificant at T > 200°C	N/A	N/A	N/A	Minubayeva & Seward (2010)
FPMD	Up to 300 °C	$[MoO_2(OH)_2 \cdot (H_2O)_2]^0$is the true structure of the molybdic acid in solution	Molybdic acid dehydrates at elevated T; $[MoO_4]^{2-}$ predominates in neutral and basic pH At acidic conditions, protonated species can exist.	Mo-O 1.74-1.76 Mo-OH 1.79-1.95 Mo-H_2O 2.40	N/A	Liu et al. (2013)
XRF & *K*-edge XAS	MoO_3 in 1M H_2O_2 at 400-600°C	$[MoO_4]^{2-}$ is most likely the predominant speciation $[HMoO_4]^-$ & $[H_2MoO_4]^0$ may be present	N_O = 3.6 - 4 (oxygen coordination number)	1.7 at all T	N/A	Yan et al. (2011)

Methods	Conditions/Solution composition	Results/Conclusions	Coordination/ geometry	Mo-O *d* (Å)	Mo-Cl or Mo-S *d* (Å)	Study
Solubility experiment	MoS_2 in 0-5 m NaCl 200-350 °C CO_2 partial P 0.69-172 bar Pyrite-pyrrhotite-magnetite buffer	Solubility of MoS_2(s) increases with decreasing fS_2(g), increasing fO_2(g) and fluid salinity	N/A	N/A	N/A	Wood et al.(1987)
Electron photometry & atomic absorption spectrometry	MoO_3 (<0.1 ppm - >10 ppm) in 0.1-4.0 M NaCl buffered by Fe_3O_4 , Fe_2O_3 , FeS_2, FeS 300-400 °C, saturated water-vapor pressure	Increasing activity of H_2S leads to a decrease of MoS_2(s) solubility. Increasing fO_2(g) and NaCl concentrations lead to an increase of MoS_2 solubility. Increasing T has a positive effect with molybdenum solubility	Higher fO_2 and pH favor formation of complexes where Mo is in its high oxidations state, Mo^{6+}	N/A	N/A	Cao (1989)
ICP-MS on synthetic fluid inclusions	MoS_2(s) in NaCl(±HCl)-bearing aqueous fluids. 600-800 °C, 200 MPa Various fO_2-fS_2	Mo solubility increases with increasing T, concentration of NaCl and fO_2(g), but decreases with increasing fS_2(g) and HCl.	$[NaHMoO_2S_2]$(aq) likely accounts for solubility of MoS_2(s)	N/A	N/A	Zhang et al. (2012)
UV-vis spectroscopy	$[MoO_4]^{2-}$ and $[MoS_4]^{2-}$ solutions + NaCl (for ionic strength) in N_2-filled glove box at ambient conditions	$[MoO_4^{2-}] \rightarrow [MoS_4^{2}]$ conversion may be very slow, intermediate thiomolybdates can be predominant in anoxic systems	N/A	N/A	N/A	Erickson & Helz (2000)
XAFS	Samples of lacustrine euxinic sediments	Mo is scavenged from euxinic waters as Mo-polysulfide species like $[Mo(IV)O(S_4)S^{2-}]$ & $[Mo(IV)S(S_4)S^{2-}]$	Mo(VI) compounds undergo reduction to Mo(IV) compounds before deposition in sediments	1.69-1.74	Mo-S 2.24-2.38	Dahl et al. (2013)

A more recent experimental study by Hurtig & Williams-Jones (2014a) suggests that the solubility of MoO_3 in H-O-Cl-S-bearing vapor and low- to intermediate density fluids increases with increasing P/T conditions and oxygen fugacity – unlike Ulrich & Mavrogenes (2008) who suggested that solubility of Mo is not pressure dependent. The study proposed that the dissolution of MoO_3 at 300-500 °C happens via the complexes' reaction with water and formation of hydrated $MoO_3(H_2O)_y$ species, with the value of y being between 2 and 8. This species are suggested to predominate under the investigated conditions, and the only other species which authors think may be significant under similar conditions in nature are unhydrated molybdenum oxo-chloro complexes (e.g. $[MoO_2Cl_2]^0$). These species may predominate at high acidity and low pressure.

Rempel et al. (2006) came to the same conclusion as the foregoing study, having found out that solubility of MoO_3 increases exponentially with fugacity of water, most likely due to the formation of gaseous hydrated complexes ($MoO_3 \cdot nH_2O$; n = 1 to 3.4).

There are a couple of other experimental studies that investigated Mo complexation with chloride alongside oxygen/hydroxy groups/water under hydrothermal conditions. Borg et al. (2012) investigated the speciation of Mo(VI) in H_2O-HCl-NaCl brines at 600 bar and up to 385 °C by *in situ* X-ray absorption spectroscopy. Their EXAFS fits and *ab initio* XANES calculations reveal that tetrahedral molybdate species (e.g., $[HMoO_4^-]$ or $[MoO_4^{2-}]$) are the major Mo species in basic to near neutral hydrothermal fluids, while chloride complexes with distorted octahedral geometry (proposed stoichiometry: $MoO_2Cl_n(H_2O)_{4-n}^{-(n-2)}$) will become significant only in highly acidic fluids under the P/T conditions of the experiment. The authors mention, however, that because an increasing temperature favours Mo-oxo-chloro complexation, it is not unreasonable to assume that such complexes may exist in less acidic solutions under higher P/T conditions. This was also suggested by Ulrich & Mavrogenes (2008). Dadze et al. (2018) studied solubility of crystalline MoO_3(s) in aqueous solutions of $HClO_4$ at 300 °C with a maximum chloride concentration of 1 m and a pressure of 10 MPa. Their group's results were in agreement with the study of Borg et al. (2012), concluding that the most probable speciation at their conditions was $MoO_2(OH)_2Cl^-$ (coordinated water omitted).

When it comes to research conducted on chloride-free solutions, Minubayeva & Seward (2010) performed an UV spectrophotometric study to determine the thermodynamic properties for the ionization of molybdic acid, H_2MoO_4, at vapour-saturated pressures and temperature ranging between 30 and 300 C° and various pH. According to their results, the transport of Mo in sulphur-poor hydrothermal fluids occurs in the form of the $HMoO_4^-/MoO_4^{2-}$ species, while H_2MoO_4 is insignificant at temperatures above 200 °C. At elevated temperatures (~ 300 °C), $HMoO_4^-$ is the dominant species at acidic conditions, while MoO_4^{2-} takes over at neutral to basic conditions. This is in accordance with the results of Borg et al. (2012). **Figure 1.2** was created in Geochemist Workbench (Bethke, 2008) in order to present the data on Mo-O speciation under different conditions obtained by Minubayeva & Seward (2010). The two figures summarize the dependency of molybdenum speciation on temperature, pH and oxygen fugacity. Additionally, the stability fields of molybdenite (MoS_2) under the same conditions are presented for comparison.

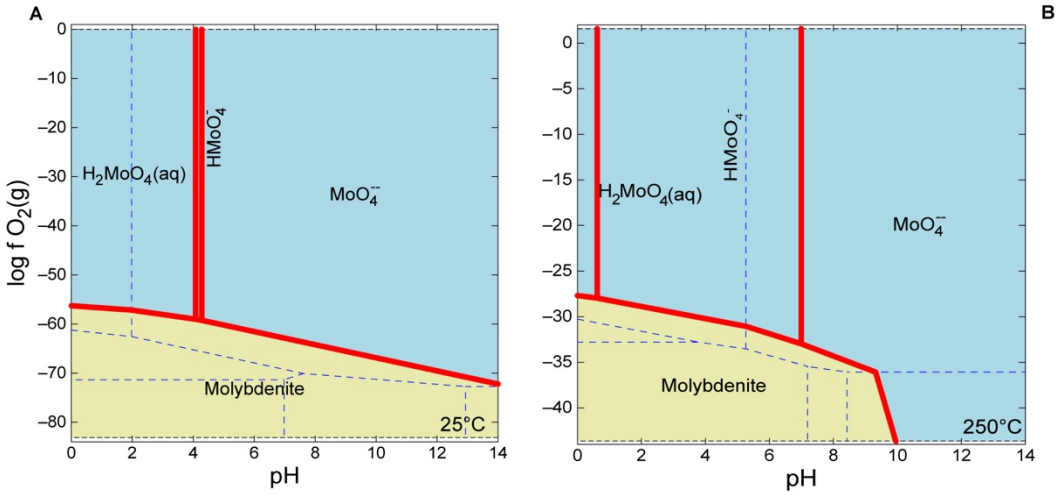

Figure 1.2. The figures show the stability fields of Mo-O species according to Minubayeva & Seward (2010) and molybdenite (the data is from www.factsage.com) depending on the temperature, pH and oxygen fugacity. **A**: T= 25 °C, P=1,013 bar, activity (a) (main)- 10^{-3}, aH_2O= 1, $a[SO^{2-}_4]$=0.1, $a[Ca^{2+}]=10^{-15}$. **B**: T= 250 °C, P=39,74 bar, activity (a) (main)- 10^{-3}, aH_2O= 1, $a[SO^{2-}_4]$=0.1, $a[Ca^{2+}]=10^{-15}$

Liu et al. (2013) determined the aqueous structure of molybdic acid (H_2MoO_4) up to 300 °C using *ab initio* molecular dynamics (FPMD) in combination with free-energy perturbation methods. The authors ruled out that the true structure of molybdic acid is temperature- and pH-dependent. At ambient conditions the acid exists as $[MoO_2(OH)_2 \cdot (H_2O)_2]$; with an increase of T, it gradually dehydrates to a distorted tetrahedral complex $[MoO_2(OH)_2 \cdot (H_2O)_{0.5}]^0$ at 200 °C, and becomes $[MoO_2(OH)_2]^0$ at 300 °C. The calculated acidity constants confirm the previously

mentioned conclusions of Borg et al. (2012) and Minubayeva & Seward (2010): [MoO_4^{2-}] is dominant at near-neutral to basic conditions while protonated species become prominent under gradual acidification.

An *in situ* XRF and Mo K-edge XAS measurements conducted by Yan et al. (2011) found out that MoO_3 is highly soluble in 1M H_2O_2 (H_2O_2 is a weak acid) aqueous supercritical fluids at 400-600 °C. The predominant speciation was determined to be [MoO_4^{2-}] under the conditions investigated. However, Yan et al. (2011) mention that the protonated complexes [$HMoO_4^-$] and [H_2MoO_4]^0 may be present though the hydrogen atoms could not be detected due to the limitation of the technique.

There is an agreement among the authors of the aforementioned studies that the molybdate anion, [$Mo(VI)O_4^{2-}$], dominates Mo speciation under neutral and basic conditions, while under acidic conditions protonated species are common. However, there is a discrepancy between several authors when it comes to the structure of protonated species. Tossel (2005), Ulrich & Mavrogenes (2008), Oyerinde et al. (2007) and Hurtig & Williams-Jones (2014a) propose [$MoO_3 \cdot nH_2O$] as the most likely structure, while Liu et al. (2013) suggested [$MoO_2(OH)_2$]^0 at elevated temperatures. The experiments of Borg et al. (2012) and Dadze et al. (2018) on Cl-bearing fluids, came to a similar conclusion, proposing formation of Mo-O-Cl complexes with increasing acidity.

Although molybdenite, MoS_2, is the dominant Mo-bearing economic mineral, there has been a very limited amount of research on solubility and speciation of Mo in sulphur-bearing hydrothermal systems. This is due to the fact that Mo solubility is inhibited in the presence of reduced sulphur (e.g. Wood et al. 1987; Cao, 1989), and hence Mo speciation is more difficult to investigate under these conditions (Zhang et al., 2012). One of the pioneering studies was done by Wood et al. (1987). This group investigated the solubility of MoS_2 in NaCl-CO_2-H_2O solution from 200 to 350 °C, and came to the conclusion that molybdenite had a very limited solubility at the conditions of the experiment. Cao (1989) demonstrated that the activity of H_2S has a profound effect on solubility of molybdenite at 300-400˚C: an increase in the activity of H_2S by 1 log unit results in a decrease in the solubility of MoS_2 by two orders of magnitude. On the other hand, an increase in both O_2 fugacity and NaCl concentration leads to a higher amount of the metal being dissolved in the fluid. The experimental study of Zhang et al. (2012)

at 600-800 °C and 200 MPa is in good agreement with these results. In addition, Zhang et al. (2012) suggests a possible formation of thiomolybdate species and their complexation with Na^+, forming $NaHMoO_2S_2$. This complex possibly accounts for the dissolution of Mo under the conditions of the experiment. Note that Zhang et al. (2012) and Wood et al. (1987) investigated the solubility of MoS_2 in Cl^- bearing fluids, thus both sulphur and chloride were present in the experimental solution; yet these studies found no evidence for chloride complexing.

The importance of molybdenum in paleoenvironmental research (Crusius et al., 1996; Arnold et al., 2004; Algeo & Lyons, 2006) has served as a catalyst for new studies on this metals' complexation with sulphur (see Chapter 1.2.3). Erickson & Helz (2000) conducted an experimental study by UV-vis spectroscopy to investigate molybdate to thiomolybdate conversion ($MoO_4^{2-} \rightarrow MoS_4^{2-}$) in terms of thermodynamics and kinetics. According to them, the process occurs in 4 steps, each of the steps being successively slower. Low pH and availability of acidic compounds make the conversion faster. However, Erickson & Helz (2000) point out that in natural environments where redox fluctuations can occur, transitional species MoO_3S^{2-}, $MoO_2S_2^{2-}$ and $MoOS_3^{2-}$ can predominate although they are thermodynamically unstable. Dahl et al. (2013) took this research a step further by investigating the mechanism of Mo incorporation into sediments after the molybdate-thiomolybdate conversion. The results of their XAS study on sulfidic lacustrine sediments present a novel view on the formation of Mo-rich sediments in euxinic environments by demonstrating that MoS_2 is not the main form of molybdenum found there (as it was proposed by Francois, 1988; Emerson & Huested, 1991; Calvert & Pedersen, 1993). Dahl et al. (2013) proposed that Mo (VI) is first reduced to Mo(IV) via a reaction with zerovalent sulphur and then scavenged from the water column as reactive Mo-polysulphide species like $Mo(IV)O(S_4)S^{2-}$ or $Mo(IV)S(S_4)S^{2-}$, which in turn precipitate through interacting with amorphous FeS phases, forming Fe-Mo-S compounds.

Although Mo-O-Cl and Mo-O-S complexes have been a point of focus in several experimental and theoretical studies, the research of Dadze et al. (2018) is the only one which provided a thermodynamic stability constant for a Mo-O-Cl complex. Apart from this, there are no kinetic/thermodynamic data available, which would have been relevant for the current study.

1.4 Study scope

Understanding the mechanisms for transport and deposition of Mo under geological conditions is undoubtedly important for our comprehension of crustal geochemistry, as well as it can provide us with knowledge required for sustainable mineral discovery and exploration (Brugger et al., 2010).

The goal of this work is to gain new insights into molecular-level speciation of Mo(VI) in hydrothermal Cl^-- and HS^--bearing brines up to magmatic hydrothermal conditions by means of *ab initio* molecular dynamics simulations. A further aim of this work is to provide reliable theoretical data in order to cross-check some of the existing experimental research which is mentioned in Chapter 1.3.

In this study I aim to answer the following questions:

1) Thesis Chapter 3: Which Mo(VI)-Cl-O species are likely to be stable at ambient to porphyry-like P/T conditions. Do the results of my MD simulations support the existing experimental data?
2) Thesis Chapter 4: Which Mo(VI)-S-O complexes are likely to be stable at porphyry-like conditions? In this chapter I investigate the speciation of molybdenum in S-bearing high P/T fluids, thus providing completely new theoretical data. These data are generated based on an unpublished experimental study conducted by my research group in July 2018 (the details are outlined in Chapter 4 and Appendix).
3) Thesis Chapter 5: A brief summary of the results and possible implications for molybdenum geochemistry.
4) Thesis Chapter 6: In this chapter I present the conclusions of my research in the light of other studies. I will also come up with some ideas for future work, based on what I have learnt through my own work and a few gaps in knowledge reported by other authors.

2 Methods

2.1 Advantages of computational chemistry methods

Over the past decades, we have gained more knowledge about the formation of metal deposits through different disciplines such as: stable isotopes, fluid inclusions, phase equilibrium and solubility experiments, *in situ* spectroscopic studies of element speciation in ore fluids, and computer simulations of reactive transport (Seward & Barnes, 1997). An accurate understanding of the thermodynamics of the important minerals and gaseous and aqueous species underpins the further development of a quantitative understanding of ore transport and deposition. Recently, and a number of experimental studies investigated the stability and coordination structure of aqueous metal complexes under hydrothermal conditions common for ore formation processes (e.g. molybdenum in Borg et al., 2012 and Hurtig & Williams-Jones, 2014a; gold in Hurtig & Williams-Jones, 2014b; copper in Liu, et al., 2008), providing valuable information about the behaviour of different metals in ore- related fluids.

Along with the solubility experiments we also need information on molecular structures of aqueous complexes (Mei et al. 2015). These data are key to the correct interpretation of solubility data, for assessing the existence of yet uncharacterized complexes, and for the construction of accurate thermodynamic models that can be used to extrapolate beyond the limited range of conditions covered by experiments. *In situ* spectroscopy provides direct determination of the speciation of the aqueous complexes (Sherman, 2001). X-ray Absorption Spectroscopy (XAS) is widely used as well, due to this method's sensitivity to electronic structures (Mei et al., 2013) and the penetrative nature of X-rays, which allows for *in situ* measurements of solutions at high pressures and temperatures (e.g. Seward et al., 1996; Fulton et al., 2001; Testemale et al., 2005; Liu et al., 2007; Tian et al., 2012).

Though experimental studies have provided most of the structural and thermodynamic data, which has helped us to understand metal mobility in hydrothermal fluids, it is obvious that all experimental methods have their inherent weaknesses. For example, even the most modern experimental equipment has its limitations when it comes to reproducing physical conditions for ore formation processes such is high P and T. Luckily, the improvement of computational methods, such as quantum mechanics simulations and classical molecular dynamics can now provide us with new independent information to cross-check the experimental results.

The two main methods in computational chemistry that will be used in combination in this study are quantum mechanical (QM) calculations and classical molecular dynamics (MD) simulations.

2.2 Classical MD

The classical MD approach is based on the approximation of the potential energy and forces acting on each atom, to two- and three-body potentials. These potentials are either empirically derived or fitted to potentials in finite clusters which are calculated by quantum mechanical methods. A simple pairwise interaction is the most widely used approach where it is assumed that the force between two atoms is not influenced by the positions of the other atoms in the simulation box.

Each inter-atomic potential normally implements a short-range repulsive-attractive force and a long-range Coulombic force (Sherman, 2010) as for example in the following equation, which is commonly implemented in classical MD software (e.g., Refson, (2001)):

$$U_{ij} = 4\varepsilon_{ij}\left[\left(\frac{\sigma_{ij}}{r_{ij}}\right)^{12} - \left(\frac{\sigma_{ij}}{r_{ij}}\right)^{6}\right] + \frac{q_i q_j}{r_{ij}}$$

Eq 2.1

In **Eq 2.1**, U_{ij} is the interaction between ions *i* and *j,* which we calculate by using Lennard-Jones potential which describes short-range interactions (Verlet, 1967) in the first term of the equation, and Coulomb force (second term of the equation) which describes long-range interactions between ions. The charges of ions *i* and *j* are respectively q_i and q_j and r_{ij} is the distance between them. ε_{ij} and σ_{ij} are the potential parameters for the ions and are calculated according to the following equation(**Eq 2.2**) using the parameters for single ions:

$$\varepsilon_{ij} = \sqrt{\varepsilon_i \varepsilon_j} \qquad \text{and} \qquad \sigma_{ij} = \frac{\sigma_i + \sigma_j}{2}$$

Eq 2.2

In this study the MD simulation boxes contain a metal-complex surrounded by the molecules of water and additional ions. Correct representation of water molecules is very important for a successful calculation, but is also challenging to achieve. Over the years, a number of models using rigid water molecules with a fixed O-H bond length and a fixed H-O-H angle has been developed. The most significant difference between these models is in the partitioning of the charge between the atoms (Sherman, 2010). Some examples include MCY water model by Matsuoka et al. (1976); TIPS2 and TIP4P by Jorgensen (1982) and Jorgensen et al. (1983); and Simple Point Charge (SPC) by Berendsen et al. (1987). The most widely applied in classical MD is however the Extended Simple Point Charge (SPC/E) by Berendsen et al. (1987) (**Fig 2.1**).

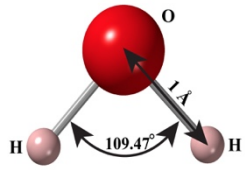

Figure 2.1 Graphic representation of the water molecule according to the SPC/E model Berendsen et al. (1987)

As **Fig 2.1** shows, the SPC/E water molecule is represented by three point charges in a fixed geometry, where the O-H distance is 1 Å and the H-O-H angle is 109.47° which is just slightly different from that in the gas phase (104.5°). Despite its simplicity, this model accurately reproduces the thermodynamic, structural and dielectric properties of water, especially along the liquid-vapour coexistence curve (Guissani & Guillot, 1993). These qualities are of great importance when it comes to simulating metal complex speciation and solvation in aqueous solutions (Sherman, 2010).

Classical MD methods can be used to simulate large scale systems containing thousands of atoms to over several hundreds of picoseconds and even nanoseconds of simulation time (Sherman, 2010). In this study, the size of the simulation box does not exceed 313 atoms, since larger amounts become intractable for *ab initio* simulations. Nevertheless, even this number of atoms initially requires the fundamental approximations of the classical MD approach. It makes it possible to obtain the initial configurations for each simulation, and especially the positions of water molecules, whilst avoiding dealing with too many degrees of freedom in the system.

On the other hand, unless simulating solutions of alkali and alkaline earth elements, where the interactions are of mainly electrostatic (ionic) character (Sherman, 2001), classical MD methods alone are not enough for obtaining reliable information on metal-ligand-solvent interactions. This is due to the fact that an interaction of a metal-ligand complex with the surrounding solvent is complicated and simple pairwise potentials are not sufficient. A classical MD simulation would require heavy parametrization but at the same time it would not give any information on the formation and breaking of covalent bonds (Terrier et al., 2010). For instance, when working with transition metals (e.g. Au, Cu, Ni, Zn, Mo), the interatomic interactions need to be described by quantum mechanical methods (Sherman, 2010).

2.3 *Ab initio* (first principles) MD

Ab initio molecular dynamics has advanced from molecular orbital (MO) theory, which started to develop in the early days of quantum mechanics in the 1930's. Among the pioneers in the development of MO theory are Friedrich Hund, Robert Mulliken, John Lennard-Jones and John C. Slater. Nowadays, MO theory has evolved into a well-trusted and accurate method for calculating molecular wavefunctions based directly on the fundamental equations of quantum mechanics (Pople & Beverige, 1970).

Molecular orbital theory provides an accurate description of electronic configuration only for one-electron molecules, however its approximate description of many-electron molecules is sufficiently good as well. Approximate MO theories are grounded in the mathematical foundation of molecular orbital theory, however they include a number of simplifications to the computational procedure (Pople & Beverige, 1970).

Density functional theory (DFT) (e.g. Parr & Yang, 1989) is the most commonly used approximation method for studying systems of geological relevance. The fundamental idea of DFT is that the total energy of a system in its ground state can be described by the means of functionals (a functional is a function of a function) of the electronic charge density (Sherman 2010).

The core of Car-Parinello method (CPMD) (Car & Parinello, 1985), which is used in this study, is implementation of DFT by defining the extended Lagrangian function, which describes the dynamics of the entire system:

$$L = \sum_i \tfrac{1}{2}\mu \int_\Omega d^3 r \left|\dot{\Psi}_i\right|^2 + \sum_I \tfrac{1}{2} M_I \dot{R}_I^2 + \sum_v \tfrac{1}{2}\mu_v \dot{a}_v^2 - E[\{\Psi i\},\{R_I\},\{a_v\}]$$

Eq 2.3

In equation **2.3**, the first term utilizes the constraint that the one-electron Kohn-Sham orbitals (ψ_I) are orthonormal with Lagrange multipliers; the second term describes the classical kinetic energy of the nuclei with mass M and coordinates R; the third term is the kinetic energy of the wavefunctions with fictitious mass μ; the last term is the Kohn-Sham total energy described as a function of the electronic charge density (represented as a function of the orbitals ψ_I), nuclear positions (R_I) and external constraints on the system (α_v) (Sherman, 2010)

On the practical level, DFT in CPMD is employed by the means of a plane-wave basis set of atomic orbitals and pseudopotentials. Plane-wave representation simplifies the computational aspect of calculations, but it has to be taken into account that plane waves are delocalized in space, thus they cannot be used to correctly describe the localized orbitals of the core electrons. That is where pseudopotentials come into the picture. The energy of the core electrons is simulated by subjecting the valence electrons to a pseudopotential, which simulates their effect on the valence electrons (Sherman, 2010). The correct choice of the functionals and the pseudopotentials is the basis for a realistic representation of the interactions between a metal, ligands and the solvent. When it comes to DFT-based molecular dynamics, it is only computationally possible to use generalized gradient approximation functionals. Becke-Lee-Yang-Parr (BLYP) functional (Becke, 1988; Lee et al., 1988) has been proven to give a satisfactory description of liquid water (Laasonen et al.,1993; VandeVondele et al, 2005), and it also works well to describe the behaviour of different ions in aqueous solutions (Heuft & Meijer 2003-2005; Hunt & Sprik, 2005). In this study, BLYP pseudopotentials will be used in combination with local density approximation functional (LDA) (Kohn & Sham, 1965).

CPMD has proved itself to be a reliable method for investigation of metal complexation and reactivity in solutions. It has been successfully applied in a number of studies to describe solvation of various cations in water (Terrier et al., 2010). The following *ab initio* studies are

especially representative, because their results on bond distances between metal cations and their ligands show good agreement with the data derived from XAS experiments conducted on the same complexes.

Table 2.1

Comparison of bond distances in metal complexes derived from MD and XAS/EXAFS

Metal complex	Metal-ligand bond distance (Å)*	
	MD	XAS
$[CuCl_2]^-$	2.15 (Sherman, 2007)	2.152 (Brugger et al., 2007a)
	2.13 (Mei et al., 2013a)	2.12-2.13 (Fulton et al., 2000a,b)
$[Cu(HS)_2]^-$	2.16 (Mei et al., 2013a)	2.149 (Etschmann et al., 2010)
$[AuCl_2]^-$	2.27-2.32 (Mei et al., 2014)	2.267 (Pokrovski et al., 2009a)
$[Au(HS)_2]^-$	2.36 (Liu et al., 2011)	2.29 (Pokrovski et al., 2009b)
$[AgCl_2]^-$	2.38 (Pokrovski et al., 2013)	2.38 (Pokrovski et al., 2009b)
$Pb(ClO_4)_2$	2.65-2.63 (Etschmann et al., 2018)	2.59-2.54 (Etschmann et al. 2018)

* Distances between metals Cu, Au, Ag, Pb and their respective ligands Cl^-, HS^-, and O^{2-}

Qualitative data such as bond distances and the formation and breaking down of metal-ligand bonds are undoubtedly important and represent the first step on the way to understanding the behaviour of transitional metals in hydrothermal fluids. However, these data alone are not enough to predict metal transport and speciation in natural or simulated fluids: thermodynamic properties for the formation of stable aqueous species are required. The good news is that based on the qualitative data, we can model thermodynamic properties of related metal complexes, which in turn will provide a much more solid basis to our understanding of hydrothermal ore formation (Brugger et al., 2016).

In theory, thermodynamic properties can be derived from *ab initio* simulations that run much longer than the exchange rate between ligands in a given reaction. In the case of aqua-chloro complexes of transition metals, the experimental data summarised by Burgess (1978), Table 11.4 and later Sharps et al. (1993) show that the ligand exchange rates are in the range of ns to μs. Given very high computational cost (outlined in sections 3.3 and 4.3) and limited

availability of the essential computational resources (such as a supercomputer), such calculations are currently out of reach.

Luckily, a couple of techniques have been developed which enable us to obtain thermodynamic properties of aqueous species of transitional metals within currently available computing resources. Essentially, we need a way to force the reaction to happen. The way to do this is by using a constraint force between the metal cation and the ligand of interest. One of the methods designed to perform such calculations is called ab initio Thermodynamic Integration.

2.4 *Ab initio* Thermodynamic integration

Ab initio thermodynamic integration (Sprik, 1998; Sprik & Ciccotti, 1998) is a computational method which makes it possible to calculate the free energy of chemical reactions involved in the formation of metal complexes (Sherman, 2010). The first step is to choose a predefined reaction path. For example, the following reaction(Mei et al., 2013):

$$[Cl\text{-}Cu\text{-}Cl]^{-} + H_2O = [H_2O\text{-}Cu\text{-}Cl]^{0} + Cl^{-} \qquad (1.1)$$

Then, the distances between the Cu cation and one of its ligands will be constrained to certain values, which are chosen based on the results of *ab initio* MD. Knowing at which distance the ligand is bonded to the metal as well as at which distance the bond is absent (which means that the interaction between the metal and the ligand is negligible), lets us choose several (>10) distances between and slightly beyond these values at which we will measure the constraint force *f*(r) that is required to maintain the ligand at the chosen distance. Since the constraint force depends on the configuration of the complex and its hydration sphere, the mean constraint force is obtained by running a simulation and averaging the force over a time frame that is large enough to sample many possible configurations (usually 7-10 ps). This way, the mean constraint force is calculated as a function of all constrained distances. The free energy of ligand exchange reaction can then be calculated by integrating the time-averaged constraint force *f*(r) over the constrained distances *r* according to the following equation (**Eq 2.4**):

$$\Delta_r A_{a \to b} = -\int_a^b \langle f(r) \rangle dr$$

Eq 2.4

Although in literature thermodynamic properties of metal complexes are presented in terms of free Gibbs energy at constant pressure, when it comes to *ab initio* MD it is preferred to calculate ΔA, which is Helmholtz free energy at constant volume, due to fact that calculations at constant pressure are computationally challenging for first principle techniques (Haile, 1992).

$$\Delta G^{r} = \Delta \mathrm{A}_{a \to b} + V \int_{p0}^{p} dp$$

Eq 2.5

In **Eq. 2.5**, $\int_{p_0}^{p} dp$ represents the change in free energy due to the change in pressure during the ligand exchange reaction at constant volume. According to Mei et al. (2013), the energy difference between ΔA and ΔG is small, so that the Helmholtz free energy is a good approximation of the Gibbs free energy of the reaction:

$$\Delta_r G = \Delta A_{\ a \to b}$$

Eq 2.6

This approximation (**Eq 2.6**) has been used in several studies with a great success, to name a few: Bühl et al. (2006, 2008); Habershon & Manolopoulos (2011); Mangold et al. (2011); and Mei et al. (2013; 2015).

The next step is to calculate the standard state Gibbs free energy of the reaction, $\Delta_r G^{\Theta}$, which is a hypothetical value for 1 molal concentrations where infinite dilution properties apply (infinite dilution refers to the chosen standard state, that assumes that the individual ions interact only with bulk water, and not with each other, so it doesn't matter how much solvent we add, the properties of the solute will not change). This is done by using the previously calculated $\Delta_r G$ in the following equation:

$$\Delta_r G^{\Theta} = \Delta_r G + RT \ln \frac{C_{A\gamma A} \times C_{B\gamma B}}{C_{C\gamma C} \times C_{D\gamma D}}$$

Eq 2.7

C_i in **Eq. 2.7** stands for concentrations of reactants or products of the reaction A+B → C+D, while γ_i are their corresponding activity coefficients (Mei et al., 2013).

In general, interactions among neutral complexes are much weaker than between charged complexes, so we follow the common geochemical convention and assume that activity coefficients of neutral species are equal to unity at infinite dilution. But in case of charged species being present in the investigated solution, we use the B-dot extension of the Debye-Hückel theory (**Eq 2.8**) (Helgeson et al., 1981; Mambote et al., 2003; Zeng et al., 2008), because of its wide-spread acceptance in thermodynamic studies of hydrothermal systems.

$$\log \gamma_i = - \frac{z_i^2 A_\gamma I^{1/2}}{1 + \dot{a}_i B_\gamma I^{1/2}} + \dot{B}_\gamma I$$

Eq 2.8

Here, $\dot{a}_i$ is the ion size parameter in Ångstrøm, Z_i is the charge of ion, I is the ionic strength, $A\gamma$ and $B\gamma$ are defined in Table 1 and Table 2 in Helgeson (1969). $\dot{B}\gamma$ is an empirical parameter which value can be found in Helgeson & Kirkham (1974), Table 26. After $\Delta_r G^\Theta$ has been obtained, the formation constants (K^Θ) can be calculated from the equation **2.9**:

$$\Delta_r G^\Theta = - RT \ln K^\Theta$$

Eq 2.9

Equations **2.1-2.9** are implemented in the computational software used in this work.
All *ab initio* simulations in the current study were performed using the resources provided by the Pawsey Supercomputing Facility, Perth, WA.

Following the success of several research groups (see **Table 2.1**) the current study will combine classical and *ab initio* methods in order to generate new computational data. A classical MD code Moldy (Refson, 2001) will be used to obtain the initial atomic configurations of each simulation. As explained in section 2.2, this saves us a lot of computational resources and makes the calculation manageable. Further on, the obtained initial configuration is treated quantum mechanically in an *ab initio* software CPMD (Car & Parinello, 1985), giving us

insights into the formation and break up of metal-complexes as a function of pressure, temperature and solution composition. The detailed setup of the simulations will be given in chapters 3.3 and 3.4.

3 Mo(VI) speciation in hydrothermal Cl-bearing brines up to magmatic hydrothermal conditions (750 °C, 2 kbar)

3.1 Introduction

The most common Mo-bearing mineral is molybdenite ($Mo(IV)S_2$) (Rickard, 2012), which occurs in porphyry-style Mo ore deposits as well as a by-product in Sn-W-Mo ores and Cu-Au porphyries. In porphyry- style deposits, the source of Mo is granitic melts, where the element occurs as Mo(VI) and Mo(IV) (Ryabchikov et al., 1981; Candela & Holland, 1984; Wood et al., 1987; Stemprok, 1990; Holzheid et al., 1994; O'Neill & Eggins, 2002). However, in hydrothermal fluids Mo is expected to be transported in its hexavalent state (Minubayeva & Seward, 2010; Hurtig & Williams-Jones, 2014a).

The importance of Cl^- as one of the major anions in porphyry fluids is beyond doubt (e.g Roedder et al., 1984). Although there has been a number of studies investigating complexation between molybdenum and chloride, the results are somewhat unclear. Earlier studies tend to agree that chloride species don't play a significant role in transport of molybdenum in hydrothermal fluids (e.g. Kudrin, 1989; Keppler; & Wyllie, 1991), however a study by Borg et al. (2012) demonstrated that Mo-O-Cl complexes become important species at elevated temperatures and high acidity, as well as Dadze et al. (2018) documented complexation of Mo with Cl^- at low to moderate concentration of chloride. Due to the physical limitations of the experimental methods, the highest temperature applied in these studies did not exceed 400 °C (Borg et al., 2012) (there have been experiments on Mo speciation in Cl^- -bearing vapor which were conducted at higher T, but the research on low-density systems is beyond the scope of the current study). Given that the P/T conditions of formation of Mo porphyry deposits are higher (350-800 °C/300-1500 bar (Hurtig & Williams-Jones, 2014a), it is a key part of the thesis, that theoretical calculations can answer questions about possibilities that cannot be explored experimentally.

3.2 Study scope

By conducting a series of *ab initio* MD simulations followed by an *ab initio* thermodynamic integration calculation, this study aims to:

1) bring more clarity in regards to the importance of Mo(VI)-chloro complexes at conditions up to 750 °C/ 2kbar. This computationally generated data will be used to cross-check the experimental results of Borg et al. (2012).
2) investigate the possible speciation of Mo-O-Cl complexes at ambient to high P/T conditions
3) document coordination changes during simulations at different P/T conditions
4) resolve the ambiguity related to the structure of protonated Mo-O species under acidic conditions
5) derive the stability constant of a selected Mo-O-Cl species at high P/T conditions

3.3 Methods

The general information about the methods and theory was set out in Chapter 2.

The initial atomic configurations for the Mo-Cl complexes investigated in this study (**Table 3.1**) were generated by a classical MD code Moldy (Refson, 2001). Pair potentials for Mo-Cl and Mo-O interactions were modified from cluster calculations for Zn-O and Zn-Cl (Harris et al., 2001), and the SPC/E model (Berendsen et al., 1987; Smith and Dang, 1994) is used to describe water molecules. The densities of the investigated systems were calculated by the SOWAT code, which implements an equation of state of NaCl-bearing solutions (Driesner, 2007; Driesner & Heinrich, 2007). The simulations were performed in an NVT ensemble (Sherman, 2007), which means that the temperature, volume and composition of the simulation box remained constant. In such ensemble, the pressure of the system is reflected by the choice of the density of the system, i.e. the volume of the simulation box. Since there is only one molybdenum atom in each box, Mo is essentially at infinite dilution and there are no Mo-Mo interactions. Our aim is to simulate conditions relevant for natural NaCl solutions; hence, densities were chosen to correspond to a total equivalent NaCl salinity of 6 molal (i.e., the used

density corresponds to that of the NaCl solution with the same chlorine molality as the simulation box). With this assumption, water-water interactions most closely reflect conditions in concentrated NaCl solutions).

Then, the *ab initio* MD calculations were performed by the means of CPMD- Car-Parinello molecular dynamics code (Car & Parinello, 1985). The LDA exchange-correlation functional, which is an approximation method applied to solve **Eq. 2.3** (Lee, Yang and Parr, 1988) and BLYP pseudopotentials (Becke et al., 1988) were used in order to reduce the number of explicit electrons as well as to set a cutoff radius (80 Ry) in the plane wave expansion. Periodic boundary conditions were applied in order to minimize surface effects. Nosè thermostat (implemented in the software) was used to control the temperatures of ions and electrons.

Twenty-one *ab initio* simulations with seven distinct initial configurations were conducted at three different pressure- and temperature conditions (**Table 3.1**), representing ambient conditions as well as supercritical fluid conditions which are found in magmatic-hydrothermal systems. All initial configurations were octahedral, with the Mo^{6+} ion being surrounded by 6 ligands. The ligands are chloride anions, water molecules and oxygen anions.

Starting with $MoCl_6$ in simulation 1a, the number of Cl^- anions is decreased while the number of water molecules bonded to Mo^{6+}, is increased and the last configuration studied is 1g, $Mo(H_2O)_6$. The content of each simulation box corresponds to a fluid of 6 molar Cl^-. All simulations were performed for 16 to 19 picoseconds (see in **Tables 3.2-3.4**).

Unlike field work and experimental research, *ab initio* MD simulations are neither physically demanding nor dangerous, however the costs involved in generating computational data are impressively high. It took about 20160 CPU hours to produce one ~17 ps long simulation. To test the same complex at three different P/T conditions required ~60480 CPU hours. An amount of 423360 CPU hours was used in order to produce the results presented in section 3.4.1. Thermodynamic integration consumed ~138240 CPU hours. Given that a cost of one CPU hour is 40 cents, the very minimum amount of money used to generate the results described in this chapter is $224620. The actual cost was in fact much higher due to several failed attempts as well a considerable amount of CPU hours was used on the purpose of learning the method.

Table 3.1 Simulation setup for molybdenum oxo-chloro complexes

Job no.	Simulation cell content (number of atoms)	Initial configuration & Solution composition	T (°C)	P (bar)
1a	1 Mo, 6 Cl, 55 O, 110 H	$[MoCl_6]^0$ + 55 H_2O	25	1
			350	500
			750	2000
1b	1 Mo, 6 Cl, 55 O, 110 H	$[MoCl_5(H_2O)]^0$ +1 (Cl^-)+ 54 H_2O	25	1
			350	500
			750	2000
1c	1 Mo, 6 Cl, 55 O, 110 H	$[MoCl_4(H_2O)_2]^0$ +2 (Cl^-) + 53 H_2O	25	1
			350	500
			750	2000
1d	1 Mo, 6 Cl, 55 O, 110 H	$[MoCl_3(H_2O)_3]^0$ +3 (Cl^-) + 52 H_2O	25	1
			350	500
			750	2000
1e	1 Mo, 6 Cl, 55 O, 110 H	$[MoCl_2(H_2O)_4]^0$+4 (Cl^-) + 51 H_2O	25	1
			350	500
			750	2000
1f	1 Mo, 6 Cl, 55 O, 110 H	$[MoCl_1(H_2O)_5]^0$+5 (Cl^-) + 50 H_2O	25	1
			350	500
			750	2000
1g	1 Mo, 6 Cl, 55 O, 110 H	$[Mo(H_2O)_6]^0$+ 6 (Cl^-) + 49 H_2O	25	1
			350	500
			750	2000

In addition to *ab initio* MD simulations, one *ab initio* Thermodynamic Integration calculation (see **Table 3.5** for details of the TI simulations) was conducted in order to estimate the stability of the ligand-exchange reaction of interest; this TI calculation is based on 16 individual constrained simulations. The *ab initio* MD results presented in Chapter 3.4.1 of this thesis, gave us an idea of which Mo-aqua-chloro complexes are stable at three different P/T conditions. Taking a step further we could now obtain thermodynamic properties for the configurations of interest using *ab initio* TI method described in detail in Chapter 2.4.

The final configuration of simulation 1e at 750 °C, 2 kbar, $[MoCl(OH)(O)_2]^0$, was stable for 17.5 ps (see **Table 3.4**). While $[MoO_2(OH)_2]^0$ is a stable final configuration of simulations 1f

and 1g. Both species have the same geometry and the only difference between them is in the exchange of Cl^- for OH^-. However, the role of chloride complexes in high temperature fluids cannot be evaluated from simulations only. This is a limitation of *ab initio* simulations, since the short simulation times do not allow for the equilibrium species to be assessed in most ligand exchange reactions. Thermodynamic integration is one of the methods that allows to bypass this limitation, and the two configurations obtained at 750˚C are an excellent case study where *ab initio* TI can be applied in order to investigate the energetics of the ligand exchange reaction. The predefined reaction path in this study is the following:

$$[MoO_2(OH)(Cl)]^0 + H_2O = [MoO_2(OH)_2]0 + [HCl]^0 \qquad (3.1)$$

In order to obtain the free energy of the ligand exchange reaction, and determine the stability of the complexes, the distance between Mo and Cl was fixed at sixteen different values, as presented in the **Table 3.5**. The force which is acting between the Mo ion and the chloride anion was measured during each simulation and then integrated over the constrained (Mo-Cl) distance. The resulting value was used to calculate the free energy of the reaction according to the **Eq. 2.4**. This equation is implemented in a MatLab code, which was used to perform the calculation.

The *ab initio* TI calculations were conducted with the same technical specifications as *ab initio* MD calculations using the CPMD code (Car & Parinello, 1985), with an additional parameter COORSP. The function of this parameter is to fix the coordination number of one selected ion (Mo in the case of this study) with respect to only one selected ligands (Cl^- in this study).

The data generated by Moldy and CPMD were processed by a free software VMD and MatLab in order to visualize the simulations and create images (**Figures 3.1-3.5)**, and to calculate the values presented in **Table 3.2-3.5**.

3.4 Results

3.4.1 Ab initio molecular dynamics simulations

The general trends observed at three different P/T conditions are linked to changes in hydration, geometry and charge. Due to the short lengths of the simulations, it is not possible to decide based purely on the results of the MD simulations, which configurations would be stable over longer time (e.g. if speaking in terms of seconds, instead of picoseconds). What is described in the text as "stable" configuration refers to a configuration which has remained unchanged during the length of the simulation, or which was stable during at least the last half of the simulation.

It seems clear that the aqua-complexes deprotonate with an increase of temperature and pressure. At 25 °C, four out of seven configurations (1d, 1e, 1f and 1g) retained at least one water molecule in the end of the simulation (**Table 3.2**). At 350 °C, configurations 1c, 1d, and 1e retained one water molecule; however, the bonding distances indicate that in all three cases this molecule is only very loosely bonded to the Mo-Cl complex and the final configuration is not stable (**Table 3.3**). As the kinetic energy significantly increases at 750 °C and 2 kbar, the water molecules deprotonate at the very start of the simulation, with only 1e, 1f and 1g retaining one or two OH^- groups (**Table 3.4**). Under this P/T condition, no water molecules remained bonded to Mo^{6+} in the final configuration.

Higher pressure and temperature lead to a decrease in coordination number. While all final configurations at ambient conditions are still octahedral – or interchanging between square pyramidal and octahedral, e.g. 1b, 1d and 1c, at 350 °C/500 bar, some complexes become stable in tetrahedral configuration (e.g. 1f). At 750 °C/2 kbar four out of seven initially octahedral configurations lose 2 of their ligands by the end of the simulation.

It is also clear that charged species can to some extent exist in a solution at ambient conditions, for example 1b, 1c and 1d, although none of these configurations remained unchanged throughout the simulation. At 350 °C there are two final configurations which involve a charged species, and at 750° C all final configurations are neutral except for 1b.

When it comes to changes which can be observed for the same initial configuration at different P/T conditions, $[MoCl_6]^0$ is the only initial configuration that has remained stable over the

whole simulation, which can be seen from **Figure 3.1**. The only noticeable thing is that the Mo-Cl bond distances, as well as their respective standard deviation factors, progressively increase with an elevation of T and P, being highest at 750 °C/2 kbar (**Tables 3.2-3.4**). It is also clear that this configuration is stable enough to prevent complexation of Mo^{6+} with O^{2-} which exist in the solution as water molecules.

Unlike $[MoCl_6]^0$, the $[Mo(H_2O)_6]^0$ configuration (**Fig 3.1**) underwent significant changes during the simulations. At ambient conditions the complex loses 5 H^+ in the very beginning of the simulation (it is not visible from the pictures). This results in a formation of a charged species $[MoO_2(OH)(H_2O)_3]^+$, which exists until 12 ps when the OH^- deprotonates, leading the molecule to become neutral again; the final configuration is an octahedral species, $[MoO_3(H_2O)_3]^0$.

This transition is clearly represented in the change of the bond distance between Mo^{6+} and the oxygen anion that lost its hydrogen at 12 ps. **Table 3.2** shows that until 12 ps the bond distance was 1.922 Å, and after 12 ps it became 1.750 Å. In this study is has been clear that the bond distance between Mo^{6+} and O^{2-} is indicative of whether the molybdenum ion is bonded to a water molecule, a hydroxy group or and oxygen anion. The longest bond distances of over 2 Å indicate that the ligand is H_2O; a bond of ~1.8-1.9 Å means that the ligand is an OH^-, while the shortest bond distance of ~1.7 Å is between Mo^{6+} and O^{2-}. The initial complex $[Mo(H_2O)_6]^0$ deprotonates and forms a neutral tetrahedral species $[MoO_2(OH)_2]^0$ during the simulations at 350 °C and 750 °C. In both cases the final configurations are very stable over the length of the simulations.

The first Mo^{6+} complex with mixed oxo-chloro ligands, $[MoCl(H_2O)_5]^0$, retained octahedral configuration at ambient conditions (**Fig. 3.2**). However, it underwent deprotonation resulting in three out of the initial five water molecules breaking down to two O^{2-} and one OH^- in the very beginning of the simulation. The final configuration, $[MoClO_2OH(H_2O)_2]^0$ has been stable for the entire 17.5 ps, although one of the water molecules exhibits slight fluctuations in its bond length, with an average Mo-O distance of 2.389 Å and a standard deviation of 0.160 Å (**Table 3.2**) – values which are just a bit too high to indicate a stable bond. The picture is quite different at 350 °C/500 bar. The initial configuration breaks down to two metastable tetrahedral complexes. The final configuration interchanges between the charged $[MoClO_3]^-$ with three O^{2-} and the neutral $[MoCl(OH)O_2]^0$. The ligand exchange happens over periods of time of a

few picoseconds. The 750 °C/2000 bar simulation presents a different result. Until 6.2 ps the complex had 5 ligands: three OH^- groups, one O^{2-} and one unstably bonded Cl^- (**Table 3.4**). At 6.2 ps the Cl^- broke away from the complex and at about the same time one of the OH^- lost its hydrogen resulting in a formation of a neutral tetrahedral species $[Mo(O)_2(OH)_2]^0$ that remained stable until the end of the simulation at 18.7 ps.

The next configuration studied, $[MoCl_2(H_2O)_4]^0$, underwent deprotonation of two out of its initial four water molecules, resulting in a (meta-)stable final configuration $[MoCl_2O_2(H_2O)_2]^0$ (**Fig. 3.2**). This is not the case for the same initial configuration at 350 °C/500 bar: under these conditions the final configuration $[MoCl_2O_2]^0$ shows some dynamic interaction with an extra water molecule. Throughout the length of the simulation this neutral tetrahedral complex gets loosely bonded to a water molecule forming a square pyramidal complex $[MoCl_2O_2]^0 \cdot H_2O$. The bond with the water molecule is very unstable and at time disappears entirely (for example between 12 and 14 picoseconds).

Initial configuration $[MoCl_3(H_2O)_3]^0$ is clearly unstable at ambient conditions (**Fig. 3.3**). The final configuration is a square pyramidal molybdenum-chloro-aqua-complex $[MoCl_2O_2(H_2O)]^0$ with one unstable Cl^- ligand. In the initial configuration $[MoCl_3(H_2O)_3]^0$ one water rapidly loses two hydrogens, forming $[MoCl_3O(H_2O)_2]^+$; after approximately 1 ps, the third chloride anion breaks off, and another water molecule loses its hydrogens, forming the final $[MoCl_2O_2(H_2O)]^0$ configuration. However, the third Cl^- remains in the solvation shell of the complex, bonding to the complex in the first shell for very short time intervals throughout the rest of the simulation; this Cl^- is also close to a bonding distance with Mo^{6+} during the last 2 ps, formally resulting in the formation of a charged complex $[MoCl_3O_2(H_2O)]^-$.

Higher P/T conditions of 350 °C/500 bar lead to a break-down of the initial octahedral geometry. At approximately 4.5 ps the pentahedral complex $[MoCl_3O_2]^-$ loses one chloride and forms a neutral $[MoCl_2O_2]^0 \cdot H_2O$, where one water molecule is weakly bonded for several picoseconds at a time (**Fig. 3.3-(b1)**). At 750 °C/2 kbar, the initial configuration rapidly forms a neutral tetrahedral molybdenum-chloro-oxo complex $[MoCl_2(O)_2]^0$. **Figure 3.3-(c1)** shows deprotonation of one water molecule at ~1 ps, which is indicated by the shortening of the bond distance between the respective oxygen anion and Mo^{6+} from approximately 2.5 Å to 1.7 Å. $[MoCl_2(O)_2]^0$ then remains stable for the remaining time of the simulation.

The most obvious change for the initial configuration $[MoCl_4(H_2O)_2]^0$ at 25 °C is deprotonation of its two water molecules which happens after less than 1 ps of the simulation (**Fig. 3.3**). Two out of four initial Cl^- ligands remain tightly bonded to Mo^{6+}, whereas the third Cl^- has a weaker bond with an average length of 2.569 Å (**Table 3.2** and **Fig. 3.3-(a)** for $MoCl_4(H_2O)_2$, yellow line in the graph). The forth Cl^- remains within 3.5 Å of Mo^{6+} for most of the simulation time, which is indicative of a weak bond. The blue line in the figure shows that it attaches to the complex for short periods of time, otherwise it remains in the solution in the proximity of the complex. The geometry changes to square pyramidal when the forth Cl^- is not bonded. Unlike the results at the ambient conditions, in the final configuration at 350 °C/500 bar all four chloride ligands are more stable, with shorter bond lengths (**Table 3.3**). The geometry changes between square pyramidal and octahedral as well, but at this temperature the sixth ligand is a weakly bonded water molecule. The picture changes at 750 °C/2 kbar, with the final configuration being a neutral, stable configuration with five ligands, $[MoCl_4O]^0$. Here, both the O^{2-} ligand as well as chloride ligands remain firmly bonded during the length of the simulation.

The last configuration studied is $[MoCl_5(H_2O)]^0$ (**Fig. 3.4**). $[MoCl_5O]^-$ is the final complex at both ambient conditions and at 350 °C/500 bar. The fifth Cl^- ligand is very unstable under both conditions, but it has a slightly shorter bond to Mo^{6+} at higher temperature and pressure. The bond length at 350 °C is 2.678 Å which indicates a more stable bond as opposed to 2.761 Å at 25 °C/1 bar. The only H_2O molecule undergoes deprotonation at the very beginning of both simulations and becomes a firmly bonded oxygen anion. High pressure and temperature conditions of 750 °C/2 kbar lead to the breakdown of the initial octahedral geometry to five-fold geometry with a ligand exchange taking place at about 6.3-6.5 ps. At 6.3 ps, the forth Cl^- ligand in $[MoCl_4O]^0$ breaks off and almost at the same time a water molecule bonds to the complex. After about 1 ps this molecule is exchanged by another water molecule (the orange line gets substituted by a blue line in **Fig.3.4-(c)**), which rapidly deprotonates and forms a stable O-Mo bond with the complex at 12 ps. Interestingly enough, at the same time one of the Cl^- ligands becomes unstable (the purple line in **Fig.3.4-(c)**). The simulation was not long enough to say with confidence whether the third Cl^- would remain bonded or if the charged, square pyramidal configuration $[MoCl_3(O)_2]^-$ would further break down to a tetrahedral complex.

Table 3.2 Initial & final geometrical properties for the simulations of Mo(VI)-Cl- H_2O complexes at 25 °C, 1 bar.

Job no.	Simulation time (ps)	Initial configuration	Final species	Mo-Cl			Mo-O			O-H		
					d (Å)	σ_{Cl} (Å)		*d* (Å)	σ_O (Å)		*d* (Å)	σ_H(Å)
1a	17,16	$[MoCl_6]^0$	$[MoCl_6]^0$	Cl(1)	2.346	0.068						
				Cl(2)	2.384	0.196						
				Cl(3)	2.343	0.067						
				Cl(4)	2.347	0.067						
				Cl(5)	2.357	0.077						
				Cl(6)	2.360	0.075						
1b	17,15	$[MoCl_5(H_2O)]^0$	$[MoCl_5O]^- \leftrightarrow [MoCl_4O]^0$	Cl(1)	2.366	0.063	O(1)	1.711	0.083			
				Cl(2)	2.761	0.233						
				Cl(3)	2.405	0.080						
				Cl(4)	2.360	0.060						
				Cl(5)	2.371	0.066						
1c	16,97	$[MoCl_4(H_2O)_2]^0$	$[MoCl_3O_2]^- \leftrightarrow [MoCl_4O_2]^{2-}$	Cl(1)	2.449	0.076	O(1)	1.721	0.040			
				Cl(2)	2.569	0.124	O(2)	1.752	0.009			
				Cl(3)	2.395	0.067						
				Cl(4)*								
1d	16,14	$[MoCl_3(H_2O)_3]^0$	$[MoCl_3O_2(H_2O)]^- \leftrightarrow [MoCl_2O_2(H_2O)]^0$	Cl(1)	3.727	0.708	O(1)	1.720	0.037			
				Cl(2)	2.429	0.094	O(2)	1.748	0.100			
				Cl(3)	2.350	0.058	O(3)	2.231	0.104	H(1)	1.018	0.033
										H(2)	1.015	0.035

*-unstable bond

Job no.	Simulation time (ps)	Initial configuration	Final species	Mo-Cl			Mo-O			O-H		
					d (Å)	σ_{Cl} (Å)		*d* (Å)	σ_{O} (Å)		*d* (Å)	σ_{H} (Å)
1e	17,38	$[MoCl_2(H_2O)_4]^0$	$[MoCl_2O_2(H_2O)_2]^0$	Cl(1)	2.387	0.059	O(1)	1.719	0.022			
				Cl(2)	2.377	0.053	O(2)	2.460	0.130	H(1)	1.004	0.029
										H(2)	1.005	0.031
							O(3)	1.736	0.025			
							O(4)	2.333	0.105	H(1)	1.003	0.028
										H(2)	1.004	0.025
1f	17,57	$[MoCl(H_2O)_5]^0$	$[MoClO_2OH(H_2O)_2]^0$	Cl(1)	2.452	0.074	O(1)	2.387	0.111	H(1)	0.995	0.032
										H(2)	1.004	0.031
							O(2)	2.389	0.160	H(1)	0.994	0.027
										H(2)	1.004	0.028
							O(3)	1.733	0.036			
							O(4)	1.740	0.047			
							O(5)	1.943	0.048	H(1)	1.008	0.029
1g	17,14	$[Mo(H_2O)_6]^0$	$[MoO_2(OH)(H_2O)_3]^+ \rightarrow [MoO_3(H_2O)_3]^0$				O(1)	1.744	0.043			
							O(2)	2.310	0.112	H(1)	1.014	0.036
										H(2)	0.996	0.028
							O(3)	2.353	0.103	H(1)	0.999	0.029
										H(2)	1.001	0.030
							O(4)	1.744	0.038			
							O(5)*	1.922-1.750	0.056-0.032	H(1)**	1.034	0.067
							O(6)	2.263	0.130	H(1)	1.025	0.113
										H(2)	1.004	0.028

*- deprotonation /change of bond length at 12 ps **- bonded until 12 ps.

Table 3.3 Initial & final geometrical properties for the simulations of Mo(VI)-Cl- H_2O complexes 350 °C, 500 bar.

Job no.	Simulation time (ps)	Initial configuration	Final species	Mo-Cl			Mo-O			O-H	
					d (Å)	σ_{Cl} (Å)		*d* (Å)	σ_O (Å)	*d* (Å)	σ_H(Å)
1a	16,88	$[MoCl_6]^0$	$[MoCl_6]^0$	Cl(1)	2.377	0.108					
				Cl(2)	2.370	0.094					
				Cl(3)	2.372	0.100					
				Cl(4)	2.373	0.109					
				Cl(5)	2.375	0.105					
				Cl(6)	2.380	0.106					
1b	16,94	$[MoCl_5(H_2O)]^0$	$[MoCl_5O]^- \leftrightarrow [MoCl_4O]^0$	Cl(1)	2.678	0.316	O(1)	1.747	0.144		
				Cl(2)	2.415	0.104					
				Cl(3)	2.408	0.116					
				Cl(4)	2.412	0.107					
				Cl(5)	2.401	0.094					
1c	17,08	$[MoCl_4(H_2O)_2]^0$	$[MoCl_4O]^0 \leftrightarrow [MoCl_4O]^0 \cdot H_2O$	Cl(1)	2.401	0.117	O(1)	1.710	0.083		
				Cl(2)	2.378	0.101	O(2)*				
				Cl(3)	2.382	0.090					
				Cl(4)	2.383	0.092					

*-loosely bonded water, see also Fig. 3.3.

Job no.	Simulation time (ps)	Initial configuration	Final species	Mo-Cl			Mo-O			O-H		
					d (Å)	σ_{Cl} (Å)		*d* (Å)	σ_O (Å)		*d* (Å)	σ_H(Å)
1d	17,13	$[MoCl_3(H_2O)_3]^0$	$[MoCl_3O_2]^- \rightarrow [MoCl_2O_2]^0 \cdot H_2O$	Cl(1)	2.550	1.893	O(1)	1.724	0.051			
				Cl(2)	2.353	0.102	O(2)	1.723	0.052			
				Cl(3)	2.353	0.092	O(3)*					
1e	16,82	$[MoCl_2(H_2O)_4]^0$	$[MoCl_2O_2]^0 \leftrightarrow [MoCl_2O_2]^0 \cdot H_2O$	Cl(1)	2.359	0.101	O(1)	1.724	0.050			
				Cl(2)	2.358	0.090	O(2)	1.720	0.039			
							O(3)**					
1f	16,81	$[MoCl(H_2O)_5]^0$	$[MoClO_3]^- \leftrightarrow [MoCl(OH)O_2]^0$	Cl(1)	2.340	0.075	O(1)	1.798	0.079	H(1)***	1.084	0.171
							O(2)	1.761	0.068	H(2)****	1.066	0.118
							O(3)	1.768	0.068			
1g	17,22	$[Mo(H_2O)_6]^0$	$[MoO_2(OH)_2]^0$				O(1)	1.743	0.048			
							O(2)	1.899	0.061	H(1)	1.024	0.064
							O(3)	1.741	0.044			
							O(4)	1.902	0.063	H(1)	1.024	0.102

*- loosely bonded water **- loosely bonded water *** -bonded from 3 to 10 ps **** -bonded from 14 to 16.8 ps

Table 3.4 Initial & final geometrical properties for the simulations of Mo(VI)-Cl- H_2O complexes at 750 °C, 2 kbar.

Job no.	Simulation time (ps)	Initial configuration	Final species		Mo-Cl			Mo-O		O-H	
					d (Å)	σ_{Cl} (Å)		*d* (Å)	σ_O (Å)	*d* (Å)	σ_H(Å)
1a	17,41	$[MoCl_6]^0$	$[MoCl_6]^0$	Cl(1)	2.388	0.121					
				Cl(2)	2.401	0.141					
				Cl(3)	2.396	0.140					
				Cl(4)	2.406	0.144					
				Cl(5)	2.392	0.131					
				Cl(6)	2.390	0.127					
1b	18,68	$[MoCl_5(H_2O)]^0$	$[MoCl_4O]^0 \rightarrow$ $[MoCl_3(O)_2]^-$		2.432	0.168	O(1)	1.707	0.037		
				Cl(1)*							
				Cl(2)	2.398	0.147	O(2)**	1.728	0.038		
				Cl(3)***	2.438	0.228					
				Cl(4)	2.399	0.196					
1c	18,89	$[MoCl_4(H_2O)_2]^0$	$[MoCl_4O]^0$	Cl(1)	2.383	0.137	O(1)	1.701	0.063		
				Cl(2)	2.415	0.172					
				Cl(3)	2.380	0.131					
				Cl(4)	2.372	0.118					
1d	18,64	$[MoCl_3(H_2O)_3]^0$	$[MoCl_2(O)_2]^0$	Cl(1)	2.325	0.105	O(1)	1.724	0.068		
				Cl(2)	2.327	0.107	O(2)	1.720	0.049		

*- bonded until 6.3 ps **- bonded from 11.7ps ***-becomes unstable after 12ps

Job no.	Simulation time (ps)	Initial configuration	Final species	Mo-Cl			Mo-O				O-H	
					d (Å)	σ_{Cl} (Å)		*d* (Å)	σ_O (Å)		*d* (Å)	σ_H (Å)
1e	18,48	$[MoCl_2(H_2O)_4]^0$	$[MoCl(OH)(O)_2]^0$	Cl(1)	2.3424	0.1100	O(1)	1.7313	0.0566			
							O(2)	1.9069	0.0657	H(1)	1.0103	0.0657
							O(3)	1.7243	0.0420			
1f	18,77	$[MoCl(H_2O)_5]^0$	$[MoCl(O)(OH)_3]^0 \rightarrow [MoO_2(OH)_2]^0$	Cl(1)*	2.5266	0.1884	O(1)	1.9387	0.0899	H(1)	0.9970	0.0429
							O(2)**	1.9267-1.7528	0.0841-0.0814	H(1)***	0.9980	0.0363
							O(3)	1.9333	0.0892	H(1)****	0.998-1.0069	0.0547-0.0583
							O(4)	1.7272	0.0531			
1g	17,60	$[Mo(H_2O)_6]^0$	$[MoO_2(OH)_2]^0$				O(1)	1.7385	0.0556			
							O(2)	1.9321	0.0951	H(1)	0.9980	0.0436
							O(3)	1.9266	0.0804	H(1)	1.0056	0.0621
							O(4)	1.7345	0.0504			

*-bonded until 7.5 ps **-deprotonation/change of bond length at 6.2ps ***- bonded until 6.2ps ****- hydrogen exchange at 7.2ps

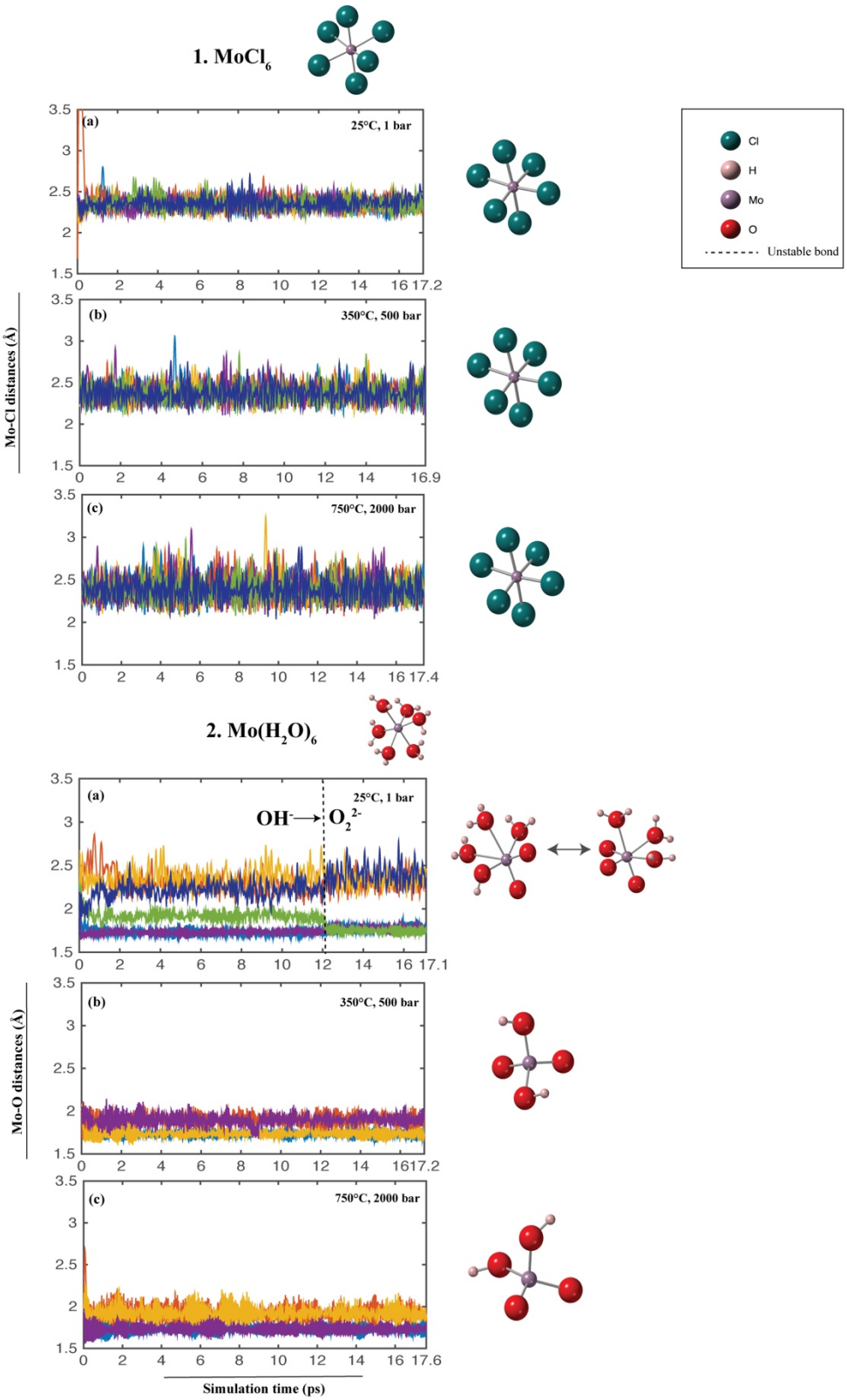

Figure 3.1 Graphic representation of the results of the simulations for $MoCl_6$ and $Mo(H_2O)_6$ complexes.

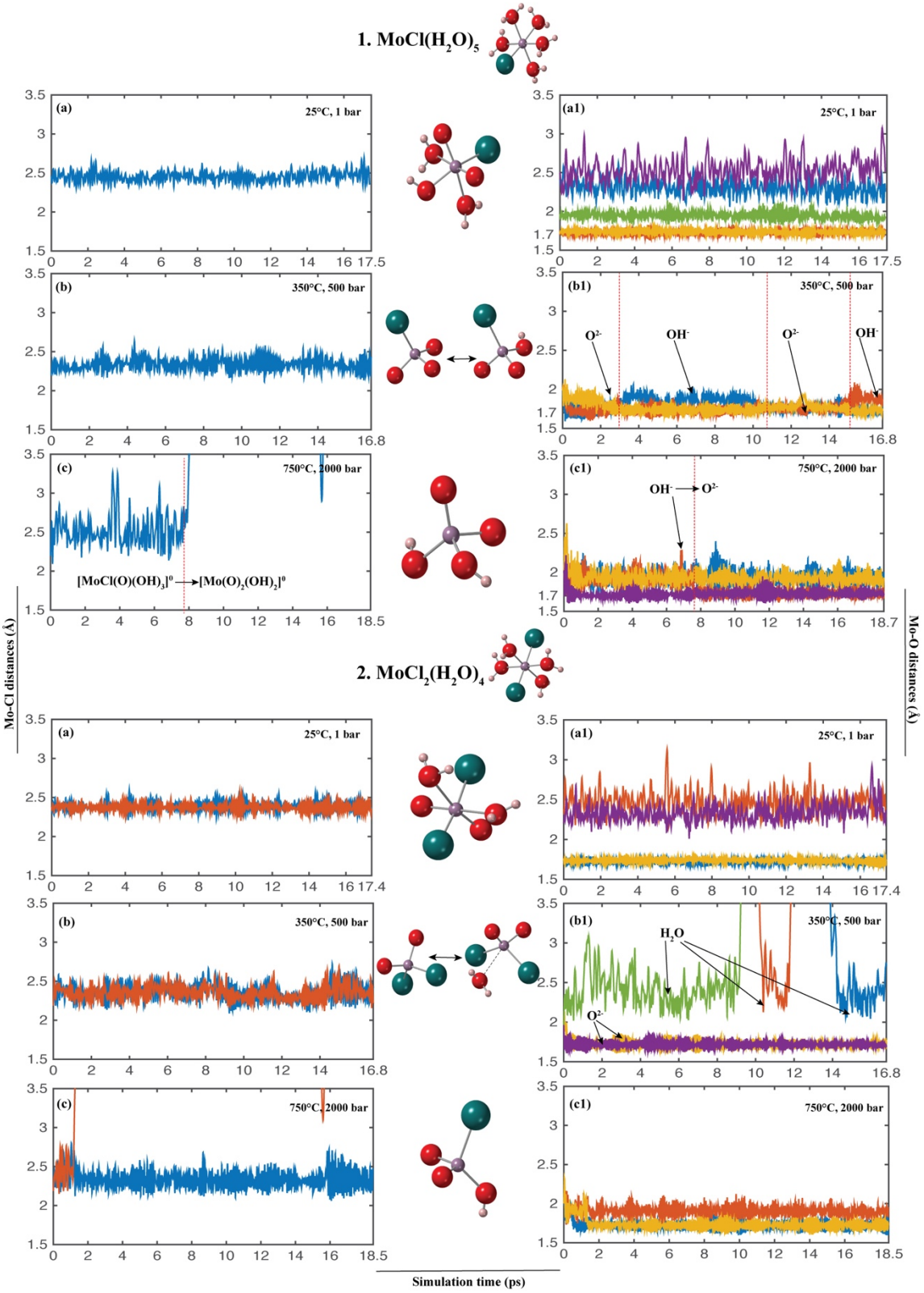

Figure 3.2 Graphic representation of the results for *ab initio* simulations for [$MoCl(H_2O)_5$] and [$MoCl_2(H_2O)_4$] complexes.

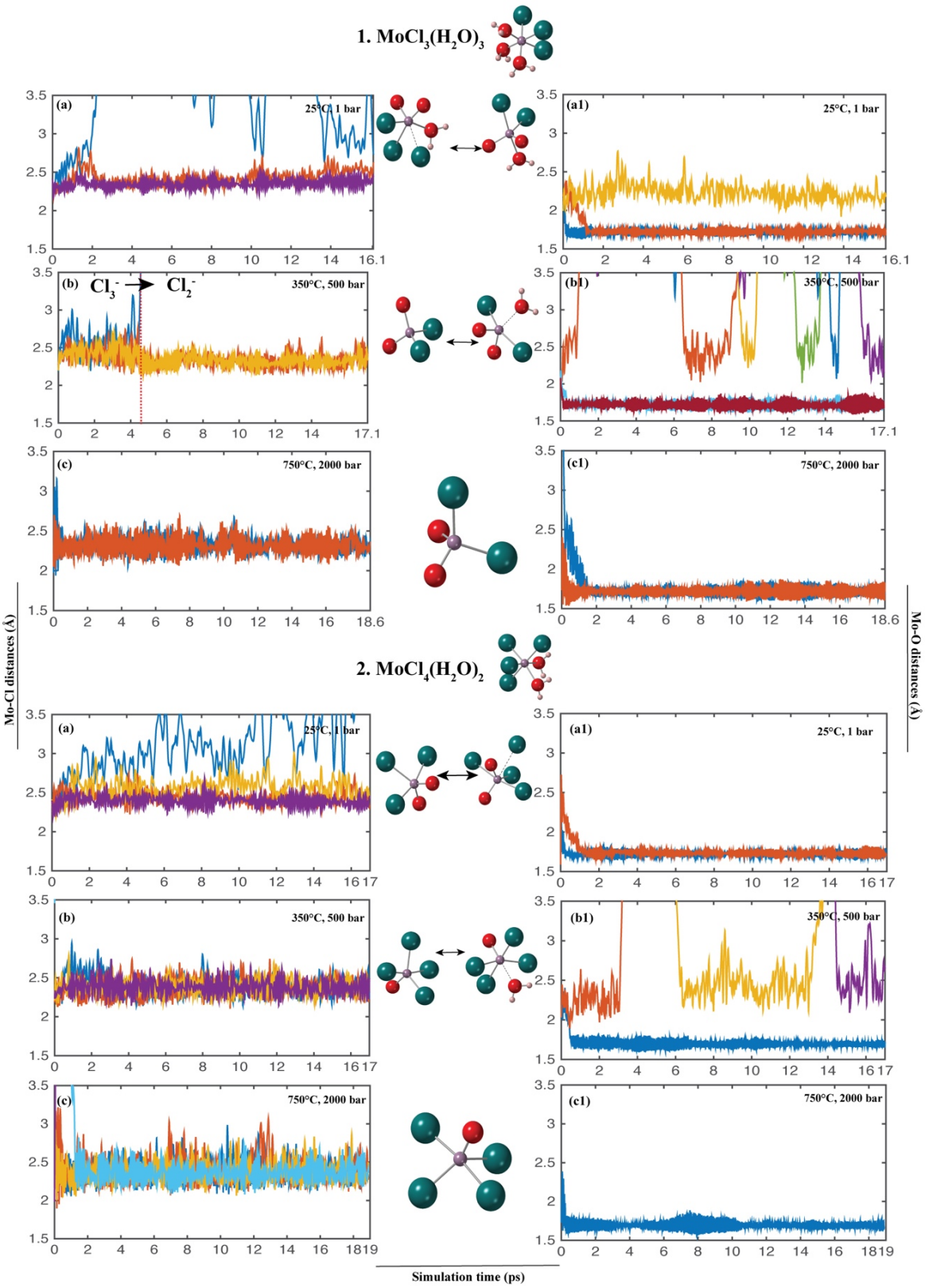

Figure 3.3 Graphic representation of the results for *ab initio* simulations for [$MoCl_3(H_2O)_3$] and [$Mo_4(H_2O)_2$] complexes.

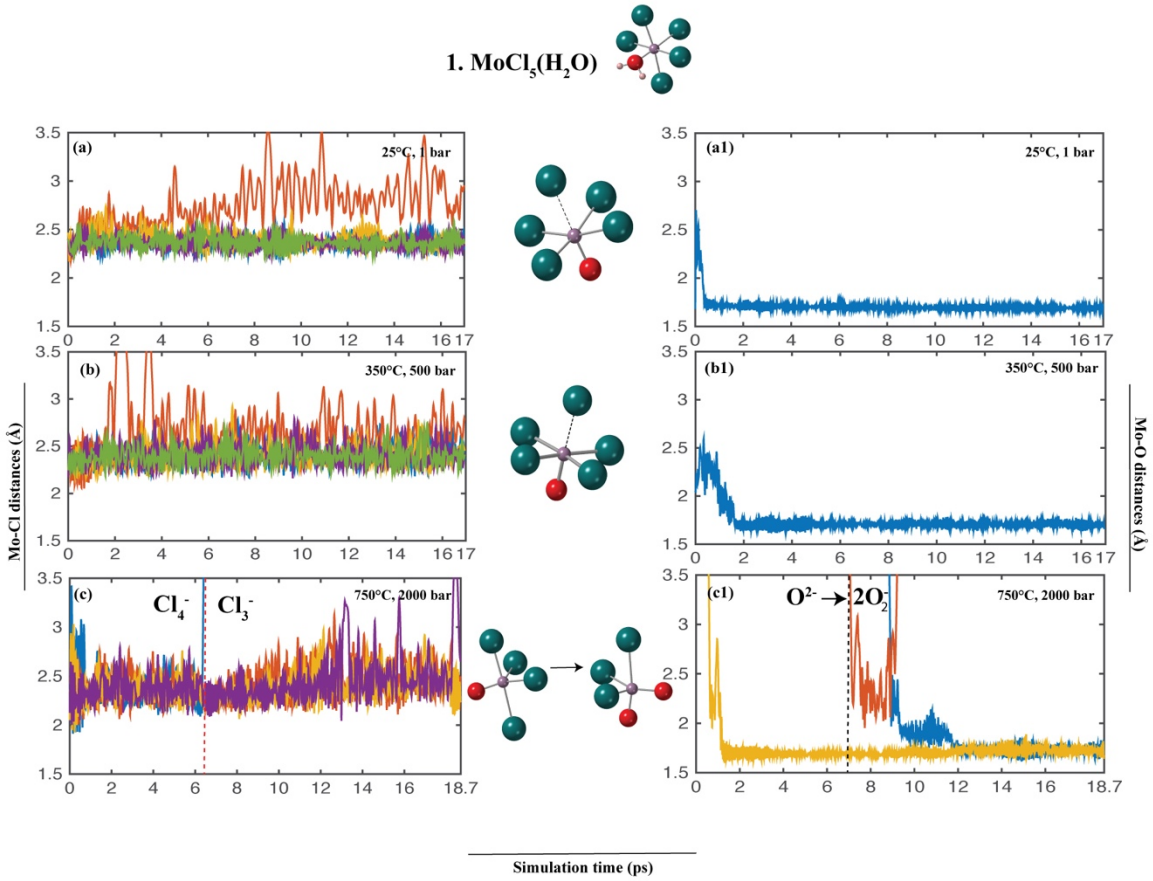

Figure 3.4 Graphic representation of the results for *ab initio* simulations for [$MoCl_5(H_2O)$] complexes.

3.4.2 Ab initio thermodynamic integration

In **Table 3.5** we can see that the shortest bond distance between Mo and the chloride anion is 2.33 Å. This bond length was chosen based on the results of *ab initio* MD. **Table 3.4** shows that the average length of a stable Mo-Cl bond at 750 °C/2 kbar is between 2.3 and 2.4 Å. At this distance the system is very close to a state of equilibrium, and the force is close to 0 (kJ $Å^{-1}$ mol^{-1}). This is presented in **Figure 3.5**, which also shows the geometrical configuration of the cluster during the simulation. The initial geometrical configuration has not changed. During the following simulations, the Cl^- was fixed farther and farther away from Mo^{6+}, which led to big changes in the magnitude of the force and consequently changes in the equilibrium of the system. With the increasing Mo-Cl distance, an external force must be applied in order to

maintain the bond length at a fixed value. This is due to the attraction force acting between Mo^{6+} and Cl^{-}.

Table 3.5 Constraint distances and results for the reaction $[MoO_2(OH)(Cl)]^0+H_2O = [MoO_2(OH)_2]^0+HCl$ at 750°C, 2 kbar. Detailed results for simulations (a)-(e) are presented in **Fig. 3.5**.

Simulation no	Simulation time (ps)	Constraint *d* Mo-Cl (Å)	Force (kJ $Å^{-1}$ mol^{-1})	Error
1(a)	9.3	2.33	-14.74	0.15
2	8.9	2.4	-85.77	0.15
3	8.9	2.47	-128.58	0.18
4	9.3	2.53	-141.73	0.18
5(b)	9.3	2.73	-169.76	0.19
6	9.3	2.93	-110.85	0.18
7(c)	8.6	3.1	-71.66	0.42
8(d)	9.2	3.2	41.39	0.25
9	8.9	3.3	62.37	0.24
10	8.8	3.5	52.68	0.27
11	8.8	3.7	44.17	0.27
12	8.8	3.9	25.40	0.26
13	8.7	4.1	19.63	0.27
14	10.1	4.3	14.86	0.25
15	8.8	4.7	6.24	0.32
16(e)	9.7	5.2	1.11	0.19

In **Figure 3.5-(a)**, this is reflected in the force curve going steeply down until it reaches its maximum absolute value of -169.76 kJ $Å^{-1}$ mol^{-1} at 2.73 Å. During this simulation, the initial configuration underwent several changes resulting in formation of new transitional complexes. A further increase in the Mo-Cl bond length leads to a decrease in the magnitude of the force, meaning that the attraction between Mo^{6+} and the chloride anion decreases. Nevertheless, the system is still quite far from the equilibrium state, and the initial configuration undergoes a couple of changes during the simulation at 3.1 Å (see (c) in **Fig. 3.5**). There is a big jump in

the absolute magnitude of the force (69.7299 kJ $Å^{-1}$ mol^{-1}), which happens during simulation (d) compared to simulation (c), although the difference in the bond length is only 0.1 Å. This energy change reflects that an abrupt change in the dynamics of the reaction takes place between these two points. Up until 3.1 Å, the behaviour of Cl^- was dominated by its attraction to Mo^{6+}, hence the negative magnitude of the force. Between 3.1 Å and 3.2 Å the barrier for ion exchange reaction gets activated and from 3.2 Å the effect of the outer solvation shell has a stronger influence on the chloride anion, which means that it is now more energetically preferable for Cl^- to stay in the solution as HCl than to form a bond with the Mo^{6+} complex. From this point and onwards, the magnitude of the force becomes positive. Although at 3.2 Å the equilibrium state is not yet reached, **Fig. 3.5** shows that the final complex at 3.2 Å is the same as at 5.2 Å. This confirms that the configuration on the right side of the reaction 3.1 is now stable.

Beyond the distance of 4.3 Å, the attraction between Mo^{6+} and Cl^- is negligible and the force curve flattens out until it reaches 0 kJ $Å^{-1}$ mol^{-1} for the last simulation with the Mo-Cl bond length of 5.2 Å. At this point, the formation of $[MoO_2(OH)_2]^0$ + HCl is strongly preferred.

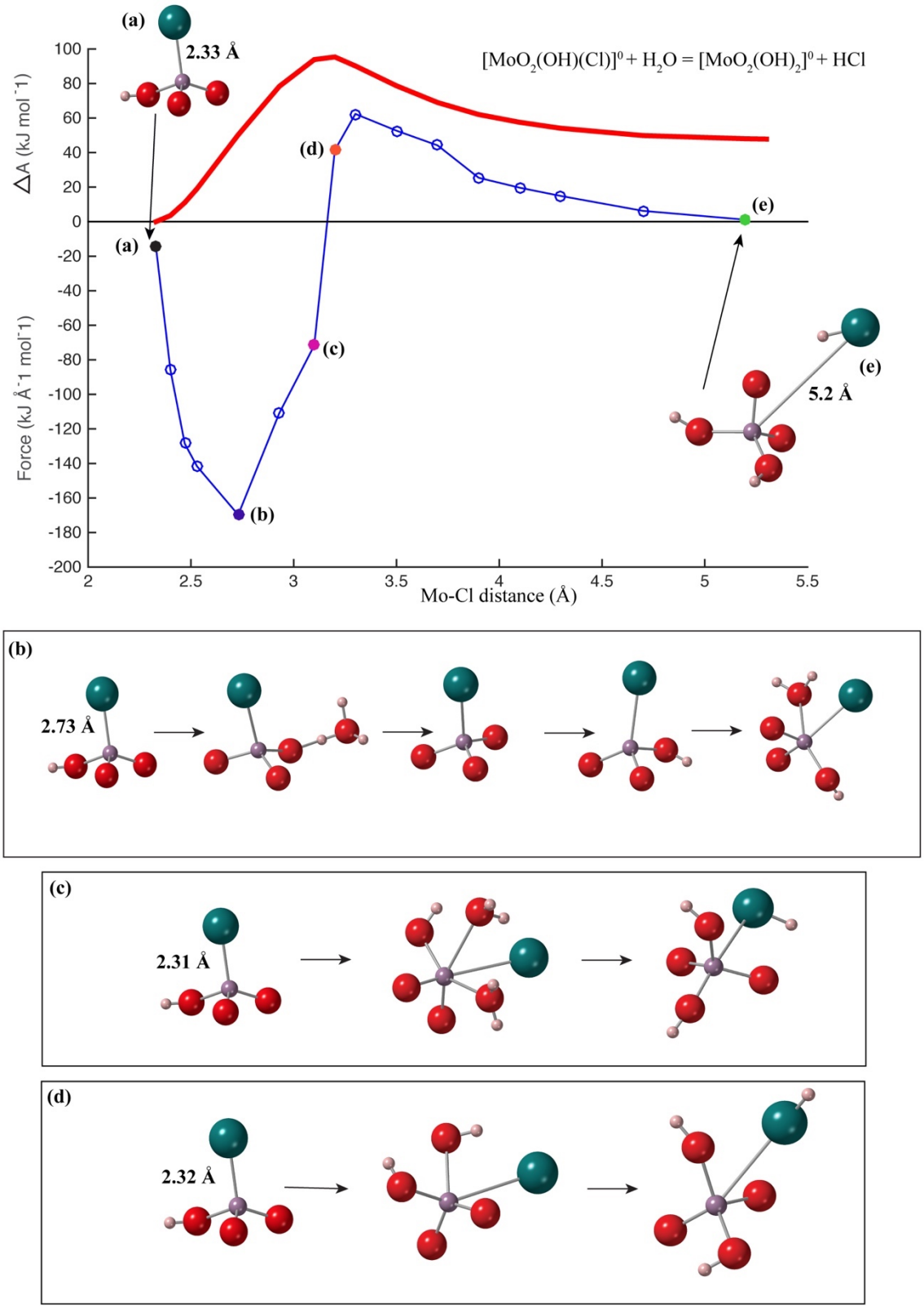

Figure 3.5 Graphic representation of the results for *ab initio* thermodynamic simulations at 750 °C, 2 kbar. The blue line represents the force, while the red line is the integral of the force. The circles on the blue line mark the magnitude of the force at different Mo-Cl bond distances. The colored circles (a-e) are the values of specific interest mentioned in the text.

The values and the shape of the force curve contain information about the dynamics of the stepwise ligand exchange reaction. But it is the change in free energy for the reaction 3.1 that determines which complex is energetically preferred. Helmholz free energy ($\Delta A_{a\rightarrow b}$) for reaction 3.1 was calculated by integration of the constraint mean force over the fixed lengths of the Mo-Cl bonds using **Eq 2.4**. According to **Eq 2.6,** we can safely assume that the value of the Gibbs free energy for the reaction 3.1 is a close approximation to the Helmholz free energy.

The shape of the integral curve reveals that the value of the free energy is 0 when the configuration $[MoO_2(OH)(Cl)^0$ is stable, and it is +47.827 kJ mol^{-1} when $[MoO_2(OH)_2]^0$ is stable. This means that $[MoO_2(OH)_2]^0$ has a much higher free energy and is therefore less energetically favorable.

Knowing the magnitude of change in the free energy, we can find the stability constant for the reaction 3.1. As we can see, there are no charged species on either side of the reaction, which means that $\ln K \cong \Delta G$ and there is no need to calculate the activity coefficient, so that we do not need to use **Eq 2.7** and **2.8.** Using **Eq 2.9**, we get:

$$\ln K = \frac{-\Delta G}{RT} = \frac{47827\ J\ mol^{-1}}{8.314\ J \times 1023\ K} = -5.62$$

$$\ln(10) = 2.302,\ \log K = \frac{-5.62}{2.30} = -2.44$$

As we can see, logK for the reaction 3.1 at 750 °C/2 kbar is -2.44. This value reflects a strong tendency of Cl^- to react with $[MoO_2(OH)_2]^0$ and form $[MoO_2(OH)Cl]^0$.

3.5 Discussion

It is important to emphasise that although there exists a number of experimental and theoretical studies on Mo-O-Cl complexation under hydrothermal conditions (see section 1.3 in this thesis), none of them used exactly the same conditions, initial speciation and method as the current study, hence all comparison / discussion with regards to the previous research is limited.

In the current study, all simulations at all P/T conditions were performed in 6 molal Cl^-. Borg et al. (2012) used similar conditions in their experiment. The relevant data from their study is presented in **Table 3.6**. However, while discussing the similarities & contradictions between the current computational study and the experimental data mentioned above, one has to be aware that there is a significant difference in the two approaches. The MD technique allows the initial configurations to be chosen with a great precision and document any changes to the complexes during the simulation. This is not the case when it comes to EXAFS experiments. In Borg et al.'s (2012) study, the solid $[Na_2MoO_4{\cdot}2H_2O]^0$ dissolved in water was used as the source of Mo(VI) with addition of NaCl and HCl. Then the *K*-edge XANES spectra for several Mo-O-Cl compounds were measured. The aqueous Mo(VI) species were determined on the basis of the energy of their spectra compared to previously acquired data.

Table 3.6 Summary of the refined EXAFS parameters for highly acidic solutions S9b and S11. *N*- number of ligands, *d*- bond length between Mo and ligand (from Borg et al. 2012)

Sample number	S11	S9b	S9b	S9b
Sample composition	0.23 m Na_2MoO_4; 4.3 m NaCl; 1.81 m HCl	0.23 m Na_2MoO_4; 6.21 m HCl	0.23 m Na_2MoO_4; 6.21 m HCl	0.23 m Na_2MoO_4; 6.21 m HCl
T °C/ P bar	340/600	25/600	166/600	340/600
N_O	1.2	2.3; 1.4	2.3; 1.6	1.1
N_{Cl}	4.6	1.3	2.1	5.1
$N_{\ tot\ ligands}$	5.8	4.6	6	6.2
$d_{Mo\text{-}O}$(Å)	1.650	1.698; 2.22	1.707; 2.25	1.647
$d_{Mo\text{-}Cl}$(Å)	2.391	2.41	2.41	2.39

The results of *ab initio* MD simulations (**Tables 3.2-3.4**) conducted at ambient conditions show slight changes to the initial configurations, where loss of hydrogens and/or release of the water molecules from the complex is the most noticeable process. All final configurations at these conditions are distorted octahedral or square pyramidal species, with 6 and 5 ligands respectively. The kinetics of the ligand exchange reactions at ambient conditions is expected to be slower than under higher P/T (e.g., Sharps, 1993) so this is quite reasonable that we could only observe minor changes to the initial complexes (at the same time it means that we may not observe the thermodynamically stable complexes either). However, the lengths of the Mo-O and Mo-Cl bonds derived from the MD runs are in a very good agreement with the experimental values of Borg et al. (2012) (**Table 3.6**) as well as other studies (e.g., Oyerinde

et al., 2007; Tossel 2005; Liu et al., 2013). One very important fact that has to be mentioned about the EXAFS experimental method is that it cannot detect hydrogen atoms, so if one of the ligands is OH^-, the measurements will only reveal the oxygen and the possibility of hydrogen atoms will be evaluated based on the Mo-O bond lengths and the shape of the observed spectra. **Table 3.6** shows that two different values for Mo-O bond distances were recorded in the experiment. *Ab initio* simulations can resolve such ambiguities in the final configurations including number of hydrogens which are elusive in experiments. The *ab initio* results show that the longest Mo-O bonds are between Mo and first shell H_2O. All bond lengths longer than 2 Å mean that the ligand is water; 1.8 Å- 2 Å tell us that Mo is bonded to an OH^- group, while bond lengths shorter than 1.8 Å (typically 1.6-1.75 Å) help identify the ligand as an oxygen anion.

Borg et al. (2012) suggest that the Mo speciation in their solution at room temperature was dominated by a mixture of octahedral complexes $[MoO_2Cl(H_2O)_3]^0$ and $[MoO_2Cl_2(H_2O)_2]^0$. This is confirmed by simulation 1e in the current study which resulted in a complex $[MoO_2Cl_2(H_2O)_2]^0$ and simulation 1f which has final configuration $[MoO_2Cl(OH)(H_2O)_2]^0$ (**Table 3.2**). As the temperature of the experiment increased first to 166 °C and then to 340 °C the authors report an increase in the number of chloride ligands (up to 5 at 340 °C) as well as loss of hydrogens by water molecules bonded with the complex. The latter trend is also evident from the MD simulations, however the picture is not very clear when it comes the effect of temperature on the number of Cl^- ligands (this will be discussed in the next paragraph). At 340 °C, Borg et al. (2012) suggested that the dominant species are most likely $[MoOCl_5]^-$. This species has been confirmed to exist as a metastable final configurations of simulation 1b (**Table 3.3**) together with $[MoCl_4O]^0$. The latter complex may have been detected in the experimental study as well, however it is less likely than the $[MoOCl_5]^-$ complex, according to their statistics.

The results for *ab initio* simulations at 750 °C/ 2 kbar offer an unprecedented insight into the behavior of Mo-O-Cl complexes at high P/T conditions. The tendency to form 4-fold complexes following dehydration / loss of hydrogens is even more evident at 750 °C/ 2 kbar than it was at 350 °C/ 500 bar. The same feature has been reported by several other authors working with transition metals, including Fe(II) (Testemale at el., 2009), Co(II)(Liu et al., 2011), Zn(II) (Mei et al., 2015).

The decrease of the dielectric constant of water (solvent) and ligand-field energy stabilization as a function of temperature has been suggested as the driving force behind the 6-fold to 4-fold change in geometry (e.g. Susak & Crerar, 1985). However, according to the current study, the tetrahedral complexes formed only for the initial configurations with the number of Cl^- ligands ≤ 3. For simulations 1a, 1b &1c, the final complexes were octahedral in case of 1a, and square pyramidal in case of 1b & 1c at both 350 °C/ 500 bar and 750 °C/ 2 kbar.

One possible explanation can be that it's more energetically demanding to break Mo-Cl bonds than Mo-O bonds. This can be explained by the results of *ab initio* MD thermodynamic integration performed at 750 °C/ 2 kbar in the current study. The log*K* value of the reaction $[MoO_2(OH)(Cl)]^0 + H_2O = [MoO_2(OH)_2]^0 + [HCl]^0$ is -2.44, which tells us th at the species on the right hand side is much more stable under given conditions than the species on the left hand side. This means that Mo- Cl complexation is more energetically favorable and hence these bonds are unlikely to break during an *ab initio* MD simulation. However, this suggestion is based on the observations of the results presented in this chapter, there is no available thermodynamic data to support this. Brugger et al. (2016) states that the common scientific view is that enthalpy (binding energy) is defining for the geometry of complexes. For some transition metals such as Ni^{2+} and Co^{2+} the extra energy of the 6-fold ligand field will be stabilizing thus making octahedral coordination preferable (Crerar et al., 1985). With increasing temperature, however, the effect of entropy can win over the enthalpy contribution to the free energy and lead to a change in coordination (e.g Crerar et al., 1985; Susak & Crerar, 1985; Sherman 2007;2010). Although in the current study neither enthalpy nor entropy effects have been investigated, judging from the observed trend that coordination changes depend on the nature of ligands, it is not unreasonable to assume that chloride ligands contribute to the stability of the 5- and 6- fold complexes to such an extent that it overcomes the effect of entropy even at high temperature (which is also evident from the thermodynamic integration calculation). Having said that, there is definitely a need for more in depth research of the exact mechanism of the coordination changes of Mo complexes and the effect of different ligands on this process.

The *ab initio* MD simulations in the current study give a direct insight into the structure of molybdic acid at highly acidic conditions. The results of simulation 1g (**Figure 3.1 (2)**) show

that at high P/T $[H_2MoO_4]^0$ exists as $[Mo(O)_2(OH)_2]^0$ which is in agreement with the theoretical study of Liu et al., (2013), while contradicting the conclusion of Tossel (2005), Ulrich & Mavrogenes (2008), Oyerinde et al. (2007) and Hurtig & Williams-Jones (2014a) who proposed $[MoO_3 \cdot nH_2O]^0$ as the true structure. This lack of agreement with several of the previous studies is not surprising given that the setup of a theoretical study (like mine and Liu et al. (2013)) is very different than experimental research. Tossel (2005) and Oyerinde et at. (2007) used DFT and a dielectric continuum method to model the solution, which can result in inaccurate predictions. Mei et al. (2013b) gives a comprehensive comparison of the two methods and examples of the differences in the results that they produce. When it comes to the studies of Ulrich & Mavrogenes (2008) and Hurtig & Williams-Jones (2014a), it is worth to mention that solubility experiments don't produce reliable stoichiometry data, and it is fairly difficult to compare to the results of these studies. The complex $[Mo(O)_2(OH)_2]^0$ was one of the species investigated by thermodynamic integration which has shown that it's less favourable than $[MoO_2(OH)(Cl)]^0$. The reason for why Mo-Cl complexation has not been observed is likely to be that ~ 17 ps of simulation time is not long enough for the ligand exchange to occur.

According to the *ab initio* simulations, several Mo-O-Cl species may be present in the solution under the same conditions. But it is unclear which of these species can exist/ co-exist in a natural hydrothermal fluid. It is important to remember that an *ab initi*o box, however sophisticated computational method it was generated by, is a very simplified model of a real solution and has several unavoidable limitations, such as a very short timeframe, exaggerated pH due to the small amount of atoms in the cell and an inability to model solutions with very low acidity (at least 1m of Cl^- , HS^- , OH^- (or any other ligand of interest) has to be added and at the same time it's not possible to add a lot of water to dilute the solutions, because even 100+ water molecules would make the simulation unreasonably slow and very expensive). So the simulations alone don't provide certain answers, but they do give a clear idea of which species can exist under given conditions. Combining the method with *ab initio* thermodynamic integration plus having a few experimental studies on the same species available, we can obtain important new data on speciation and thermodynamic properties of metal-ligand complexes under an unlimited range P/T conditions.

4 Mo(VI) speciation in hydrothermal S-bearing brines up to magmatic hydrothermal conditions (750 °C, 2 kbar)

4.1 Introduction

Molybdenite is the most common Mo-bearing phase that occurs naturally. It's appears in many different geological environments such as Mo- and Co-Mo porphyries, W-Mo quartz veins, skarns and uranium sandstones. Such a variety of hosting environments means that the mineral is found at temperatures encompassing almost the entire range of hydrothermal conditions, from less than 200 °C in sedimentary U-Mo deposits (Tugarinov et al., 1973) to over 600 °C in Mo-porphyry deposits (Hall et al., 1974; Bloom, 1981; White et al., 1981). This feature of molybdenite deposits makes it obvious that there is a need for more knowledge about the mobility of Mo in ore-forming fluids over a wide range of geochemical conditions. This information can be acquired by investigating the solubility of Mo-S species as a function of temperature, pressure, oxygen- and sulphur fugacity as well as fluid composition. In combination with the knowledge of Mo speciation under hydrothermal conditions it will bring about a broad understanding of the mechanisms of Mo transport and ore formation (Cao 1989).

The previously mentioned lack of investigation of Mo solubility and speciation in S-bearing fluids (see Section 1.3) had lead members of my research group to a decision to obtain new experimental data. As a result, a series of *in situ* XAS experiments was conducted in July 2018 at the European Synchrotron Research Facility in Grenoble, France. The collected data (see Appendix) show speciation of Mo-S-O species under different P/T and acidity conditions. The *ab initio* MD simulations in the current thesis were designed to cross-check these experimental results, and to extend the investigations of Mo speciation in sulphur-bearing fluids to higher temperature and pressure ranges relevant for the molybdenum ore formation, which are beyond the experimental capabilities.

4.2 Study scope

The aim of this work is to generate independent *ab initio* MD data which would:

1) serve to confirm the interpretation of the XAS data collected during the experiment in July 2018.
2) investigate the stability of the same species as in the experiment (the experimental data for 300 °C)
3) study the effects of concentration of HS^- on the behaviour of Mo-O-S species
4) document if there are any other configurations present than MoO_4^{2-} and MoS_4^{2-}, for example MoS_2 and $MoOS_3^{2-}$.
5) provide information on any configuration changes which may occur under different P/T conditions.

In addition, a series of three *ab initio* simulations will be conducted in order to gain preliminary insights into the stability of $[MoO_4]^{2-}$ under basic conditions in order to cross-check the experimental results.

4.3 Method

The general information about the methods and theory is presented in Chapter 2. The initial atomic configurations for the Mo-S complexes investigated in this study (**Table 4.1**) were generated by the classical MD code Moldy (Refson, 2001). Pair potentials for Mo-S and Mo-O interactions were modified from cluster calculations for Y-O and Y-Cl (Guan et al., 2019) and SPC/E model (Berendsen et al., 1987; Smith and Dang, 1994) was applied to describe water molecules. The previously mentioned CPMD code (Car & Parinello, 1985) was used to conduct the *ab initio* MD calculations. The simulations were run under constant pressure, temperature and with a constant composition (NVT-ensemble). The same parameters were used as for the Mo-Cl calculations in Chapter 3: BLYP pseudopotentials (Becke et al., 1988), LDA exchange-correlation functional (Lee, Yang and Parr, 1988) and a cutoff gradient of 80 Ry in order to minimize an unnecessary expansion of the wavefunction. Nosè thermostat within the CPMD code was applied to control the temperatures of both the electrons and the ions.

Because small systems like the ones investigated in this study are prone to significant surface effects, periodic boundary conditions were used in order to eliminate these. The densities of the systems were calculated by the SOWAT code, which implements the equation of state of NaCl-bearing solutions (Driesner, 2007; Driesner & Heinrich, 2007); the densities correspond to NaCl solutions with the same molality of HS^- in the simulations.

Eleven *ab initio* MD simulations with five different initial configurations were performed to investigate the speciation of Mo-S-O complexes at three P/T conditions of interest (**Table 4.1**). The choice of the P/T conditions was based on the unpublished experimental data collected by my research group in July 2018 (the data is presented in the Appendix). However, in these XAS experiments quality data could only be collected to 300 °C, and the only pressure investigated was 800 bar. Taking advantage of the *ab initio* methods and their lack of restrictions when it comes to P/T conditions, in this study it was decided to generate independent computational data for the P/T range that is representative of the natural processes leading to the formation of Mo porphyry deposits. All initial configurations are tetrahedral, i.e. Mo^{6+} ion has 4 ligands in the first coordination shell. The ligands are hydrosulphide anions, hydroxy groups and water molecules. All initial configurations carry a charge; thus it was necessary to bring the simulation cell to neutrality by adding free ions to the solution – HS^-, OH^- and Na^+.

The initial configuration 1a & 1c are identical while 1b & 1d (**Table 4.1**) are very similar with H_2O being substituted by OH^- in 1d and a different charge of the initial species. However, the molar concentration, density (as well as the size of the simulation box) and number of atoms are different. The amount of hydrosulfide in simulations 1a and 1b is equivalent to 6 m HS^-. Simulations 1c and 1d represent more diluted fluids. A lower HS^- concentration was achieved by substituting free hydrosulphide anions with hydroxy groups as well as an addition of 45 water molecules. One kilogram of H_2O is equivalent to 55.51 moles of H_2O, so simulation cell 1c with a 100 moles of water and 4 moles of HS^- has an HS^- concentration of 2.2 m. Respectively, simulation 1d with 2 moles of HS^- has 1.1 m HS^-. These two simulations were only performed at 350 °C/ 800 bar.

Table 4.1 Simulation setup for molybdenum oxo-sulphur complexes

Job no.	Simulation cell content (number of atoms)	Initial configuration & Solution Composition	T (°C)	P (bar)
1a	1 Mo, 6 S, 55 O, 116 H	$[Mo(HS^-)_4]^{2+}$ + 2(HS^-) +55 H_2O	350	800
			500	800
			750	2000
1b	1 Mo, 6 S, 55 O, 116H	$[Mo(HS^-)_2(H_2O)_2]^{4+}$ + 4(HS^-) +53 H_2O	350	800
			500	800
			750	2000
1c	1 Mo, 4 S, 102 O, 206 H	$[Mo(HS^-)_4]^{2+}$ + 2(OH^-) +100 H_2O	350	800
1d	1 Mo, 2 S, 104 O, 206 H	$[Mo(HS^-)_2(OH^-)_2]^{2+}$ + 2(OH^-) +100 H_2O	350	800
1e	1 Mo, 3 Na, 60 O, 111H	$[MoO_4]^{2-}$ +3(Na^+) +1(OH^-) + 55 H_2O	350	800
			500	800
			750	2000

The importance of $[MoO_4]^{2-}$ is evident from the studies of Oyerinde et al. (2007), Minubayeva & Seward (2010) and Borg et al. (2012). Although this configuration could have been presented in Chapter 3, alongside the $[Mo(H_2O)_6]^0$, it was chosen to include it in this chapter because the formation of S-bearing complexes involves substitution of oxygen by sulphur in tetrahedral $[MoO_4]^{2-}$.

The cells in simulations 1c and 1d contain 313 atoms, which made the simulations very slow and very expensive. Simulation 1c consumed 31680 CPU hours and cost $12672, while 1d used 34560 CPU hours, $13824. These are important numbers to consider when planning to generate new *ab initio data* in order to avoid waste of recourses.

4.4 Results

Detailed results are presented in **Tables 4.2-4.4** and **Figures 4.1-4.3.**

Three *ab initio* MD simulations with the initial configuration $[Mo(HS^-)_4]^{2+}$ and 6 m HS^- showed that complexation between Mo and O did not occur at any stage under any of the three P/T conditions investigated at such a high HS^- concentration. At 350 °C/800 bar, Mo^{6+} bonded with five ligands, thus forming a $[Mo(HS)_3S_2]^-$ complex with a square pyramidal geometry;

this configuration formed at 0.5 ps and remained the same to the end of the simulation. Three of the ligands are hydrosulphide groups and have longer bond lengths with Mo than the two S^{2-} ligands (**Table 4.2 & Figure 4.1**). The same $[Mo(HS^-)_4]^{2+}$ initial configuration remained tetrahedral at the same pressure but at a higher temperature of 500 °C. The only change after over 17 ps of simulation is the deprotonation of three hydrosulphide ligands, with $[Mo(HS^-)S_3]^-$ being the final species from 8 ps onwards. The same is true for 750 °C/2 kbar , except for that in the resulting tetrahedral configuration two of the initial ligands underwent loss of hydrogens, to form $[Mo(HS^-)_2S_2]^0$ (**Figure 4.1 (2)**).

The second complex investigated in the 6 m HS^- solution, $[Mo(HS^-)_2(H_2O)_2]^{4+}$, exhibits more changes. In fact, the two waters in the initial configuration got replaced by two sulphur ligands in the very beginning of each simulation at all three P/T conditions. The final complex remained tetrahedral, with three S^{2-} ligands and one hydrosulphide group at 350 and 500 °C /800 bar ($[Mo(HS^-)S_3]^-$), and two HS^- and two S^{2-} at 750 °C and 2 kbar ($[Mo(HS^-)_2S_2]^0$.

Lowering the HS^- concentration to 2.2 m clearly affected the course of simulation 1c for the $[Mo(HS^-)_4]^{2+}$ complex. **Figure 4.2** shows that complexation with an oxygen anion happened at about 2 ps as well as there is a water molecule present in the second shell from 2 to 12 ps. The initial tetrahedral configuration became square pyramidal when an oxygen bonded with the complex, but at 12 ps one hydrosulphide ligand broke off and the final configuration is 4-fold $[MoS_3O]^{2-}$. One unexpected feature of this complex is that the bond length Mo-O is 2.034 Å, which is longer than Mo-OH bonds in simulation 1d and Mo-O bonds in 1e.

Table 4.2 Initial & final geometrical properties for the simulations of Mo(VI)-S- H_2O complexes at 350 °C, 800 bar.

Job no.	Sim. time (ps)	Initial configuration	Final species	Mo-S			S-H			Mo-O			O-H		
					d (Å)	σ_S (Å)		*d* (Å)	σ_H (Å)	*d*(Å)	σ_O(Å		*d*(Å)	σ_H(Å)	
1a	17,48	$[Mo(HS^-)_4]^{2+}$	$[Mo(SH^-)_3(S^{2-})_2]^-$	S(1)	2.161	0.061									
		+2HS^-		S(2)	2.285	0.161	H(1)*	1.364	0.0392						
				S(3)	2.509	0.143	H(1)	1.361	0.0329						
				S(4)	2.506	0.125	H(1)	1.364	0.0431						
				S(5)	2.463	0.111	H(1)	1.361	0.0253						
1b	17,88	$[Mo(HS^-)_2(H_2O)_2]^{4+}$	$[Mo(SH^-)_2(S^{2-})_2]^0 \rightarrow Mo(SH^-)(S^{2-})_3]^-$	S(1)	2.162	0.066									
		+4HS^-		S(2)	2.326	0.101	H(1)**	1.371	0.052						
				S(3)	2.381	0.091	H(1)	1.372	0.051						
				S(4)	2.160	0.070									
1c	15,7	$[Mo(HS^-)_4]^{2+}$	$[Mo(S^{2-})_2(HS^-)_2(O^{2-})]^{2-} \cdot H_2O \rightarrow [Mo(O^{2-})(S^{2-})_3]^{2-}$	S(1)	2.213					O(1)***	2.034				
		+2OH^-		S(2)	2.412		H(1)##	1.362		O(2)****					
				S(3)#	2.478		H(1)	1.363							
				(S4)	2.181										
1d	17,4	$[Mo(HS^-)_2(OH^-)_2]^{2+}$	$[Mo(HS^-)_2(OH^-)_2]^{2+} \cdot H_2O$	S(1)	2.341	0.095	H(1)	1.377	0.042	O(1)	1.914	0.062	H(1)	0.998	0.036
		+2OH^-		S(2)	2.344	0.095	H(2)	1.373	0.02	O(2)	1.902	0.072	H(1)	1.001	0.040
										O(3)*****					
1e	18,86	$[MoO_4]^{2-}$	$[MoO_4]^{2-}$							O(1)	1.814	0.043			
										O(2)	1.809	0.048			
										O(3)	1.810	0.048			
										O(4)	1.810	0.052			

*- bonded until 7 ps **-bonded until 14ps ***- from 2.5 ps ****- loosely bonded water 2-12 ps water *****- loosely bonded water 9.8-11.2 ps #- until 12 ps ## -goes away at 12 ps

Table 4.3 Initial & final geometrical properties for the simulations of Mo(VI)-S- H_2O complexes at 500 °C, 800bar.

Job no.	Sim. time (ps)	Initial configuration	Final species	Mo-S			S-H			Mo-O			O-H	
					d (Å)	σ_S (Å)		*d* (Å)	σ_H (Å)		*d* (Å)	σ_O(Å)	*d* (Å)	σ_H(Å)
1a	17,41	$[Mo(HS^-)_4]^{2+}$ +2HS^-	$[Mo(SH^-)(S^{2-})_3]^-$	S(1)	2.405	0.098	H(1)	1.370	0.054					
				S(2)	2.175	0.061								
				S(3)	2.276	0.116	H(1)*	1.376	0.063					
				S(4)	2.170	0.059								
1b	17,41	$[Mo(HS^-)_2(H_2O)_2]^{4+}$ +4HS^-	$[Mo(SH^-)(S^{2-})_3]^-$	S(1)	2.195	0.091								
				S(2)	2.198	0.092								
				S(3)	2.241	0.106	H(1)**	1.392	0.099					
				S(4)	2.429	0.161	H(1)	1.374	0.066					
1e	18,81	$[MoO_4]^{2-}$	$[MoO_4]^{2-}$							O(1)	1.813	0.053		
										O(2)	1.816	0.058		
										O(3)	1.812	0.055		
										O(4)	1.814	0.059		

* - bonded until 8 ps **- bonded until 4.2 ps

Table 4.4 Initial & final geometrical properties for the simulations of Mo(VI)-S- H_2O complexes at 750 °C, 2 kbar.

Job no.	Sim. time (ps)	Initial configuration	Final species	Mo-S			S-H			Mo-O			O-H	
					d (Å)	σ_S (Å)		*d* (Å)	σ_H (Å)		*d* (Å)	σ_O(Å)	*d* (Å)	σ_H(Å)
1a	17,41	$[Mo(HS^-)_4]^{2+}$ +2HS^-	$[Mo(SH^-)_2(S^{2-})_2]^0$	S(1)	2.160	0.080								
				S(2)	2.385	0.102	H(1)	1.384	0.082					
				S(3)	2.164	0.088								
				S(4)	2.391	0.119	H(1)	1.3836	0.086					
1b	17,38	$[Mo(HS^-)_2(H_2O)_2]^{4+}$ +4HS^-	$[Mo(SH^-)_2(S^{2-})_2]^0$	S(1)	2.385	0.107	H(1)	1.370	0.042					
				S(2)	2.185	0.109	H(1)*	1.374	0.031					
				S(3)	2.164	0.089								
				S(4)	2.376	0.143	H(1)**	1.378	0.072					
1e	17,15	$[MoO_4]^{2-}$	$[MoO_4]^{2-}$							O(1)	1.833	0.090		
										O(2)	1.813	0.059		
										O(3)	1.813	0.061		
										O(4)	1.814	0.063		

* - bonded until 2.2 ps **-bonded after 2.3 ps

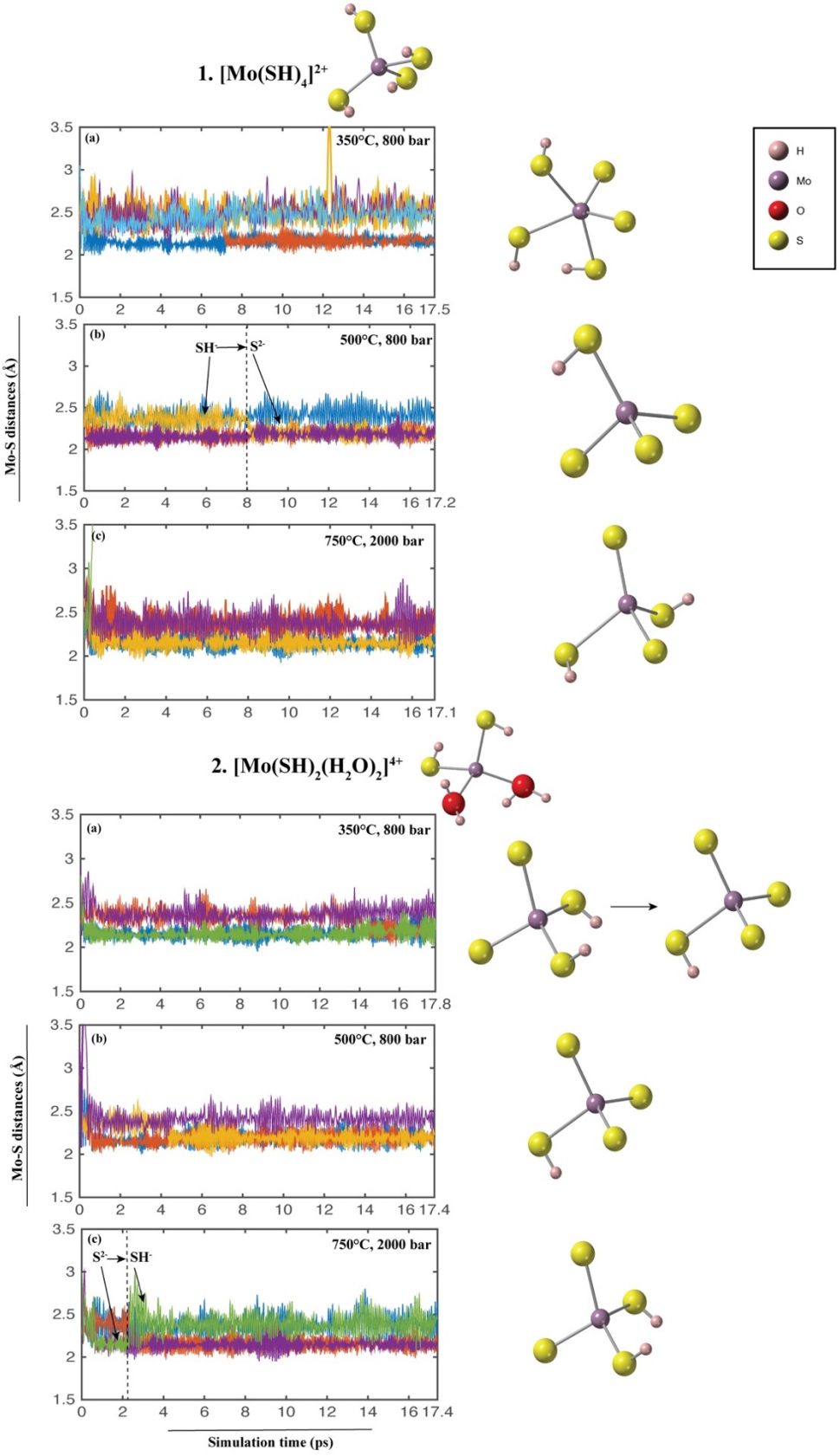

Figure 4.1 Graphic representation of the results of the simulations for $[Mo(HS^-)_4]^{2+}$ and $[Mo(HS^-)_2(H_2O)_2]^{4+}$, 6 m HS^-.

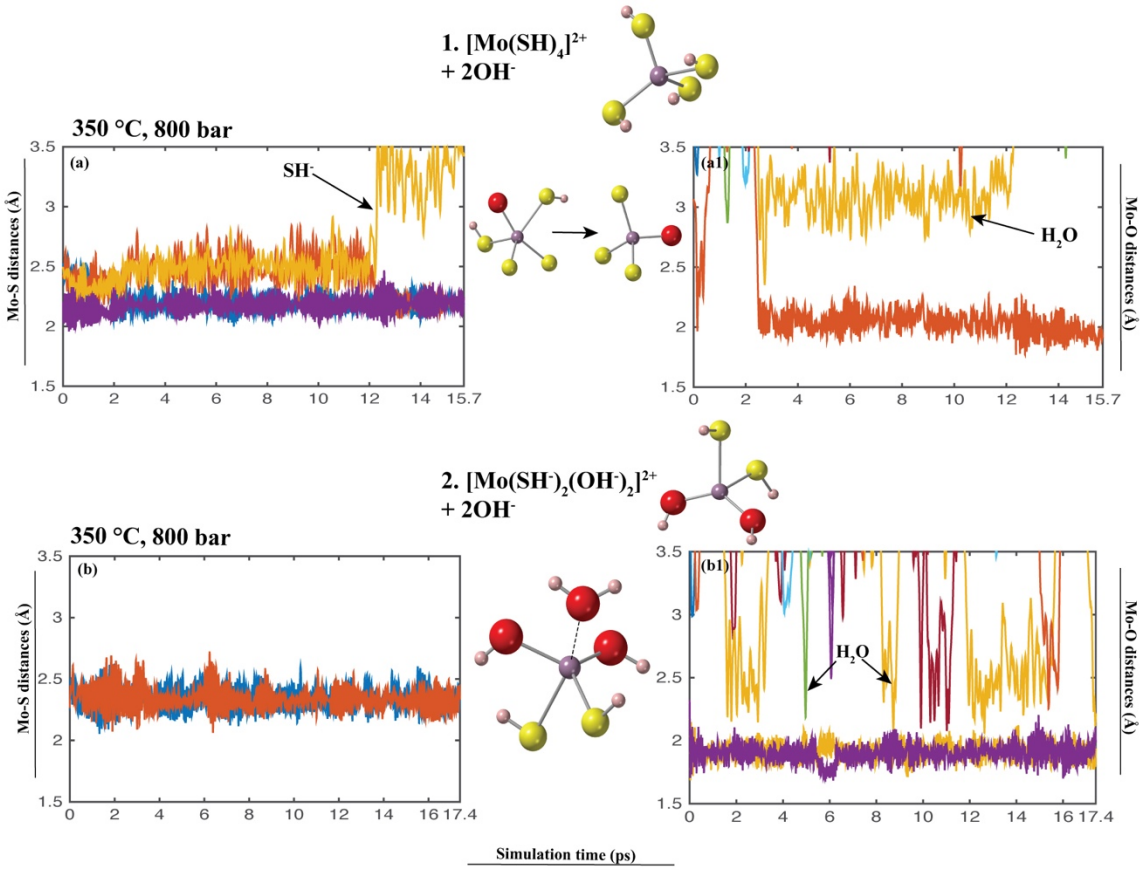

Figure 4.2 Graphic representation of the results of the simulations for $[Mo(HS^-)_4]^{2+}$ (2.2 m HS^-) and $[Mo(HS^-)_2(OH^-_2]^{2+}$ complexes (1.1 m HS^-).

An even lower HS^- concentration for the initial configuration $[Mo(HS^-)_2(OH^-)_2]^{2+}$, 1.1 m of hydrosulphide in the simulation cell 1d, confirms that a decreased HS^- makes Mo-O complexation more favourable compared to simulation 1b. The only change which happens during this simulation is an addition of a loosely bonded second shell water, resulting in the final configuration $[Mo(HS)_2(OH)_2]^{2+} \cdot H_2O$

When it comes to simulation 1e for complex $[MoO_4]^{2-}$, the initial configuration remained unchanged during all three runs at three different P/T conditions (**Figure 4.3**). The bond lengths Mo-O are stable and very similar at all temperatures.

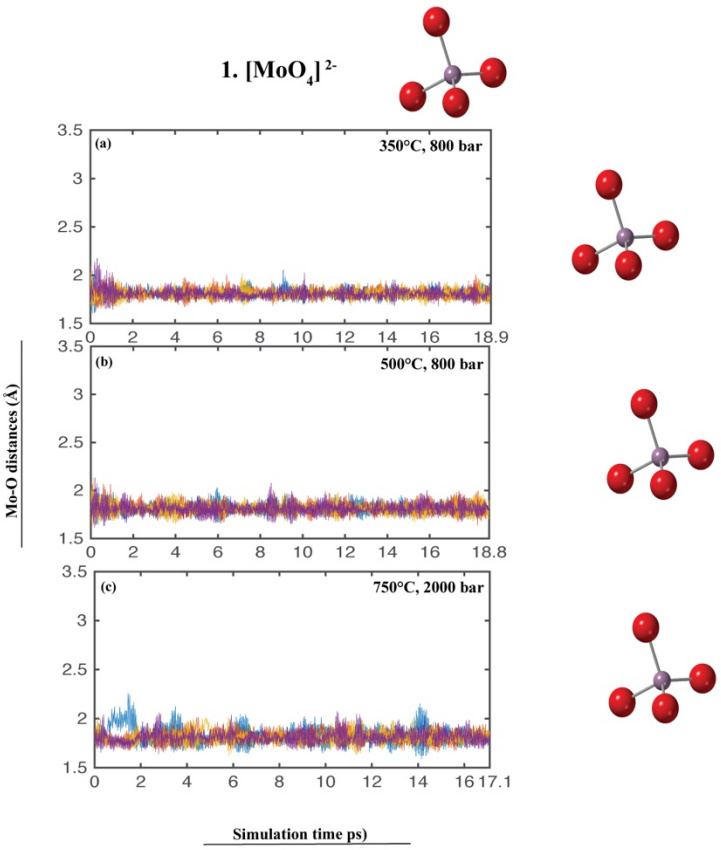

Figure 4.3 Graphic representation of the results of the simulations for $[MoO_4]^{2-}$.

4.5 Discussion

Simulation 1a with the initial configuration $[Mo(HS^-)_4]^{2+}$ and an HS^- concentration of 6 m showed very few changes at the two highest P/T conditions investigated, except for the loss of hydrogens has been detected, which lead to a change of charge at both conditions. However, at 350 °C/ 800 kbar, a fifth ligand bonded with the complex, thus forming a square pyramidal configuration $[Mo(SH^-)_3(S^{2-})_2]^-$ which remained stable during the length of the simulation. Pentahedral Mo-O-S complexes have formed also during simulations 1c and 1d, however these were metastable. It is interesting to note that 5-fold geometry appeared only at at 350 °C/ 800 kbar, not at the higher P/T conditions. The results of *ab initio* simulations for Mo-Cl complexes in Chapter 4 have shown that Mo can have both five and six ligands even at high P/T conditions. However additional research on the energetics behind the formation and stability of such configurations is needed in order to provide a theoretical explanation for this observation.

The complexation between Mo-S and oxygen did not occur in simulations 1a and 1b at any P/T conditions. Moreover, the two water ligands in the initial configuration $[Mo(HS^-)_2(H_2O)_2]^{4+}$ (**Fig. 4.1**) detached from the complex in the very beginning, and were replaced by sulphur and / or hydrosulphide ligands, indicating a strong preference for formation of Mo-S bonds at these conditions. This observation is in a good agreement with the experimental data where it has been noted that the higher the HS^- concentration, the more formation of Mo-S bonds is favoured. The highest concentration used in the experiment was 2 m HS^-, so it is not unreasonable to assume that this trend would be even more pronounced with 6 m HS^- in the simulation box. Bostick et al. (2003) also reported that MoO_4^{2-} goes over to MoS_4^{2-} with the increase in sulphur concentration, however their X-ray Absorption Spectroscopy experiment was performed at ambient conditions and the concentrations of HS^- were very low.

The effect of HS^- on the speciation is obvious when we compare results of simulation 1a and 1c, where the same initial configuration $[Mo(HS^-)_4]^{2+}$ was subjected to different concentration of hydrosulphide. Lowering HS^- concentration to 2.2 made it possible for hydrosulphide anion to become replaced by an oxygen anion at the very beginning of the simulation 1c. The same observation applies to simulations 1b and 1d. The concentration of HS^- in 1d is 1.1 m , and the initial configuration $[Mo(HS^-)_2(OH^-)_2]^{2+}$ retained both OH^- groups as well as attracted a second shell water.

Table 4.5 Results of the experimental data and *ab initio* MD simulations performed under similar conditions.

Conditions	Experiment	*ab initio* MD	Experiment	*ab initio* MD
	Sol 5	1 d	Sol 6	1c
m HS^-	1.1	1.1	2	2.2
T (°C)/P (bar)	300/800	350/800	300/800	350/800
N_O	2.0	2	1.3	1
N_S	2.0	2	1.9	3
$N_{tot\ ligands}$	4	4	3.2	4
$d_{Mo\text{-}O}$(Å)	1.73	1.902;1.914	1.72	2.034
$d_{Mo\text{-}S}$ (Å)	2.25	2.341;2.344	2.22	2.213;2.412;2.181

Table 4.5 compares the results of *ab initio* MD simulations 1d and 1c with the results of the EXAFS refinement of the experimental solutions with similar P-T condition and HS^- concentrations. There is a very good agreement between the experimentally derived number of

ligands and Mo-S bond lengths with the MD values. The Mo-O bond distances derived from the MD simulations are about 0.2-0.3 Å longer than experimental values. Similar longer MD bond distances have been obtained by previous studies (Liu et al., 2017).

The simulations offer a more detailed information about the bond length. In case of simulation 1d, it also shows clearly that all four ligands are bonded to a hydrogen (**Fig. 4.2 (2) & Table 4.2**), plus that there is a second shell water present in the vicinity of the complex. The XAS results don't provide such details and this fact illustrates the importance of the *ab initio* MD method when it comes to interpretation and extrapolation of experimental data.

The second pair of data compared in the **Table 4.5**, Sol 6 and simulation 1c with ~2 m HS^- shows some discrepancies when it comes to the number of ligands. According to the experiment, solutions containing high concentration of HS^-, like Sol 6 will experience a reduction in the number of ligands with increasing T (note, 300 ^oC is the highest temperature of the experiment, while 350 ^oC was the lowest temperature in the computational study). The observed coordination in Sol 6 was 3 ligands, according to the experiments. This has not been seen in simulation 1c, which resulted in a tetrahedral thiomolybdate species $[Mo(O^{2-})(S^{2-})_3]^{2-}$. However, the timeframe of simulations is not long enough to enable us to draw definite conclusions about the stability of the investigated species.

The earlier studies have proposed that the molybdate anion, $[MoO_4]^{2-}$ is one of the most significant molybdenum species in geological environments. In relation to low P/T environments, the molybdate anion is important because it is the starting point for a series of reactions leading to its conversion to tetrathiomolybdate, a process which is believed to take place in anoxic/euxinic environments (Dahl et al., 2013; Bostick et al., 2003; Erickson & Helz, 2000). When it comes to hydrothermal conditions, the complex is believed to predominate in high-density crustal fluids under neutral and basic conditions, according to Minubayeva & Seward (2010). Simulation 1e (**Fig. 4.3**), which investigated the stability of the molybdate anion at three different P/T conditions, revealed no changes to the initial configuration, which may serve as an indicator of the stability of this species at the given conditions, thus confirming the experimental data mentioned above.

The presence of charged species has been observed under all investigated conditions (also for the Mo-O-Cl species in Chapter 3). According to the equation in the DEW model (Sverjensky et al., 2014), at room temperature, the dielectric constant of water is very high, 78, which means that water is a polar solvent. At 750 °C, this constant is only 10, which means that is can still carry some charged species although its properties as a solvent are greatly reduced.

To sum this up, the data obtained from MD simulations in this study is in a very good agreement with the XAS data collected in July 2018 (**see Table 4.5**), however the MD data offer more detailed information about bond lengths and the nature of the ligands (see **Figure 4.1-4.3** & **Table 4.2-4.4**) as well as expand the range of investigated P/T conditions. The computational results confirm that hydrosulphide concentration has an effect on the stability and nature of the Mo-O-S complexes, where lower HS^- concentration (2.2 and 1.1 m) makes it possible to form Mo-O bonds, which was not observed at high HS^- concentration (6 m).

5 Geological implications

Figure 5.1 presents the predominance fields of the molybdate species as a function of T and pH along with the sulphidic species and a quartz-muscovite-K-feldspar buffer which are important in relation to hydrothermal fluids. It was generated using the thermodynamic data from Minubayeva & Seward (2010) and The Geochemist Workbench software (Bethke, 2008). The dependence of each plotted reaction upon T and pH was calculated using HCh package (Shvarov & Bastrakov, 1999).

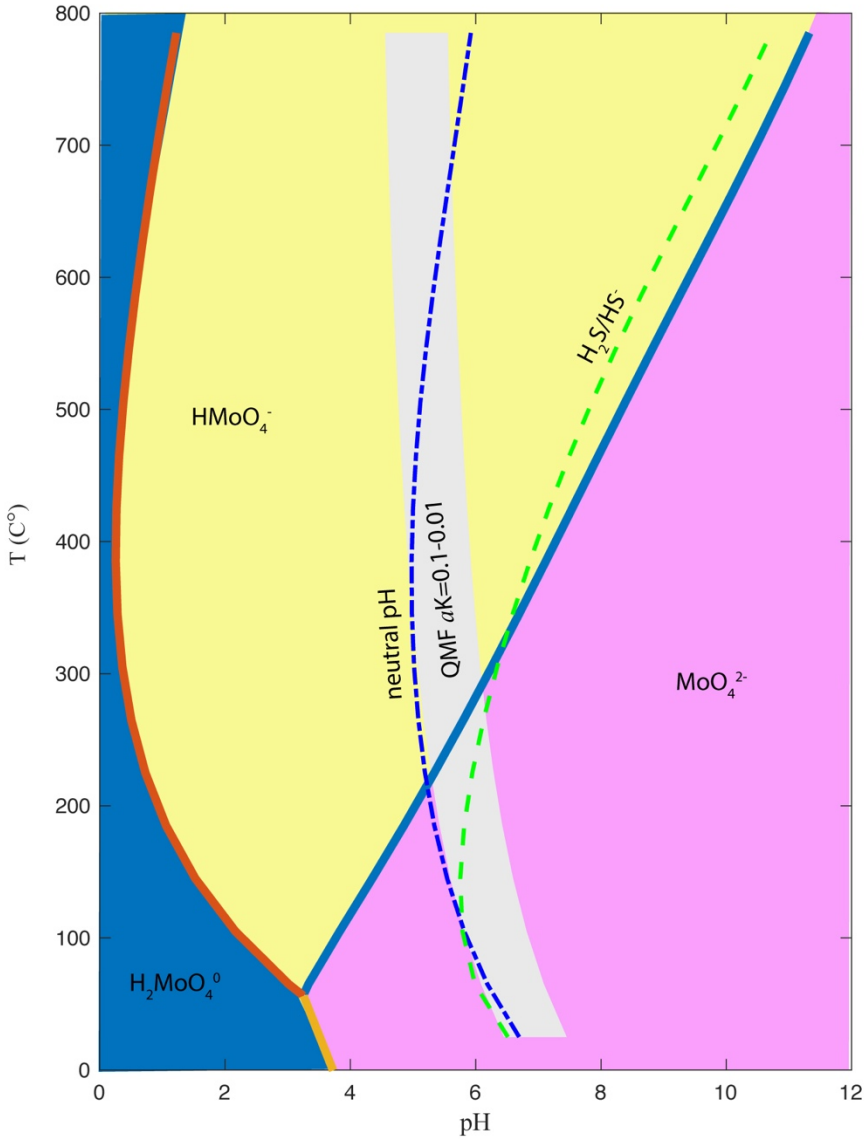

Figure 5.1 Speciation of Mo(VI) as a function of temperature and pH, calculated using the thermodynamic properties from Minubayeva and Seward (2010). The curves for neutral pH ($aH^+ = aOH^-$), $aH_2S(aq) = aHS^-$, and quartz-muscovite-K-feldspar for aK^+ ranging from 0.1 to 0.01 (grey area). The plot is generated in MatLab.

Although there is no experimental data at temperature as high as 800 °C, the figure can serve as a prediction of the speciation of Mo-O-H species at these conditions. The protonated species $HMoO_4^-$ has a big stability field which extends into the basic conditions with increasing temperature and takes over MoO_4^{2-}. The grey area on the picture represents the "potassic core", which is a part of the intrusion buffered by QMF buffer, where Mo-bearing minerals crystallize (**Figure 1** in Cooke et al., 2014). Initially, the magmatic intrusion will be very hot (≈800 °C), but during the interaction with the host rock, it will cool down to about 300 °C. The temperature of the hydrothermal fluids infiltrating the intrusion will decrease too. At such conditions, the species responsible for the Mo transport would be the protonated $HMoO_4^-$ complex, according to **Figure 5.1** and the molybdate anion will not be important. However, this would apply to a chlorine-free system, which is likely not to be the case for porphyry systems Cooke et al., 2014.

Figure 5.2 presents a calculation which extrapolates for the effects of pH and salinity.
pH plays an essential role in controlling mineral solubility and speciation of elements in aqueous solutions (reviewed in Seward & Barnes, 1997; Brugger et al., 2016). A study of Galvez et al. (2016) describes how the pH of the hydrothermal fluids in subduction zones influences volatile cycles and metal distribution. Stability of Cl^--bearing molybdenum species is very dependent on pH, according to several studies (e.g., Borg et al., 2012). At acidic conditions they are stable, but not at neutral and basic conditions. Due to the limited size of the simulation cell in *ab initio* MD simulations, it is not possible to make realistic estimations about the pH based solely on the simulations. However, the results of *ab initio* thermodynamic integration in combination with other techniques can be used to analyse the effects of pH dependency on the speciation.

Based on the results presented in Chapter 3 (section 3.4.2), the molybdenum speciation in Cl^- brines at 750˚C / 2000 bar was analysed in the light of its pH dependency. **Figure 5.2** was generated by Eqbrm software (Brugger, 2007b) and shows the predicted speciation of Mo-O-Cl species under the investigated conditions based on the reaction: $K=[Cl^-][H^+]/[HCl^0]$. **Figures 5.2-a and a1** reveal that adding NaCl to a weak acidic (10^{-4} m HCl) fluid does not have a noticeable effect on the speciation, with $[MoO_2(OH)_2]^0$ being predominant. The picture

becomes different when HCl is added to a solution with a low NaCl concentration, as **Figures 5.2-b and b1** show. Here, the addition of acid will cause the chloride species to become important, in particular when pH is below 4.3. Most importantly, **Figures 5.2-c and c1** show that an addition of acid to 0.5 m NaCl, which is a very common salinity in ore fluids (e.g Seward & Barnes, 1997), will make chloride species predominant even in neutral and weak-alkaline pH.

To sum this up, the new MD results suggest that chloride species (e.g., $[MoO_2Cl(OH)]^0$) play an important role in molybdenum transport in high P/T magmatic hydrothermal systems, such as porphyry Cu-Mo deposits. While in chloride-free solutions, the most important species would be $HMoO_4^-$.

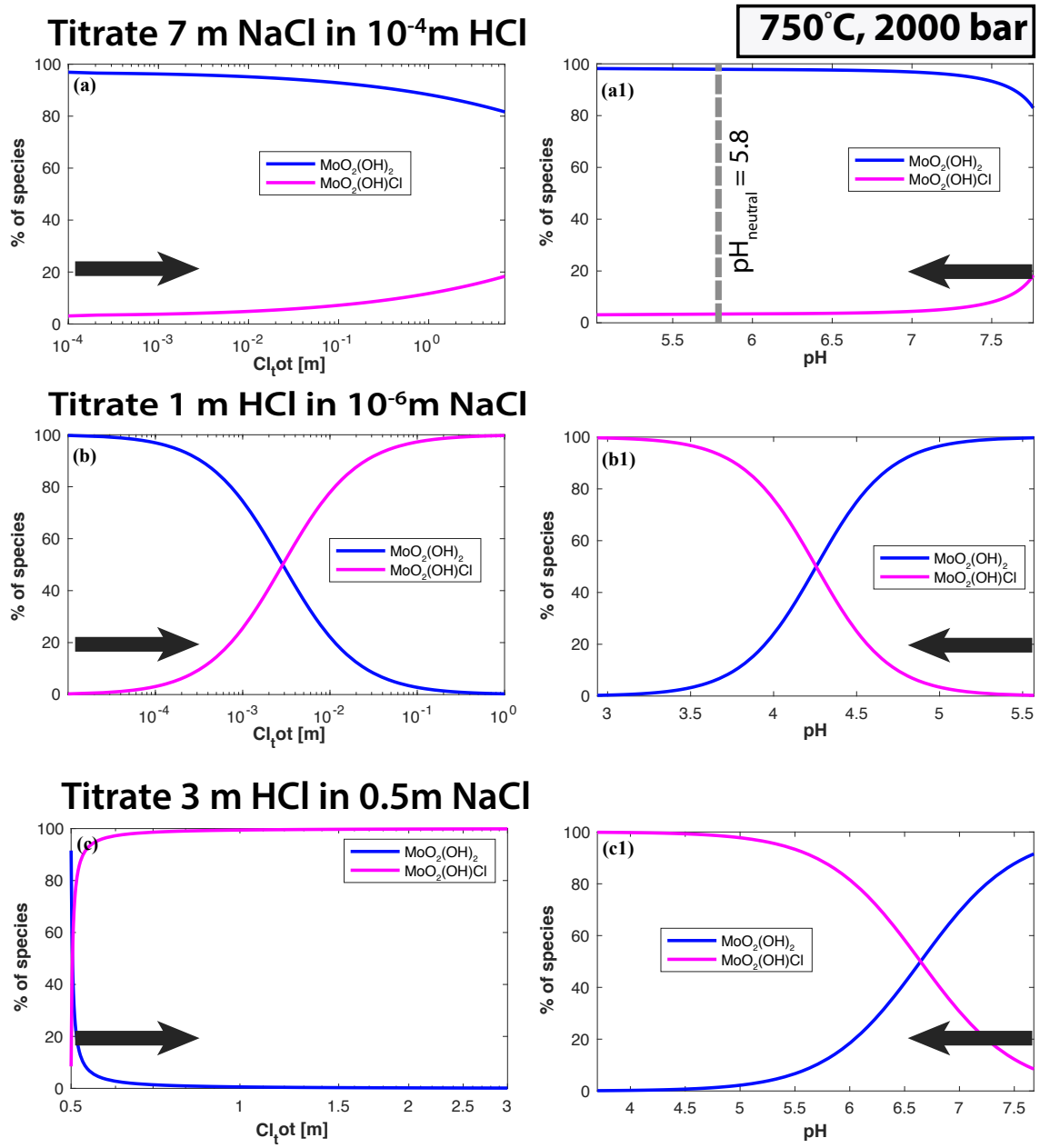

Figure 5.2. Molybdenum speciation in chloride brines at 750˚C / 2000 bar, as a function of pH and NaCl concentrations. Stabilities of the $[MoO_2(OH^-)Cl^-]^0$ complex derived from the thermodynamic integration data (see section 3.4.2). The simulations correspond to: (a, a1) titration of 7m NaCl in 10^{-4} m HCl solution; (b, b1) titration of 1m HCl in 10^{-6} m NaCl; and (c, c1) titration of 3m HCl in 0.5 m NaCl. The simulation were conducted using the Eqbrm software (Brugger, 2007). Activity coefficients for charged species were calculated using the b-dot equation, with parameters for $NaCl^-$dominated solutions at the upper limit (600˚C / 2000 bar) from Oelkers & Helgeson, (1989).

6 Conclusions and future work

6.1 Conclusions

Using *ab initio* MD simulations to investigate processes of metal-ligand complexing in hydrothermal fluids is like looking at the ore forming processes with a very powerful microscope. The method shows the behaviour of molecules which compose solid minerals and fluids around them, as well as how they interact with each other.
What we see is generated using necessary computational approximations, and is a very simplified version of what is found in nature, but it is still a very valuable knowledge. In case of this particular study, *ab initio* simulations have provided some important insights and helped to resolve ambiguities found in previous works.

First of all, the research presented in Chapter 3, confirms the values of bond lengths of Mo-O and Mo-Cl derived by experimental studies of Tossel (2005), Oyerinde et al. (2007), Borg et al.(2012) & Liu et al. (2013), as well as it offers more details about the nature of ligands (O^{2-}, OH^- or H_2O). This information is valuable because the experimental techniques are not able to detect hydrogen atoms.

Investigating Mo speciation under the conditions similar to those applied by Borg et al. (2012), the *ab initio* MD data presents a supportive evidence of Mo-Cl complexation and proves the existence of the complexes proposed by the experiment, such as $[MoO_2Cl(H_2O)_3]^0$ and $[MoO_2Cl_2(H_2O)_2]^0$ at ambient conditions as well as $[MoOCl_5]^-$ and $[MoCl_4O]^0$ at 340 °C.

The current study has generated completely new high P/T data, which does not have an experimental equivalent. Along with presenting the observed speciation, I also calculated the stability constant for the reaction
$[MoO_2(OH)(Cl)]^0 + H_2O = [MoO_2(OH)_2]^0 + HCl$ to be: ($\log K$) = -2.44. This gives a clear answer that at 750 °C / 2 kbar and a high acidity of 6 m Cl^-, the tetrahedral Cl^--bearing species is very stable and complexation with chloride is energetically favourable at these conditions.

The data presented in Chapter 3 has also confirmed that the true structure of molybdic acid is $[Mo(O)_2(OH)_2]^0$ which is in agreement with the theoretical study of Liu et al., (2013), while it contradicts the conclusion of Tossel (2005), Ulrich & Mavrogenes (2008), Oyerinde et al. (2007) and Hurtig & Williams-Jones (2014a) who proposed $[MoO_3 \cdot nH_2O]^0$ as the true structure.

In relation to natural systems, my suggestion, based on **Figure 5.1** and **5.2,** would be that in a chlorine-free system, the protonated species $HMoO_4^-$ is the main carrier of Mo, while in presence of chlorine the complexation with Cl^- is highly favourable even under neutral and mildly basic conditions.

Chapter 4 presents the first attempts to generate MD data for Mo-O-S complexation which have been successfully made. The observed bond distances Mo-S are in a good agreement with the values derived by the experimental study of July 2018 (see **3**)

The data collected also confirmed the dependency of Mo-S complexation on the HS^- concentration. Higher concentration of hydrosulphide favours the formation of Mo-S bonds. The results of the experiment of July 2018 came to the same conclusion .

Lastly, the *ab initio* MD simulations described in Chapter 4 show that the molybdate anion, $[MoO_4]^{2-}$, is stable in a basic solution at all three P/T conditions investigated. This conclusion supports the findings of Minubayeva & Seward, (2010) and Oyerinde et al. (2007)

6.2 Future work

The scientific work presented in this thesis focused on a very narrow selection of research questions while the field of metal complexation in hydrothermal fluids is a very broad topic which offers a seemingly infinite amount of ideas for future investigation. In the section below, I present some of the thoughts which crossed my mind while working on this thesis. Hopefully, they can serve as a guide for new computational and experimental studies.

- A few studies have suggested that higher P favours tetrahedrally coordinated species (Crerar et al., 1985; Le Bacq et al., 2011, Borg et al., 2012). Hurtig & Williams-Jones

(2014a) proposed that increasing T but constant P favours tetrahedral configuration because of the dehydration. However, the *ab initio* results in the current study are ambiguous. The final configurations seem to be largely dependent on the nature of ligands, and the initial complexes with > 5 Cl^- ligands remained in a 5- to 6- fold coordination during the simulations even at high P/T conditions. The effect of pressure on the coordination of Mo-O-Cl complexes can be investigated by running a series of calculations at the same temperature but different pressures.

- Several acidity conditions need be tested to check the effect of Cl^- concentration on Mo-O-Cl complexation. Some studies (Ulrich & Mavrogenes, (2008); Dadze et al., (2018)) have suggested that molybdenum oxo-chloro complexes can play an important role in Mo transport with increasing temperature even at less acidic conditions than those reported by Borg et al. (2012). For example, a simulation of $[MoO_2Cl(OH)_2]^-$ can be run with ~1 m Cl^- to see if the complex remains stable, as it was proposed by Dadze et al. (2018).
- The stability of the molybdate anion $[MoO_4^{2-}]$ can be investigated under different acidic conditions to document whether it would remain stable in a solution with low chloride concentration, in addition to being stable in neutral and basic fluids, as documented by Borg et al., 2012.
- Based on the results presented in section 3.4.1 it is evident that Mo-O-Cl complexes form several metastable configurations at 350 °C. A series of *ab initio* TI calculations can be run in order to bring more clarity about the stability of the investigated complexes at these conditions.
- To make a complete picture of the complexation patterns of Mo-O-Cl it would be useful to perform a series of *ab initio* TI calculations starting with $[MoCl_6]^0$ and substituting one chloride ligand by an oxygen ligand in the subsequent simulations until the chloride- free configuration is achieved. These calculations would map the thermodynamic changes which take place between the whole range of possible Mo-O-Cl configurations. However, such an in-depth investigation would be incredibly demanding in terms of computational recourses and time.
- *ab initio* MD simulations are a wonderful tool which can be used to investigate the conversion of $[MoO_4]^{2-}$ to $[MoS_4]^{2-}$ under ambient condition. This reaction is very important in sedimentary processes, such as burial mechanisms for Mo in sulphidic environments (e.g., Dahl et al., 2013). The conversion takes place in four steps which have been documented by Erickson & Helz, (2000). It has also been proposed (Tossel, 2005)

that the formation of $[MoS_4]^{2-}$ from $[MoO_4]^{2-}$ is thermodynamically beneficial. On the basis of this information a series of *ab initio* simulations can be performed with a following thermodynamic integration calculation, in order to describe the process computationally.

- In natural geological environments, molybdenum is likely to be exposed to both Cl^- and HS^- -bearing aqueous hydrothermal fluids (e.g Seo et al., 2012; Zhang et al., 2012). Complexation of Mo in such fluids would be undoubtedly challenging to model. However, it can be attempted to simulate a series of reactions between different Mo-O-Cl-S compounds which lead to the formation of molybdenite, as suggested by Seo et al. (2012) (Reactions 4-10).

Ab initio MD simulations are a great tool for not only cross- checking the existing experimental results but can also serve as a guide for the setup of new experiments. By suggesting a likely speciation under the conditions of interest, insights from *ab initio* simulations can make new relevant experiments more precise and thus help to avoide unnecessary waste of recourses.

7 References

Agricola, G., and Hoover, H. & Hoover, L.H. (1950) De re metallica / translated from the first Latin edition of 1556, with biographical introduction, annotations and appendices by Herbert Clark Hoover and Lou Henry Hoover, *Dover Publications,* New York

Anbar A. D., Duan Y., Lyons T. W., Arnold G. L., Kendall B., Creaser R. A., Kaufman A. J., Gordon G. W., Scott C., Garvin J. and Buick R. (2007) A whiff of oxygen before the great oxidation event? *Science,* **317**, 1903–1906.

Ardakani, O.H., Chappaz, A., Sanei, H., Mayer, B., (2016) Effect of thermal maturity on remobilization of molybdenum in black shales. *Earth Planetary and Science Letters,* **449**, 311-320.

Arnold G. L., Anbar A. D., Barling J. and Lyons T. W. , (2004) Molybdenum isotope evidence for widespread anoxia in mid- proterozoic oceans. *Science,* **304**, 87–90.

Audetat A., Dolejs D. and Lowenstern J. B. (2011) Molybdenite saturation in silicic magmas: occurrence and petrological implications. *Journal of Petrology,* **52(5)**, 891–904.

Barceloux, D. G. and Barceloux, Dr. D. (1999) Molybdenum, Journal of Toxicology: *Clinical Toxicology*, **37 (2),** 231-237

Bebout, G.E., Penniston-Dorland, S.C. (2016) Fluid and mass transfer at subduction interfaces the field metamorphic record. *Lithos,* **240–243**, 228–258.

Becke, A. D. (1988) Density-functional exchange-energy approximation with correct asymptotic behaviour. *Physical Review A,* **38**, 3098.

Beeson, K. C. and Matrone, G. (1976) The soil factor in nutrition: Animal and human. New York: Marcel Dekker

Berendsen H. J. C., Grigera J. R. and Straatsma T. P. (1987) The missing term in effective pair potentials. *Journal of Physical Chemistry A,* **91**, 6269–6271.

Bertine, K.K., Turekian, K.K., (1973) Molybdenum in marine deposits. *Geochimica et Cosmochimica Acta,* **37**, 1415-1434.

Bethke, C.M. (2008) Geochemical and biogeochemical reaction modelling (second edition). Cambridge University Press, New York. 543 pages.

Bloom, M. S. (1981) Chemistry of inclusion fluids in stockwork molybdenum deposits. *Economic Geology,* **76**, 1906-1920.

Borg, S, Liu, W, Etschmann, B, Tien, Y., Brugger, J. (2012) An XAS study of molybdenum speciation in hydrothermal chloride solutions from 25-385 °C and 600 bar. *Geochimica et Cosmochimica Acta,* **92**, 292-307.

Bortels, H. Zentralbl. 1936, *Bakteriol. Parisitenkd. Infektionskr*. **95**, 193–218.

Bostick B. C., Fendorf, S. and Helz, G. R. (2003) Differential absorption of molybdate and tetrathiomilybdate on pyrite (FeS_2). *Environmental Science & Technology,* **37**, 285-291.

Braithwaite, E. R. (1994) Molybdenum: an outline of its chemistry and uses (edited by Braithwaite, E. R. and Haber, J) *Studies in inorganic chemistry* **19**, Elsevier

Brugger, J. (2007b). Eqbrm software BeerOz, a set of Matlab routines for the quantitative interpretation of spectrophotometric measurements of metal speciation in solution. *Computers & Geosciences,* **33**, 248-261.

Brugger, J., Etschmann, B., Liu, W., Testemale, D., Hazemann, J. L. and Emerich, H. (2007a) An XAS study of the structure and thermodynamics of Cu(I) chloride complexes in brines up to high temperature (400 °C, 600 bar). *Geochim. Cosmochim. Acta*, **71**, 4920-4941

Brugger, J., Liu, W., Etschmann, B., Mei, Y., Sherman, D. and & Testemale, D. (2016). A review of the coordination chemistry of hydrothermal systems, or do coordination changes make ore deposits? *Chemical Geology*, **447,** 219–253

Brugger, J., Pring, A., Reith, F., Ryan, C., Etschmann, B., Liu, W.H., O'Neill, B. and Ngothai, Y. (2010) Probing ore deposits formation: New insights and challenges from synchrotron and neutron studies. *Radiatiation Physics and Chemistry,* **79**, 151-161.

Brumsack, H.-J. and Gieskes, J. (1983) Interstitial Water Trace-Metal Chemistry of Laminated Sediments form the Gulf of California, Mexico. *Marine Chemistry*, **14**, 89-106.

Bühl, M., Kabrede, H., Diss, R., and Wipff, G., (2006) Effect of Hydration on Coordination Properties of Uranyl(VI) Complexes. A First-Principles Molecular Dynamics Study. *Journal of the American Chemical Society,* **128**, 6357-6368.

Bühl, M., Sieffert, N., Golubnychiy, V., and Wipff, G., (2008) Density Functional Theory Study of Uranium(VI) Aquo Chloro Complexes in Aqueous Solution. *The Journal of Physical Chemistry A* **112**, 2428-2436.

Burgess, J., (1978) Metal ions in solution. Published by Ellis Horwood Ltd. Chichester and distributed by John Wiley and Sons, Chichester and New York. 481 pp.

Burguera, J.L., Burguera, M. (2007) Molybdenum in human whole blood of adult residents of the Merida State (Venezuela). *Journal of Trace Elements in Medicine and Biology,* **21 (3)** 178–183.

Calvert S. E. and Pedersen T. F. (1993) Geochemistry of recent oxic and anoxic marine sediments: implications for the geological record. *Marine Geology,* **113**, 67–88.

Candela P. A. and Holland H. D. (1984) The partitioning of copper and molybdenum between silicate melts and aqueous fluids. *Geochimica et Cosmochimica Acta,* **48**, 373–380.

Canfield D. E. (2005) The early history of atmospheric oxygen: homage to Robert M. Garrels. *Annual Review of Earth and Planetary Sciences,* **33**, 1–36.

Cao, X. (1989) Solubility of molybdenite and the transport of molybdenum in hydrothermal solutions. Ph.D. thesis, Iowa State University.

Car, R. & Parrinello, M. (1985) Unified Approach for Molecular Dynamics andDensity-Functional Theory. *Physical Review Letters* **55**, 2471-247

Chappaz, A., Lyons, T.W., Gregory, D.D., Reinhard, C.T., Gill, B.C., Li, C., Large, R.R., (2014). Does pyrite act as an important host for molybdenum in modern and ancient euxinic sediments? *Geochimica et Cosmochimica Acta,* **126**, 112-122.

Chappaz, A., Glass, J. & Lyons, T.W. (2016) Molybdenum in *Encyclopedia of Geochemistry*, Springer International Publishing

Cooke, D. R., Hollings, P., Wilkinson, J.J, Tosdal, R.M. (2014) 13.14 - Geochemistry of Porphyry Deposits, in Treatise on Geochemistry (Second Edition), Editor: Heinrich, D., Holland, H.D. and Turekian, K.K, *Elsevier*, pp. 357-381,

Cramer S. P., Hodgson K. O., Gillum W. O. and Mortenson L. E., (1978) Molybdenum site of nitrogenase – preliminary structural evidence from X-ray absorption spectroscopy. *Journal of the American Chemical Society,* **100**, 3398–3407.

Crerar, D.A., Wood, S., Brantley, S., Bocarsly, A., (1985) Chemical controls on solubility of ore-forming minerals in hydrothermal systems. *Canadian Mineralogist,* **23**, 333–352.

Crusius J., Calvert S., Pedersen T. and Sage D., (1996) Rhenium and molybdenum enrichments in sediments as indicators of oxic, suboxic and sulfidic conditions of deposition. *Earth and Planetary Science Letters,* **145**, 65–78.

Cruywagen, J.J., (1999) Protonation, oligomerization, and condensation reactions of vanadate(V), molybdate(VI), and tungstate(VI). In: Sykes, A.G. (Ed.), *Advances in Inorganic Chemistry. Academic Press*, pp. 127-182.

Dadze, T.P., Kashirtseva, G.A., Novikov, M.P., Plyasunov, A.V., (2018) Solubility of MoO_3 in aqueous acid chloride-bearing solutions at 573 K. *Journal of Chemical Engineering Data* **63,** 1827-1832.

Dahl T. W., Hammarlund E. U., Anbar A. D., Bond D. P. G., Gill B. C., Gordon G. W., Knoll A. H., Nielsen A. T., Schovsbo N. H. and Canfield D. E., (2010) Devonian rise in atmospheric oxygen correlated to the radiations of terrestrial plants and large predatory fish. *Proceedings of the National Academy of Sciences,* **107**, 17911–17915.

Dahl T. W., Canfield D. E., Rosing M. T., Frei R. E., Gordon G. W., Knoll A. H. and Anbar A. D. (2011) Molybdenum evidence for expansive sulfidic water masses in 750 Ma oceans. *Earth and Planetary Science Letters,* **311**, 264–274.

Dahl, T.W., Chappaz, A., Fitts., J.P, Lyons, T.W (2013) Molybdenum reduction in a sulfid lake: Evidence from X-ray absorption fine-structure spectroscopy and implications for the Mo paleoproxy. *Geochimica et Cosmochimica Acta,* **103** 213-231.

Dellwig, O., Beck, M., Lemke, A., Lunau, M., Kolditz, K., Schnetger, B., Brumsack, H.-J., (2007) Non-conservative behavior of molybdenum in coastal waters: coupling geo-chemical, biological, and sedimentological processes. *Geochimica et Cosmochimica Acta* **71**, 2745–2761.

Dick, A.T. (1956) Molybdenum in animal nutrition. *Soil Science*; **81**:229–236.

Driesner, T., (2007) The system H2O–NaCl. Part II: Correlations for molar volume, enthalpy, and isobaric heat capacity from 0 to 1000°C, 1 to 5000bar, and 0 to 1 XNaCl. *Geochimica et Cosmochimica Acta* **71**, 4902-4919.

Driesner, T. and Heinrich, C. A., (2007) The system H2O–NaCl. Part I: Correlation formulae for phase relations in temperature–pressure–composition space from 0 to 1000 °C, 0 to 5000bar, and 0 to 1 XNaCl. *Geochimica et Cosmochimica Acta* **71**, 4880-4901.

Emerson S. and Huested S. S., (1991) Ocean anoxia and the concentrations of molybdenum and vanadium in seawater. *Marine Chem*istry, **34**, 177–196.

Erickson B. E. and Helz G. R., (2000) Molybdenum(VI) speciation in sulfidic waters: stability and lability of thiomolybdates. *Geochimica et Cosmochimica Acta,* **64**, 1149–1158.

Etschmann, B., Liu, W., Testemale, D., Muller, H., Rae, N., Proux, O., Hazemann, J., Brugger, J., (2010) An in situ XAS study of copper(I) transport as hydrosulfide complexes in hydrothermal solutions (25–592 °C, 180–600 bar): speciation and solubility in vapor and liquid phases. *Geochimica et Cosmochimica Acta,* **74 (16)**, 4723–4739.

Etschmann, B., Mei, Y., Liu, W., Rae, N., Kappen, P., Testemale, D. and Brugger, J. (2018) Role of Pb(II) complexes in hydrothermal mass transfer: An X-ray absorption spectroscopic study. *Chemical Geology*, **502,** 88-106.

Francois R.,1988. A study on the regulation of the concentrations of some trace metals (Rb, Sr, Zn, Pb, Cu, V, Cr, Ni, Mn and Mo) in Saanich Inlet Sediments, British Columbia, Canada. *Marine Geology,* **83**, 285–308.

Fulton, J. L., Hoffmann, M. M., and Darab, J. G., (2000a) An X-ray absorption fine structure study of copper(I) chloride coordination structure in water up to 325 °C. *Chemical Physics Letters,* **330**, 300-308.

Fulton, J. L., Hoffmann, M. M., Darab, J. G., Palmer, B. J., and Stern, E. A., (2000b) Copper(I) and Copper(II) Coordination Structure under Hydrothermal Conditions at 325 °C: An X-ray Absorption Fine Structure and Molecular Dynamics Study. *The Journal of Physical Chemistry A,* **104**, 11651-11663.

Fulton, J. L., Darab, J. G., and Hoffmann, M. M. (2001) X-ray absorption spectroscopy and imaging of heterogeneous hydrothermal mixtures using a diamond microreactor cell. *Review of Scientific Instruments,* **72**, 2117-2122.

Galvez M. E., Connolly J. A. D. and Manning C. E. (2016) Implications for metal and volatile cycles from the pH of subduction zone fluids. *Nature,* **539**, 420–424.

Gaschnig R. M., Rudnick R. L., McDonough W. F., Kaufman A. J., Hu Z. and Gao S. (2014) – Onset of oxidative weathering of continents recorded in the geochemistry of ancient glacial diamictites. *Earth and Planetary Science Letters,* **408**, 87–99.

Giussani, A. (2011) Molybdenum in the Environment and its Relevance for Animal and Human Health, *Elsevier*, pp 840-846

Glass, J.B., Chappaz, A., Eustis, B., Heyvaert, A.C., Waetjen, D.P., Hartnett, H.E., Anbar, A.D., (2013) Molybdenum geochemistry in a seasonally dysoxic Mo-limited lacustrine ecosystem. *Geochimica et Cosmochimica Acta,* **114**, 204-219.

Greany, A. T., Rudnick, R. L., Gaschning, R. M., Whalen, J. B., Luais, B. & Clemens, J. D. (2018) Geochemistry of molybdenum in the continental crust. *Geochimica et Cosmochimica Acta*, **238**, 36-54

Guan, Q. Mei, Y., Etschmann, B., Testemale, D., Louvel, M. and Brugger, J. (2019) Yttrium complexation and hydration in chloride-rich hydrothermal fluids: a combined *ab initio* molecular dynamics and *in situ* X-ray absorption spectroscopy study. *Geochimica et Cosmochimica Acta, Under Review (submitted 10 Sept. 2019)*

Guissani Y, Guillot B (1993) A computer simulation study of the liquid–vapour coexistence curve of water. *Journal of Chemical Physics*, **98**, 8221–35.

Gupta, U.C., (1997) Symptoms of molybdenum deficiency and toxicity in crops. In: Molybdenum in Agriculture. *Cambridge University Press*, Cambridge, pp. 160-181.

Habershon, S. and Manolopoulos, D. E. (2011) Free energy calculations for a flexible water model, *Phys. Chem. Chem. Phys.*, 2011,13, 19714-19727

Haile, J. M. (1992) Molecular dynamics simulation: Elementary Methods. Wiley, New York

Hall, W. E., I. Friedman, and J. T. Nash. (1974) Fluid inclusion and light stable isotope studies of the Climax molybdenum deposits, Colorado. *Economic Geology,* **69**, 884-901.

Hall, J.O., (2018) Chapter 32 Molybdenum in Veterinary Toxicology, 3rd Edition, Basic and Clinical Principles, *Academic Press*, pp. 463-467

Harris, D. J., Brodholt, J. P., Harding, J. H., and Sherman, D. M., (2001) Molecular dynamics simulation of aqueous $ZnCl_2$ solutions. *Molecular Physics,* **99**, 825-833.

Heinrich, C.A., Walshe, J.L., Harrold, B.P. (1996). Chemical mass transfer modelling of ore-forming hydrothermal systems - current practice and problems. *Ore Geology Reviews,* **10 (3–6)**, 319–338.

Heinrich, C.A., Driesner, T., Stefansson, A., Seward, T.M., (2004) Magmatic vapor contraction and the transport of gold from the porphyry environment to epithermal ore deposits. *Geology,* **32 (9)**, 761–764.

Helgeson, H. C., (1969) Thermodynamics of hydrothermal systems at elevated temperatures and pressures. *American Journal of Science* **267**, 729-804.

Helgeson, H. C., Kirkham, D. H., and Flowers, G. C., (1981) Theoretical prediction of the thermodynamic behaviour of aqueous electrolytes by high pressures and temperatures; IV, Calculation of activity coefficients, osmotic coefficients, and apparent molal and standard and relative partial molal properties to 600 degrees C and 5kb. *American Journal of Science,* **281**, 1249-1516.

Helgeson, H. C. and Kirkham, D. H., (1974) Theoretical prediction of the thermodynamic behavior of aqueous electrolytes at high pressures and temperatures; II, Debye-Hückel parameters for activity coefficients and relative partial molal properties. *American Journal of Science,* **274**, 1199-1261

Helz G. R., Bura-Nakic, E., Mikac N. and Ciglenecki I., (2011) New model for molybdenum behavior in euxinic waters. *Chemical Geol*ogy, **284**, 323–332.

Helz, G.R., Miller, C.V., Charnock, J.M., Mosselmans, J. F.W., Pattrick, R.A.D., Garner, C.D. and Vaughan, D.J. (1996) Mechanism of molybdenum removal from the sea and its concentration an black shales: EXAFS evidence. *Geochimica et Cosmochimica Acta,* **60**, 3631-3642.

Henckens, M. L. C. M., Biermann, F. H. B. and Driessen, P.P.J. (2019) Mineral Resources governance: A call for establishment of an International Competence Center on Mineral resources Management *Resources, Conservation and Recycling*, **141**, 255-263

Henckens, M.L.C.M., Driessen,P.P.J., Worrell, E. (2018) Molybdenum resources: Their depletion and safeguarding for future generations, *Resources, Conservation and Recycling*, **134**, 61-69

Heuft, M. J. and Meijer, E. J., (2003) Density functional theory based molecular-dynamics study of aqueous chloride solvation. *The Journal of Chemical Physics*, **119**, 11788.

Heuft, M. J. and Meijer, E. J., (2005) Density functional theory based molecular-dynamics study of aqueous fluoride solvation. *The Journal of Chemical Physics*, **122**, 094501.

Heuft, M. J. and Meijer, E. J., (2005) Density functional theory based molecular-dynamics study of aqueous iodide solvation. *The Journal of Chemical Physics*, **123**, 094506.

Hielm,P. J. (1788) ibid **49** 288.

Holzheid A., Borisov A. and Palme H., (1994) The effect of oxygen fugacity and temperature on solubilities of nickel, cobalt, and molybdenum in silicate melts. *Geochimica et Cosmochimica Acta,* **58**, 1975–1981.

Howard, J. B. & Rees, D. C. (1996) Structural Basis of Biological Nitrogen Fixation. *Chemical Reviews,* **96**, 2965–2982.

Hunt, P. and Sprik, M. (2005) On the position of the highest occupied molecular orbital in aqueous solutions of simple ions. *ChemPhysChem* **6 (9)**, 1805-8.

Hurtig, N.C., Williams-Jones, A.E., (2014a) An experimental study of the solubility of MoO3 in aqueous vapour and low to intermediate density supercritical fluids. *Geochimica et Cosmochimica Acta,* **136 (0)**, 169–193.

Hurtig, N., Williams-Jones, A. E. (2014b) An experimental study of the transport of gold through hydration of AuCl in aqueous vapour and vapour-like fluids, *Geochimica et Cosmochimica Acta,* **127**, 305-325.

International Molybdenum Association (IMOA), (2011) Molybdenum in Iron and Steels for Clean and Green Power Generation. IMOA.

International Molybdenum Association (IMOA), (2013) Molybdenum in Power Generation, Thin Film Photovoltaic Solar Panels. IMOA/07/13.

International Molybdenum Association (IMOA), (2015) Molybdenum Uses, Molybdenum Metal & Alloys. IMOA/07/13.

Jarrell W.M., Page A.L., Elseewi A.A. (1980) Molybdenum in the environment. In: Gunther F.A., Gunther J.D. (eds) Residue Reviews. Residue Reviews, **74**. Springer, New York, NY.

Jorgensen, W. L., (1982) Revised TIPS for simulations of liquid water and aqueous solutions. *The Journal of Chemical Physics,* **77**, 4156.

Jorgensen, W. L., Chandrasekhar, J., Madura, J. D., Impey, R. W., and Klein, M. L., (1983) Comparison of simple potential functions for simulating liquid water. *The Journal of Chemical Physics,* **79**, 926.

Keppler H. and Wyllie P. J. (1991) Partitioning of Cu, Sn, Mo, W, U, and Th between Melt and Aqueous Fluid in the Systems Haplogranite–H2O HCl and Haplogranite–H2O HF. *Contributions to Mineralogy and Petrology,* **109**, 139–150.

Kesler, S. E. (1994) Mineral Resources, *Economics and the Environment*. McMillan, New York.

Kohn, W. and Sham, L. J., (1965) Self-Consistent Equations Including Exchange and Correlation Effects. *Physical Review,* **140**, A1133-A1138.

Kudrin A. V., (1989) Behavior of Mo in aqueous NaCl and KCl solutions at 300–450 °C. *Geochemistry International,* **26**, 87–99.

Krauskopf, K. B. (1972) Geochemistry of micronutrients. In Mortvedt, J.J, Giordano, P.M. and Lindsay, W.L: Micronutrients in agriculture, *Soil Sci. So. Amer.*, Madison, Wisc., p.7

Laasonen, K., Pasquarello, A., Car, R., Lee, C., and Vanderbilt, D., (1993) Car-Parrinello molecular dynamics with Vanderbilt ultrasoft pseudopotentials. *Physical Review B* **47**, 10142-10153.

Le Bacq O., Machon D., Testemale D. and Paturel A. (2011) Pressure-induced amorphization mechanism in $Eu_2(MoO_4)_3$. *Physical Review B,* **83**, 1–5.

Lee, C., Yang, W., and Parr, R. G., (1988) Development of the Colle-Salvetti correlation-energy formula into a functional of the electron density. *Physical Review B,* **37**, 785- 789.

Lerchbaumer L. and Audétat A. (2012) High Cu concentrations in vapor-type fluid inclusions: an artifact? *Geochimica et Cosmochimica Acta,* **88**, 255–274.

Liu, W., Etschmann, B., Foran, G., Shelley, M. and Brugger, J. (2007) Deriving formation constants for aqueous metal complexes from XANES spectra: Zn^{2+} and Fe^{2+} chloride complexes in hypersaline solutions. *American Mineralogist,* **92**, 761-770.

Liu, W., Brugger, J., Etschmann, B., Testemale, D., and Hazemann, J. L. (2008) The solubility of nantokite (CuCl(s)) and Cu speciation in low-density fluids near the critical isochore: An in-situ XAS study. *Geochimica et Cosmochimica Acta,* **72**, 4094-4106.

Liu, W., Mei, Y., Etschmann, B., Brugger, J., Pearce, M., Ryan, C.G., Borg, S., Wykes, J., Kappen, P., Paterson, D., Boesenberg, U., Garrevoet, J., Moorhead, G. and Falkenberg, G. (2017) Arsenic in hydrothermal apatite: oxidation state, mechanism of uptake, and comparison between experiments and nature. *Geochimica et Cosmochimica Acta,* **196**, 144-159.

Liu, X., Lu, X., Wang, R., Zhou, H., and Xu, S., (2011) Speciation of gold in hydrosulphide-rich ore-forming fluids: Insights from first-principles molecular dynamics simulations. *Geochimica et Cosmochimica Acta,* **75**, 185-194.

Liu, X., Cheng, J., Sprik, M. and Lu, X. (2013) Solution structures and acidity constants of molybdic acid , *The Journal of Physical Chemistry Letters*, **4**, 2926-2930

Lyons T. W., Reinhard C. T. and Planavsky N. J. (2014) The rise of oxygen in Earth's early ocean and atmosphere. *Nature,* **506**, 307–1215.

Mambote, R. C. M., Krijgsman, P. And Reuter, M. A. (2003). Hydrothermal precipitation of arsenic compounds in the ferric-arsenic (III)- sulphate system: thermodynamic modelling. *Miner. Eng.* **16**, 429-440.

Mangold, M., Rolland, L., Costanzo, F., Sprik, M., Sulpizi, M. and Blumberger, J. (2011) Absolute pKa values and solvation structure of amino acids from density functional based molecular dynamics simulation, J. *Chem. Theory. Comput*. **7**, 1951-1961

Mao, J.W., Pirajno, F., Xiang, J.F., Gao, J.J., Ye, H.S., Li, Y.F., Guo, B.J., (2011) Mesozoic molyb- denum deposits in the east Qinling–Dabie orogenic belt: characteristics and tectonic setting. *Ore Geology Reviews,* **43 (1)**, 264–293.

Mason, J. Thiomolybdates: mediators of molybdenum toxicity and enzyme inhibitors (1986) *Toxicol* 1986, **42**, 99-109.

Matsuoka, O., Clementi, E. and Yoshimine, M. (1976) CI study of water dimer potential surface, *J. Chem. Phys*., **64**, 1351-1361.

Mei, Y., Sherman, D. M., Liu, W., and Brugger, J., (2013b) Complexation of gold in S_3^- - rich hydrothermal fluids: Evidence from ab initio molecular dynamics simulations. *Chemical Geology*, **347**, 34-42

Mei, Y., Sherman, D. M., Liu, W., and Brugger, J., (2013a) Ab initio molecular dynamics simulation and free energy exploration of copper(I) complexation by chloride and bisulfide in hydrothermal fluids. *Geochimica et Cosmochimica Acta,* **102**, 45-64.

Mei, Y., Liu, W., Sherman, D. and Brugger, J. (2014) Metal complexation and ion hydration in low density hydrothermal fluids: Ab initio molecular dynamics simulation of Cu(I) and Au(I) in chloride solutions (25–1000°C, 1-5000bar), *Geochimica et Cosmochimica Acta*, **131**, pp. 196-212

Mei, Y., Sherman, D. M., Liu, W., Etschmann, B., Testemale, D. and Brugger, J. (2015) Zinc complexation in chloride-rich hydrothermal fluids (25-600°C): A thermodynamic model derived from *ab initio* molecular dynamics. *Geochimica et Cosmochimica Acta*, **150**, 265-284.

Mendel, R.R., (2007) Biology of the molybdenum cofactor. *Journal of Experimental Botany,***58 (9**), 2289-2296.

Miller, C. A., Peucker-Ehrenbrink, B., Walker, B. D., and Marcantonio, F., (2011). Re-assessing the surface cycling of molybdenum and rhenium. *Geochimica et Cosmochimica Acta*, **75**, 7146–7179.

Minubayeva Z. and Seward T. M. (2010) Molybdic acid ionisation under hydrothermal conditions to 300 °C. *Geochimica et Cosmochimica Acta,* **74**, 4365–4374.

Oelkers, E.H. and Helgeson, H.C. (1989) Calculation of the transport properties of aqueous species at pressures to 5 kbar and temperatures to 1000 ^{o}C. *Journal of Solution Chemistry,* **18**, 601-640.

O'Connor, G. A., Brobst, R.B., Chaney, R.L., Kincaid, R.L., McDowell, L.R., Pierzynski, G.M., Rubin, A. and Van Riper, G.G. (2001) A modified risk assessment to establish molybdenum standards for land application of biosolids. *J. Environ. Qual*. **30**, pp 1490-1507.

O'Neill H. S. C. and Eggins S. M. (2002) The effect of melt composition on trace element partitioning: an experimental investigation of the activity coefficients of FeO, NiO, CoO, MoO_2 and MoO_3 in silicate melts. *Chemical Geol*ogy, **186**, 151–181.

Ossandón, C.G., Fréraut, C.R., Gustafson, L.B., Lindsay, D.D., & Zentilli, M. (2001). Geology of the Chuquicamata Mine: A Progress Report.

Oyerinde O. F., Weeks C. L., Anbar A. D. and Spiro T. G. (2008) Solution structure of molybdic acid from Raman spectroscopy and DFT analysis. *Inorganica Chimica Acta,* **361**, 1000–1007.

Ozeki, T., Kihara, H. and Ikeda, S. (1988) Study of the equlibra in 0.003 mM molybdate acidic aqueous solutions by factor analysis applied to ultraviolet spectra. *Anal. Chem*. **60**, 2055-2059.

Ozeki T., Adachi H. and Ikeda S. (1996) Estimation of the dissolved structures and condensation reactivities of mononuclear molybdenum(VI) species in solution using the UV-absorption spectra and molecular orbital calculation DV-X alpha. *Bulletin* of *Chemical Society of Japan*, **69**, 619–625.

Parr, R.G., Yang, W. Density-Functional Theory of Atoms and Molecules, *Oxford Univ. Press*, New York, 1989.

Pearce C. R., Cohen A. S., Coe A. L. and Burton K. W., (2008) Molybdenum isotope evidence *for global ocean anoxia coupled with perturbations to the carbon cycle during the Early Jurassic Geology,* **36**, 231–234.

Pohl, W.L. (2011) Economic Geology. Principles and Practice, Wiley-Blackwell.

Pokrovski, G. S., Tagirov, B. R., Schott, J., Bazarkina, E. F., Hazemann, J.-L., and Proux, O., (2009a) An in situ X-ray absorption spectroscopy study of gold-chloride complexing in hydrothermal fluids. *Chemical Geology,* **259**, 17-29.

Pokrovski, G. S., Tagirov, B. R., Schott, J., Hazemann, J.-L., and Proux, O., (2009b) A new view on gold speciation in sulfur-bearing hydrothermal fluids from in situ X-ray absorption spectroscopy and quantum-chemical modeling. *Geochimica et Cosmochimica Acta,* **73**, 5406-5427.

Pokrovski, G. S., Roux, J., Ferlat, G., Jonchiere, R., Seitsonen, A. P., Vuilleumier, R., and Hazemann, J.-L., (2013) Silver in geological fluids from in situ X-ray absorption spectroscopy and first-principles molecular dynamics. *Geochimica et Cosmochimica Acta,* **106**, 501-523.

Pople, J.A. and Beverige, D.L. (1970) Approximate Molecular Orbital Theory, McGraw-Hill, New York.

Rajagopalan, K. V. (1988) Molybdenum: An essential trace element in human nutrition. *Annual Review of Nutrition,* **8**, 401-427.

Rankin, W.J., (2011) Minerals, Metals and Sustainability. CSIRO 2011.

Refson, K., (2001). Moldy: a portable molecular dynamics simulation program for serial and

parallel computers. *Computer Physics Commun*ication, **126**, 310 -329.

Rempel K. U., Migdisov A. A. and Williams-Jones A. E. (2006) The solubility and speciation of molybdenum in water vapour at elevated temperatures and pressures: implications for ore genesis. *Geochimica et Cosmochimica Acta*, **70**, 687–696.

Rickard, D. (2012) Metastable Sedimentary Iron Sulfides. In: *Developments in Sedimentology*. Elsevier, **65**, pp. 195-231.

Roedder, E. (1984) Fluid inclusions. *Reviews in Mineralogy,* **12**, 1-644.

Ryabchikov, I. D., V. I. Rekharsky, and A. V. Kudrin. (1981). Mobilization of molybdenum by magmatic fluids in the process of crystallization of granitic melts. *Geokhimiya,* **8**, 1243-1245.

Scheele, C. W. K. (1778) *Svenska Vetensk Akad. Handl*. **39** 217.

Scott C., Lyons T. W., Bekker A., Shen Y., Poulton S. W., Chu X. and Anbar A. D. (2008) Tracing the stepwise oxygenation of the Proterozoic ocean. *Nature,* **452**, 456–459.

Schwarz, G. and Belaidi, A.A. (2013) Molybdenum in human health and disease, *Met Ions Life Sci* **13**, 415–450.

Schwarz, G., Mendel, R.R, Ribbe, M. W. (2009) Molybdenum cofactors, enzymes and pathways. *Nature*, **460 (7257)**, 839–847.

Selby, D. and Creaser, R. A. (2001) Re-Os Geochronology and Systematics in Molybdenite from the Endako Porphyry Molybdenum Deposit, British Columbia, Canada. *Economic Geology*, **96**, 197-204.

Selby, D., Nesbitt, B.E., Muehlenbachs, K., and Prochaska, W., (2000) Hydrothermal alteration and fluid chemistry of the Endako porphyry molybdenum deposit, British Columbia. *Economic Geology*, **95**, 183–202.

Seo J. H., Guillong M. and Heinrich C. A. (2012) Separation of molybdenum and copper in porphyry deposits: the roles of sulfur, redox, and pH in ore mineral deposition at Bingham Canyon. *Economic Geology,* **107**, 333–356.

Seward, T. M., Henderson, C. M. B., Charnock, J. M. and Dobson, B. R. (1996) An X-ray absorption (EXAFS) spectroscopic study of aquated Ag^{+} in hydrothermal solutions to 350 °C. *Geochimica et Cosmochimica Acta,* **60**, 2273-2282.

Seward, T. M. & Barnes, H. L. (1997). Metal transport by hydrothermal ore fluids. In: Barnes, H. L. (Ed.), *Geochemistry of Hydrothermal Ore Deposits*. Wiley, New York.

Seward, T.M., Driesner, T. (2004) Hydrothermal solution structure: Experiments and computer simulations. In *Aqueous Systems at elevated Temperatures and Pressures: Physical Chemistry in Water, Steam and Hydrothermal Solutions* (eds. D.A. Palmer, R. Fernandez-Prini and A.H. Havey). Elsevier, pp.149-182.

Sharps, J. A., Brown Jr, G. E., and Stebbins, J. F., (1993) Kinetics and mechanism of ligand exchange of Au (III), Zn(II), and Cd(II) chlorides in aqueous solution: An NMR study from 28–98°C. *Geochimica et Cosmochimica Acta,* **57**, 721-731.

Sherman, D. M. (2001) Quantum Chemistry and Classical Simulations of Metal Complexes in Aqueous Solutions. *Reviews in Mineralogy and Geochemistry,* **42**, 273-317.

Sherman, D. M., (2007) Complexation of Cu^{+} in Hydrothermal NaCl Brines: Ab initio molecular dynamics and energetics. *Geochimica et Cosmochimica Acta,* **71**, 714-722.

Sherman, D. M. (2010) Metal complexation and ion association in hydrothermal fluids: insights from quantum chemistry and molecular dynamics. *Geofluids*, **10**, 41-57.

Shinohara, H., K. Kazahaya, and J. B. Lowenstern (1995), Volatile transport in a convecting magma column: Implications for porphyry Mo mineralization, *Geology*, **23**, 1091– 1094.

Svarov, Y. and Bastrakov, E. (1999) HCh: a software package for geochemical modelling. User's guide. AGSO (Austalian geological Survey Organisation) record 1999/25, 60pp.

Smedley,P. L. and Kinniburgh, D. G. (2017) Molybdenum in natural waters: A review of occurrence, distributions and controls. *Applied Geochemistry*, **84**, 387-432

Smith D. E. and Dang L. X. (1994) Computer simulations of NaCl association in polarizable water. *Journal of Chemical Physics,* **100**, 3757– 3766.

Sprik, M., (1998) Coordination numbers as reaction coordinates in constrained molecular dynamics. *Faraday Discussions,* **110**, 437-445.

Sprik, M. and Ciccotti, G., (1998) Free energy from constrained molecular dynamics. *Journal of Chemical Physics,* **109**, 7737-7744.

Stemprok M. (1990) Solubility of tin, tungsten and molybdenum oxides in felsic magmas. *Mineralium Deposita* **25**, 205–212

Susak, N.J., Crerar, D.A., (1985) Spectra and coordination changes of transition metals in hydrothermal solutions: implications for ore genesis. *Geochimica et Cosmochimica Acta* **49**, 555–564.

Sverjensky, D. A., Harrison, B. and Azzolini, D. (2014) Water in the deep Earth: the dielectric constant and the solubilities of quartz and corundum to 60 kb and 1200 °C, *Geochim. Cosmochim. Acta*, **129**, 125-145.

Sverdrup, H.U., Ragnarsdottir, K.V., Koca, D., (2015) An assessment of metal supply sustainability as an input to policy: security of supply extraction rates, stocks-in-use, recycling, and risks of scarcity. *Journal of Cleaner Production,* **140 (1)**, 359-372.

Takenaka S., Tanaka T., Funabiki T. and Yoshida S. (1998) Structures of molybdenum species in silica-supported molyb- denum oxide and alkali-ion-modified silica-supported molyb-denum oxide. *Journal of Chemical Physics B,* **102**, 2960–2969.

Tejada-Jimenes ,M., Chamizo-Ampudia, A., Angel, L., Aurora, G. and Emilio, F. (2018) Chapter 8 in Plant micronutrient use efficiency. Molecular and genomic perspectives in Crop Plants, pp. 137-159.

Terrier , C., Vitorge, P., Gaigeot, M-P., Spezia, R. and Vuilleumier, R. (2010) *The Journal of Chemical Physics*, **133**, 044509

Testemale, D., Argoud, R., Geaymond, O., and Hazemann, J. L. (2005) High pressure/high temperature cell for X-ray absorption and scattering techniques. *Review of Scientific Instruments,* **76**, 043905.

Testemale, D., Brugger, J., Liu, W., Etschmann, B., and Hazemann, J. L., (2009) In-situ X- ray absorption study of Iron (II) speciation in brines up to supercritical conditions. *Chemical Geology,* **264**, 295-310.

Tian, Y., Etschmann, B., Liu, W., Borg, S., Mei, Y., Testemale, D., O'Neill, B., Rae, N., Sherman, D. M., Ngothai, Y., Johannessen, B., Glover, C., and Brugger, J. (2012) Speciation of nickel (II) chloride complexes in hydrothermal fluids: In situ XAS study. *Chemical Geology,* **334**, 345-363.

Tossell, J.A., (2005) Calculating the partitioning of the isotopes of Mo between oxidic and sulfidic species in aqueous solution. *Geochimica et Cosmochimica Acta,* **69**, 2981–2993.

Tugarinov, A. I., I. L. Khodakovskiy, and A. P. Zhidikova. (1973) Physicochemical conditions for molybdenite production in hydrothermal uranium-molybdenum deposits. *Geochemistry International,* **10**, 731- 739.

Tunney, J. M., McMaster, J., Garner, C. D (2004) in *Comprehensive Coordination Chemistry*

II, ed. Mc Cleverty J.A. and Meyer, T.J., Elsevier-Pergamon, Amsterdam, **8**, chapter. 8.18, pp. 459-477.

Ulrich T. and Mavrogenes J. (2008) An experimental study of the solubility of molybdenum in H_2O and KCl-H_2Osolutions from 500 °C to 800 °C, and 150 to 300 MPa. *Geochimica et Cosmochimica Acta,* **72**, 2316–2330.

Underwood, E. J. (1977) Trace elements in human and animal nutrition, 4th ed. San Francisco: Academic Press, p. 560.

UNEP, (2011a) International Panel on Sustainable Resource Management. Working Group on Geological Stocks of Metals, Working Paper, April 6, 2011.

USGS, (2017a) Mineral Commodity Summaries 2017, Appendix B.

USGS, (2017c.)Molybdenum Statistics. (January, 2017).

USGS, (2018b) Mineral commodity summaries, January 2018, Antimony, Boron, Molybdenum.

VandeVondele, J., Mohamed, F., Krack, M., Hutter, J., Sprik, M., and Parrinello, M. (2005) *Journal of Chemical Physics*, **122**, 014515

Verlet, L., (1967) Computer "experiments" on classical fluids. I. Thermodynamical properties of Lennard-Jones molecules. *Physical Review,* **159**, 98.

Voegelin A. R., Pettke T., Greber N. D., von Niederhäusern B. and Nägler T. F. (2014) Magma differentiation fractionates Mo isotope ratios: evidence from the Kos Plateau Tuff (Aegean Arc). *Lithos,* **190–191**, 440–448.

Vorlicek, T. P., Chappaz, A., Groskreutz, L. M., Young, N., and Lyons, T. W., (2015) A new analytical approach to determining Mo and Re speciation in sulfidic waters. *Chemical Geology*, **403**, 52–57.

Wang, M., Shen, Q., Xu, G. and & Guo, S. (2014). New Insight into the Strategy for Nitrogen Metabolism in Plant Cells. *International Review of Cell and Molecular Biology*, **310**, 1-37.

White, W. H., A. A. Bookstrom, R. J. Kamilll, M. W. Ganster, R. P. Smith, D. E. Ranta, and R. C. Steininger. (1981) Character and origin of Climax-type molybdenum deposits. *Economic Geology,* **75th Anniversary version**, 270-316.

Wichard, T., Mishra, B., Myneni, S.C.B., Bellenger, J.-P.P., Kraepiel, A.M.L., (2009) Storage and bioavailability of molybdenum in soils increased by organic matter complexation. *Nature Geoscience,* **2**, 625-629.

Wille M., Kramers J. D., Nägler T. F., Beukes N. J., Schröder S., Meisel T., Lacassie J. P. and Voegelin A. R. (2007) Evidence for a gradual rise of oxygen between 2.6 and 2.5 Ga from Mo isotopes and Re-PGE signatures in shales. *Geochimica et Cosmochimica Acta,* **71**, 2417–2435.

Wood, S. A., D. C. Crerar, and M. P. Borcsik. (1987) Solubility of the assemblage pyrite-pyrrhotite-magnetite-sphalerite-galena-stibnite- bismuthinite-argenite-molybdenite in H20-NaCl-C02 solutions from 200° to 3500c. *Economic Geology,* **82**, 1864-1887.

Yan H., Mayanovic R. A., Anderson A. J. and Meredith P. R. (2011) An in situ X-ray spectroscopic study of Mo6+ speciation in supercritical aqueous solutions. *Nuclear Instruments and Methods in Physics Research Section A: Accelerators, Spectrometers, Detectors and Associated Equipment,* **649**, 207–209.

Yang J., Barling J., Siebert C., Fietzke J., Stephens E. and Halliday A. N. (2017) The molybdenum isotopic compositions of I-, S-, and A-type granitic suites. *Geochimica et Cosmochimica Acta,* **205**, 168–186.

Zajacz Z., Halter W. E., Pettke T. and Guillong M. (2008) Determination of fluid/melt partition coefficients by LA- ICPMS analysis of co-existing fluid and silicate melt inclusions: controls on element partitioning. *Geochimica et Cosmochimica Acta,* **72**, 2169–2197.

Zeng, X., Hu, H., Hu, X., Cohen, A. J. and Yang, W. (2008) Ab initio quantum mechanical/molecular mechanical simulationof electron transfer process: fractional electron approach. *J. Chem. Phys*., **128**, 124510.

Zhang, L., Audetat, A., Dolejs, D. (2012) Solubility of molybdenite (MoS_2) in aqueous fluids at 600-800 °C, 200MPa: A synthetic fluid inclusions study. *Geochimica et Cosmochimica Acta,* **77**, 175-185.

Zhong, R., Brugger, J., Tomkins, A.G., Chen, Y., Li, W., (2015b). Fate of gold and base metals during metamorphic devolatilization of a pelite. *Geochimica et Cosmochimica Acta,* **171**, 338–352.

Zoroddu, M. A., Aaseth, J., Crisponi, G., Medici, S., Peana, M., Nurchi, V. M. (2019) The essential metals for humans: a brief overview*, Journal of Inorganic Biochemistry*, **195**, 120-129.

Appendix

An XAS study of the nature of molybdenum in hydrosulphide-bearing hydrothermal solutions

By Barbara Etschmann , July 2018

Experimental method

Sample solutions

All sample solutions were prepared from analytical grade deionized water, $Na_2MoO_2{\cdot}2H_2O$ (Sigma Aldrich™-brand) and a stock 2 m NaHS solution. The NaHS stock solution was prepared by dissolving sodium hydroxide in water, and then bubbling $H_2S_{(g)}$ through the solution. The pH values calculated for a 2 m NaHS solution at 300 °C is 8.5. This method was used by Helz et al. (1993), Mosselmans et al. (1999), Etschmann et al. (2010) and Mei et al., (2016) for studies on Cu and Zn.

The solution compositions are compiled in **Table 1.**

Sample cell and XAS measurement

Molybdenum K-edge (20 000 eV) X-ray Absorption Near Edge Structure (XANES) and Extended X-ray absorption Fine Structure (EXAFS) spectra were measured at beamline 30-BM (FAME) at the European Synchrotron Radiation Facility (ESRF) in Grenoble, France. The setup at the FAME beam line has been described by Proux et al. (2005). A focused beam size of FWHM 300 x 150 μm^2 was used. The incident and transmitted beam intensity I_0 and I_1 were measured with Si diodes. A 30 element solid state fluorescence detector was used for detecting fluorescence data. The energy was calibrated with a Mo foil, such that the maximum of the first derivative was at 20 000 eV.

The high temperature-high pressure cell developed by the "Laboratoire de Cristallographie" (CNRS) was used for XAS measurements of solutions up to supercritical conditions (Testemale

et al., 2005). The cell consists of an external water-cooled high-pressure vessel equipped with three 1.5 mm thick beryllium windows enabling collection of fluorescence and transmission signals at a pressure of 800 bar. A sample solution with a mass of ~0.1 g was contained inside a glassy carbon tube with an internal diameter of 4 mm. The pressure was applied to the sample by two glassy carbon pistons, using helium as a pressure medium. The glassy carbon tube was placed inside a small cylindrical resistive heater; the heater and tube are installed inside in a water-cooled stainless steel high-pressure vessel. The temperature of the fluid at the beam location was controlled by a Eurotherm PID controller to a stability within 0.1 °C, and calibrated using measurements of the density of water as a function of temperature (e.g., Etschmann et al., 2010; Liu et al., 2011), based on the equation of state of pure water (NIST database, Lemmon et al., 2000) and the X-ray mass attenuation coefficients tabulated by Chantler, (1995). The details of the cells can be found in a several previous studies (e.g., Testemale et al., 2005; 2009; Etschmann et al., 2010; Liu et al., 2011).

XANES and EXAFS data were analysed with the HORAE package (Ravel and Newville, 2005), using FEFF version 9 (Rehr et al., 2009). 1-σ errors are reported from EXAFS analyses (HORAE package, Ravel and Newville, 2005).

Results

XANES

Mo(VI)-oxide-chloride compounds have a distinctive pre-edge (1s – 4d transition) which appears to be related to (i) the number of Mo=O bonds/Mo atom and (ii) the symmetry of the structure, the more symmetrical structures having a smaller pre-edge (Borg et al., 2012 and refs therein).

Effect of HS^- concentration: the lower the HS^- concentration, the larger the pre-edge and therefore the more Mo-O bonding (Sol14, 0.037 m HS^-), the barely noticeable pre-edge of Sol6 indicates more Mo-S bonding (highest HS^- concentration, 2 m HS^-), see line A on **Fig 1b**.

Also, the shoulder on the white line increases with increasing HS- concentration (see line B **on Fig 1b**).

Effect of increasing T: Temperature has a smaller effect on the XANES spectra than the HS^- concentration. For Sol6 (2 m HS^-) the change from 30 to 300 °C is reflected in a slight decrease in the shoulder of the white line; for Sol 5 (1.129 m HS^-), Sol15 (0.430 m HS^-) and Sol8 (0.279 m HS^-) the effect is more pronounced with an increase in the height of the pre-edge, shoulder and white line. There was no evidence of a change in the XANES spectra for Sol12 (0.070 m HS^-) but an increase in the pre-edge for Sol14 (0.037 m HS^-).
So, generally, the pre-edge increases with increasing T, indicating an increase in Mo-O bonding (**Fig. 1d**).

EXAFS

The total ligand number reduced from 4 at low temperature to < 4 at higher temperatures for solutions containing more than 0.1 m HS^-; the change being more pronounced and happening at a lower temperature with the more HS^- in solution; for Sol6 (2 m HS^-), ntot was 4 at 30 °C and reduced to ntot ~ 3 at 300 °C, whereas ntot remains ~ 4 for all measured temperatures for Sol12 (0.070 m HS^-) and Sol14 (0.037 m HS^-) (**Table 2**). A similar effect was noticed for Zn (Mei et al. 2014b; Mei et al., 2016).

For relatively high concentrations of HS-, nS decreases with increasing T (Sol5, Sol6, Sol15, Sol8); for lower HS^- concentrations nS remained roughly constant with increasing T (Sol10, Sol12, Sol14, Sol15). nO increases with increasing T for Sol5 and Sol6 (highest HS^- concentrations).

References

Borg, S, Liu, W, Etschmann, B, Tien, Y., Brugger, J. (2012) An XAS study of molybdenum speciation in hydrothermal chloride solutions from 25-385 °C and 600 bar, *Geochimica et Cosmochimica Acta* **92**, 292-307.

Chantler, J. (1995) Theoretical form factor, attenuation, and scattering tabulation for Z=1-92 from E=1-10 eV to E=0.4-1.0 MeV. Journal of Physical And Chemical Reference Data 24, 71-591.

Etschmann, B.E., Liu, W., Testemale, D., Müller, H., Rae, N.A., Proux, O., Hazemann, J.L. and Brugger, J. (2010) An in situ XAS study of copper(I) transport as hydrosulfide complexes in hydrothermal solutions (25–592 °C, 180–600 bar): Speciation and solubility in vapor and liquid phases. Geochimica et Cosmochimica Acta 74, 4723-4739.

Helz, G. R., Charnock, J. M., Vaughan, D. J., and Garner, C. D. (1993) Multinuclearity of Aqueous Copper and Zinc Bisulfide Complexes - an EXAFS Investigation. *Geochimica Et Cosmochimica Acta* **57**, 15-25.

Lemmon, E.W., McLinden, M.O. and Friend, D.G. (2000) Thermophysical properties of fluid systems. National Institute of Standards and Technology, Gaithersberg.

Liu, W., Borg, S.J., Testemale, D., Etschmann, B., Hazemann, J.-L. and Brugger, J. (2011) Speciation and thermodynamic properties for cobalt chloride complexes in hydrothermal fluids at 35-440 ˚C and 600 bar: An in-situ XAS study. Geochimica Et Cosmochimica Acta 75, 1227-1248.

Mei, Y., Sherman, D. M., Liu, W., Etschmann, B., Testemale, D. and Brugger, J. (2014b) Zinc complexation in chloride-rich hydrothermal fluids (25-600 °C): A thermodynamic model derived from *ab initio* molecular dynamics. *Geochimica et Cosmochimica Acta*, **150**, 265-284.

Mei, Y., Etschmann, B., Liu, W., Sherman, D., Testemale, D. and Brugger, J**.**, 2016. Speciation and thermodynamic properties of zinc in sulfur-rich hydrothermal fluids: insights from *ab initio* molecular dynamics simulations and X-ray absorption spectroscopy. *Geochimica Cosmochimica Acta*, 179, 32–52.

Mosselmans, J.F.W., Pattrick, R.A.D., Charnock, J.M. and Solé, V.A. (1999) EXAFS of copper in hydrosulfide solutions at very low concentrations: implications for the speciation of copper in natural waters. *Mineralogical Magazine*, **63**, 769-772.

Proux, O., Biquard, X., Lahera, E., Menthonnex, J-J., Prat, A., Ulrich, O., Soldo, Y., Trévisson, P., Kapoujyan, G., Perroux, G., Taunier, P., Grand, D., Jeantet, P., Deleglise, M., Roux, J-P. and Hazemann, J.-L. (2005) FAME: A new beamline for X-ray absorption investigations of very-diluted systems of environmental, material and biological interests. *Physica Scripta*, **115**, 970-973.

Ravel, B. and Newville, M. (2005) ATHENA, ARTEMIS, HEPHAESTUS: data analysis for X-ray absorption spectroscopy using IFEFFIT. Journal of Synchrotron Radiation 12, 537–541.

Rehr, J.J., Kas, J.J., Prange, M.P., Sorini, A.P., Takimoto, Y. and Vila, F. (2009) Ab initio theory and calculations of X-ray spectra. Comptes Rendus Physique 10, 548-559.

Testemale, D., Argoud, R., Geaymond, O., Hazemann, J.L. (2005) High pressure/high temperature cell for x-ray absorption and scattering techniques. *Rev. Sci. Instrum.* **76,** 043905.

Testemale, D., Brugger, J., Liu, W., Etschmann, B. and Hazemann, J. (2009) In-situ X-ray absorption study of iron(II) speciation in brines up to supercritical conditions. Chemical Geology 264, 295-310.

Tables

Table 1. Composition of solutions

Solution	Composition(g)	Composition (molal)	T (°C), P (bar)
Sol 5	0.0065 g $Na_2MoO_4.2H_2O$ + 3.0275 g H_2O + 4.3631 g 2m NaHS	0.004 m Mo + 1.129 m HS-	30 – 300 °C, 800 bar
Sol 6	0.0131 g $Na_2MoO_4.2H_2O$ + 10.7412 g 2m NaHS	0.006 m Mo + 2.00 m HS-	30 – 300 °C, 800 bar
Sol 8	0.0258 g $Na_2MoO_4.2H_2O$ + 11.968 g H_2O + 2.155 g 2m NaHS	0.008 m Mo + 0.279 m HS-	30 – 300 °C, 800 bar
Sol 10	0.026 g $Na_2MoO_4.2H_2O$ + 11.955 g H_2O + 2.149 g 2m NaHS + 0.810 g NaCl	0.009 m Mo + 0.278 m HS- + 0.998 m Cl-	30 – 300 °C, 800 bar
Sol 12	0.022 g $Na_2MoO_4.2H_2O$ + 10.096 g H_2O + 0.406 g 2m NaHS	0.009 m Mo + 0.070 m HS-	30 – 300 °C, 800 bar
Sol 14	0.022 g $Na_2MoO_4.2H_2O$ + 9.953 g H_2O + 0.209 g 2m NaHS	0.009 m Mo + 0.037 m HS-	30 – 300 °C, 800 bar
Sol 15	0.024 g $Na_2MoO_4.2H_2O$ + 10.974 g H_2O + 3.339 g 2m NaHS	0.007 m Mo + 0.430 m HS-	30 – 300 °C, 800 bar

Table 2. EXAFS results

ESRF July 2018 Mo **SO2=0.7 from Na2MoO4.2H2O pellet and solution**

Sol 5	**1.1 m HS-**		**χ^2_{red} = 348**		**R-factor = 0.023**		**E0 = 6.1(4)**		
T	**nO**	**rO (Å)**	**σ^2O (Å^2)**	**nS**	**rS (Å)**	**ntot**	**σ^2s (Å^2)**	**k-range**	**R-range**
30	1 (fix)	1.69(2)	0.0024(9)	3.0(2)	2.208(6)	4	0.0024(9)	2-10	1-3
100	0.5 (fix)	1.67(2)	0.0015(4)	3.5(1)	2.206(4)	4	0.0015(4)	2-11	1-3
200	1 (fix)	1.70(3)	0.003(4)	3.0(3)	2.210(8)	4	0.002(1)	2-11	1-3
300	2.0(6)	1.73(1)	0.001(4)	2.0(6)	2.25(1)	4	0.006(5)	2-11	1-3
Sol5.apj	fit11								

Sol 6	**2 m HS-**		**χ^2_{red} = 99**		**R-factor = 0.015**		**E0 = 5.9(3)**	
T	**nO**	**rO (Å)**	**nS**	**rS (Å)**	**ntot**	**σ^2 (Å^2)**	**k-range**	**R-range**
30	0.9(1)	1.71(1)	3.0(2)	2.207(4)	3.9	0.0013(6)	2-14	1-3
100	0.6(1)	1.70(2)	3.2(2)	2.206(4)	3.7	0.0013(6)	2-14	1-3
200	0.6(1)	1.71(2)	3.2(2)	2.208(4)	3.8	0.0017(6)	2-14	1-3
300	1.3(1)	1.721(9)	1.9(2)	2.220(5)	3.2	0.0011(8)	2.5-12	1-3
Sol6.apj	fit4							

Sol 8	**0.28 m HS-**		**χ^2_{red} = 646**		**R-factor = 0.065**		**E0 = 8.0(7)**	
T	**nO**	**rO (Å)**	**nS**	**rS (Å)**	**ntot**	**σ^2 (Å^2)**	**k-range**	**R-range**
30	2.5(2)	1.80(1)	1.1(2)	2.29(2)	3.6	0.003 (fix)	2-9	1-3

100	2.4(5)	1.76(1)	1.2(4)	2.25(2)	3.6	0.001(2)	2-14	1-3
200	2.4(5)	1.76(1)	1.1(4)	2.26(3)	3.5	0.001(2)	2-14	1-3
300	2.7(4)	1.76(1)	0.8(3)	2.27(3)	3.5	0.001(2)	2-14	1-3
Sol8.apj	fit4							

Sol 10	**0.28 m HS- + 1 m NaCl**		**χ^2_{red} = 500**		**R-factor = 0.055**		**E0 = 7.4(8)**	
T	**nO**	**rO (Å)**	**nS/Cl**	**rS/Cl (Å)**	**ntot**	**σ^2 (Å^2)**	**k-range**	**R-range**
30	2.5(5)	1.76(2)	1.5(3)	2.26(3)	3.5	0.002(2)	2-13	1-3
100	2.4(2)	1.76(1)	1.6(2)	2.27(1)	3.4	0.003(1)	2-11	1-3
200	2.3(4)	1.75(2)	1.7(3)	2.27(2)	3.4	0.004(2)	2-10	1-3
300	2.5(4)	1.75(1)	1.5(3)	2.28(2)	3.6	0.002(2)	2-11	1-3
Sol10.apj	fit3							

Sol 12	**0.07 m HS-**		**χ^2_{red} = 559**		**R-factor = 0.089**		**E0 = 9.4(7)**	
T	**nO**	**rO (Å)**	**nS**	**rS (Å)**	**ntot**	**σ^2 (Å^2)**	**k-range**	**R-range**
30	3.2(1)	1.78(1)	0.8 (fix)	2.28(4)	4	0.002(2)	2-11.5	1-3
100	3.2(1)	1.777(9)	0.8 (fix)	2.28(3)	3.6	0.002(1)	2-12	1-3
200	3.7(7)	1.78(1)	0.5(4)	2.31(7)	4.2	0.005(3)	2-12	1-3
300	3.2(4)	1.78(1)	0.8(1)	2.33(4)	4	0.003(2)	2-11.5	1-3
Sol12.apj	fit4							

Sol 14	**0.037 m HS-**		**χ^2_{red} = 460**		**R-factor = 0.050**		**E0 = 8.3(7)**	
T	**nO**	**rO (Å)**	**nS**	**rS (Å)**	**ntot**	**σ^2 (Å^2)**	**k-range**	**R-range**

30	3.8(5)	1.767(9)	0.4 (fix)	2.28(7)	4.2	0.002(2)	2-12	1-3
100	3.7(5)	1.771(9)	0.4 (fix)	2.27(6)	4.1	0.002(2)	2-12	1-3
200	3.3(5)	1.76(1)	0.7(1)	2.29(4)	4	0.002(2)	2-12	1-3
300	3.4(4)	1.761(9)	0.7(3)	2.29(3)	4.1	0.002(2)	2-12	1-3
Sol14.apj	fit8							

Sol 15	**0.43 m HS-**		**χ^2_{red} = 416**		**R-factor = 0.092**		**E0 = 8.3(6)**	
T	**nO**	**rO (Å)**	**nS**	**rS (Å)**	**ntot**	**σ^2 (Å^2)**	**k-range**	**R-range**
30	2.1(4)	1.76(1)	1.7 (fix)	2.26(2)	3.8	0.002(2)	2-11	1-3
100	2.1(2)	1.76(1)	1.6(2)	2.25(1)	3.7	0.001(1)	2-11	1-3
200	2.3(4)	1.75(1)	1.3(2)	2.27(2)	3.6	0.001(2)	2-11	1-3
300	2.9(4)	1.76(1)	1.2(3)	2.28(2)	4.1	0.002(2)	2-11	1-3
Sol15.apj	fit13							

Figures

Figure 1. XANES data of solutions. **(a)** Summary of all collected data as a function of temperature and solution composition. Dark blue spectrum = 30 ºC; red spectrum= maximum temperature collected; light blue spectra = temperatures in-between. **(b)** XANES spectra of all solutions at 30 ºC. **(c)** XANES spectra of all solutions at 300 ºC (virtually the same as 30 ºC). **(d)** This figure is the same as Fig 1a, but without the intermediate T, so that it is easier to see effect of increasing T.

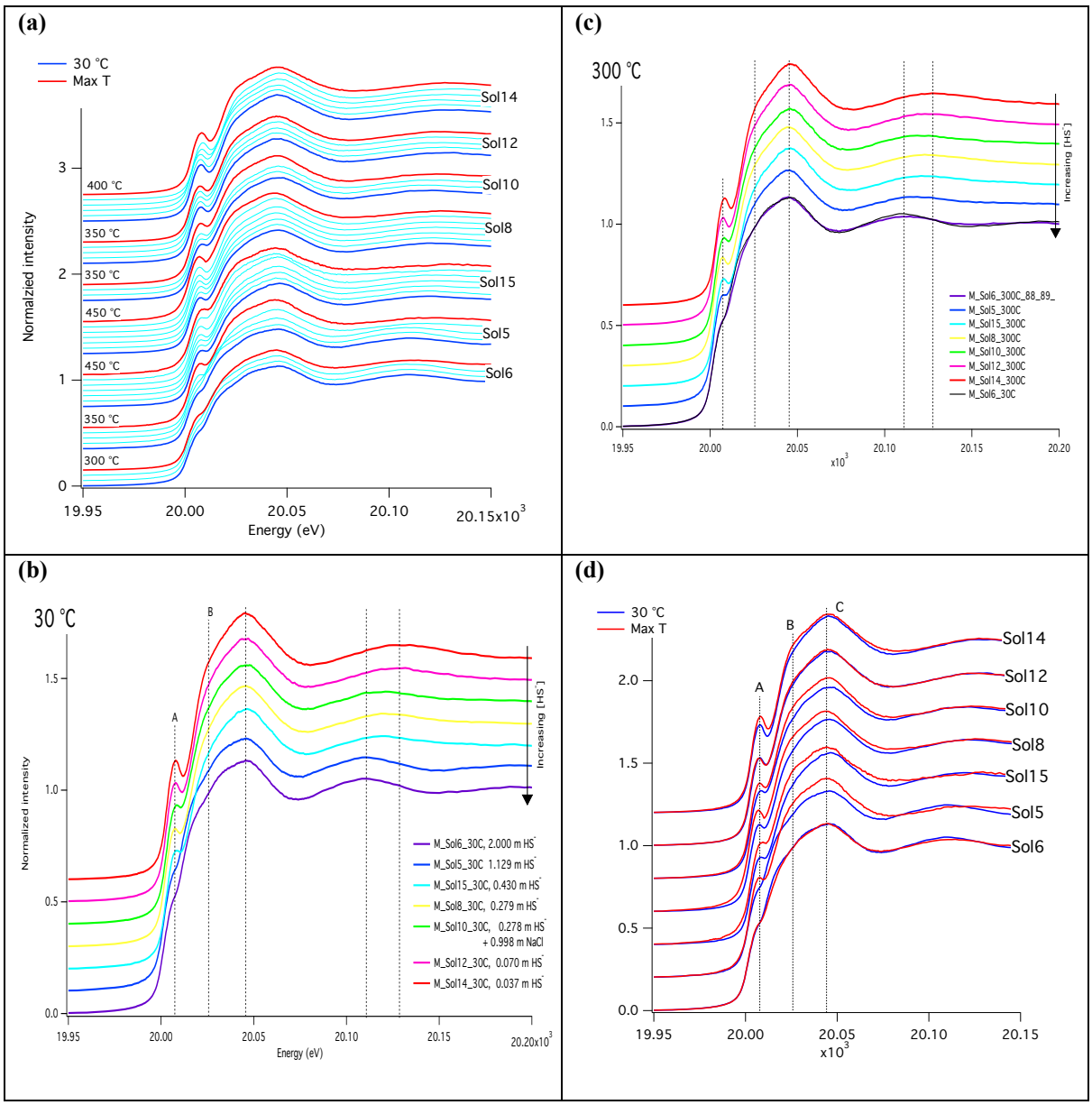

Figure 2. EXAFS spectra, (a) in K-space and (b) their Fourier transforms. Solid line = raw data, dashed line = fitted data.

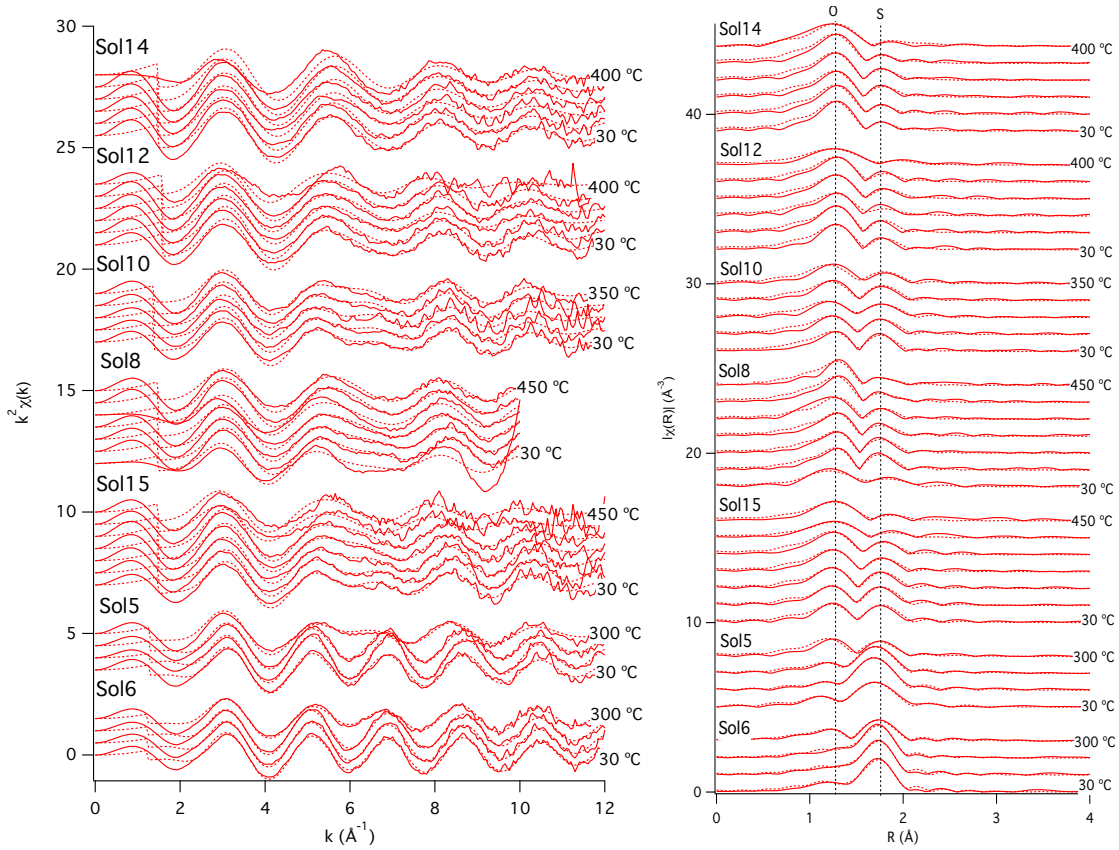

(a) (b)